

UNIVERSIDADE FEDERAL DO ESPÍRITO SANTO
CENTRO TECNOLÓGICO
PROGRAMA DE PÓS-GRADUAÇÃO EM ENGENHARIA AMBIENTAL

KAMILA FURTADO CUPERTINO

**ASSESSMENT OF THE USEPA FLUX HOOD PERFORMANCE TO MEASURE
VOLATILISATION RATE OF ODOROUS COMPOUNDS FROM PASSIVE LIQUID
SURFACES**

VITÓRIA (ES), SEPTEMBER 2022

KAMILA FURTADO CUPERTINO

**ASSESSMENT OF THE USEPA FLUX HOOD PERFORMANCE TO MEASURE
VOLATILISATION RATE OF ODOROUS COMPOUNDS FROM PASSIVE LIQUID
SURFACES**

A thesis submitted to Programa de Pós-Graduação em Engenharia Ambiental of the Centro Tecnológico at Universidade Federal do Espírito Santo, for the degree of Doctor in Environmental Engineering.

Supervisor: Prof. Dr Jane Méri Santos

Co-supervisors: Prof. Dr Ademir Abdala Prata Jr and Prof. Dr. Richard Michael Stuetz

VITÓRIA (ES), SEPTEMBER 2022

Ficha catalográfica disponibilizada pelo Sistema Integrado de Bibliotecas - SIBI/UFES e elaborada pelo autor

C974a Cupertino, Kamila Furtado, 1986-
ASSESSMENT OF THE USEPA FLUX HOOD PERFORMANCE TO MEASURE VOLATILISATION RATE OF ODOROUS COMPOUNDS FROM PASSIVE LIQUID SURFACES / Kamila Furtado Cupertino. - 2022.
154 f. : il.

Orientadora: Jane Meri Santos.

Coorientadores: Ademir Abdala Prata Junior, Richard Michael Stuetz.

Tese (Doutorado em Engenharia Ambiental) - Universidade Federal do Espírito Santo, Centro Tecnológico.

1. Pesquisa experimental. 2. Ar - Poluição. 3. Análise numérica. 4. Compostos orgânicos. I. Santos, Jane Meri. II. Prata Junior, Ademir Abdala. III. Stuetz, Richard Michael. IV. Universidade Federal do Espírito Santo. Centro Tecnológico. V. Título.

CDU: 628



UNIVERSIDADE FEDERAL DO ESPÍRITO SANTO
CENTRO TECNOLÓGICO
PROGRAMA DE PÓS-GRADUAÇÃO EM ENGENHARIA AMBIENTAL

ASSESSMENT OF THE USEPA FLUX HOOD PERFORMANCE TO MEASURE VOLATILISATION RATE OF ODOROUS COMPOUNDS FROM PASSIVE LIQUID SURFACES

Kamila Furtado Cupertino

Banca Examinadora:

Prof.^a Dr.^a Jane Meri Santos
Orientadora - PPGEA/CT/UFES

Prof. Dr. Ademir Abdala Prata Jr.
Coorientador Externo – UNSW/Austrália-UFAL

Prof. Dr. Richard Michael Stuetz
Coorientador Externo – UNSW/Austrália

Prof.^a Dr.^a Elisa Valentim Goulart
Examinador Interna – PPGEA/CT/UFES

Prof. Dr. Neyval Costa Reis Jr.
Examinador Interno – PPGEA/CT/UFES

Prof. Dr. Waldir Nagel Schirmer
Examinador Externo – Unicentro/PR

Prof. Dr. Igor Braga de Paula
Examinador Externo – PUC-Rio

Elisa Valentim Goulart
Coordenadora do Programa de Pós-Graduação em Engenharia Ambiental
UNIVERSIDADE FEDERAL DO ESPÍRITO SANTO

To my precious daughter,
Dominique Cupertino Furieri.

ACKNOWLEDGMENTS

Firstly, I would like to thank God for the grace to complete this work.

I would like to thank the professors and administrative staff of the Programa de Pós-graduação em Engenharia Ambiental (PPGEA) from Universidade Federal do Espírito Santo (UFES), and especially to my supervisor Prof. Jane Meri Santos for the encouragement and opportunities obtained throughout the development of this achievement.

I would like to thank Companhia Espírito Santense de Saneamento (CESAN) and co-workers for their support in carrying out this scientific research.

I would like to thank the Coordenação de Aperfeiçoamento de Pessoal de Nível Superior (CAPES) for financial support.

I would like to thank to the professors and administrative staff of University of New South Wales, especially to Prof. Richard Stuetz for partnership and co-supervision on this study. I am grateful for the co-supervision and friendship of Prof. Ademir Prata Jr. who helped me so many times with procedures at the Odor Lab and for so many pleasant moments during my stay in Sydney with his wife Renata and lovely daughter Victoria.

I would like to thank my NQualiar Lab colleagues for the knowledge exchanges and for making the entire development of the research easier, namely: Andressa, Brenda, Cristina, Enilene, Izabele, Jamily, Laize, Karine, Maria Clara, Matheus, Milena, Noéle, Pamela, Philippe and Ramon. For the same reasons, I also thank my colleagues at the Odour Lab: Clare, Christina, Fadhilah, James, Nhat, Philippa, Radoslaw, Rob, Ruth, Thais, Weiyang and Yating. Special thanks to Janaina, Nick, Nixon, Rui and lovely Eva for making me feel at home during my stay in Sydney.

In gratitude to family and friends, from here I speak in Portuguese: à minha mãe Marlene, obrigada por estar ao meu lado em todas as minhas decisões. Agradeço ao meu irmão Wallace por cuidar de mim desde sempre e ao meu pai Áureo (*in memoriam*), que estaria muito orgulhoso pela conclusão da tese. Agradeço aos amigos por sempre ouvirem minhas queixas com paciência, carinho e me incentivarem a continuar: Ana Beatriz, Edvânia, Larissa, Letícia, Mara Gabriela, Marcela, Natália, Rafael, Shaira, Soraya e Stênio. Agradeço à toda minha família pela torcida e pela compreensão, sobretudo nos momentos em que precisei estar ausente para o desenvolvimento deste estudo. Agradeço em especial aos meus sobrinhos: João Guilherme, Júlia, Rafaela e Thales. Por fim, agradeço ao meu esposo e melhor amigo Bruno Furieri: você é o raio de luz que ilumina, aquece meu coração e minha vida! Eu te amo com todo meu coração e agradeço a Deus pela graça de partilhar com você mais uma vitória.

ABSTRACT

Wastewater treatment plants are important sources of odorous gases to the atmosphere as nitrogen, sulphur, and volatile organic compounds (VOC). These odorous gases may cause adverse effects on human health and annoyance. Dynamic flux hoods have been used as direct methods to estimate area source emission rates from liquid gas surfaces. However, despite of being designed to achieve complete mixing and consequent homogeneous distribution of concentration inside the device, some related works pointed out that the compound can accumulate (concentration build-up) inside the flux hood, affecting sampling representativeness. Then, to investigate the performance of the device to measure volatilisation rate of odorous compounds from passive liquid surfaces, mass transfer parameters for acetic acid (gas phase-controlled compound) were assessed under various sweep air flow rates (2, 3, 5, 7 and 10 L min⁻¹) with original flux hood (No Fan) and flux hood modified by an internal fan. To assess the validity of adapting results from one compound to another, a procedure based on their Schmidt number to estimate the gas-film mass transfer coefficient inside the original USEPA flux hood for a gas phase-controlled compound (acetic acid) based on a reference compound (butyric acid) were evaluated. Finally, the bias between measured emission in laboratory and values that could be expected in the field in the absence of sampling device were evaluated by comparing the values of mass transfer obtained experimentally with the values obtained from the volatilisation model proposed by Prata-Brutsaert for two scenarios. We observed that not all fan configurations tested resulted in higher emissions inside the flux hood compared to the No Fan configuration and this is contrary to the intuitive hypothesis that the use of a fan inside the flux hood would enhance the emission of odorants measured on liquid surfaces. By using the numerical simulation technique, we could better understand the reason the fan inside the flux hood does not produce a significant increase in the emission rate. Main conclusions are specific for the fan sizes, rotation speeds and position inside the hood investigated in this work; it is possible that certain variations in these aspects may render stronger effects of the fan flow. Investigations and standardization of procedure are recommended to apply scaling up, especially in situations where the flux hood cannot be used in the field for operational reasons, so that the effect of the build-up concentration inside the flux hood may be considered.

Keywords: Enclosure devices, Volatile Organic Compounds, Emission estimation, Computational Fluid Dynamics, Laboratory simulation.

ABBREVIATIONS AND ACRONYMS

CAPES	Coordenação de Aperfeiçoamento de Pessoal de Nível Superior
CFD	Computational Fluid Dynamics
CV	Control Volume
DFC	Dynamic Flux Chamber
NQualiAr	Air Quality Research Group
PWT	Portable Wind Tunnel
RANS	Reynolds Averaged Navier Stokes
RSM	Reynolds Stress Model
SST	Shear Stress Transport
UFES	Universidade Federal do Espírito Santo
UNSW	University of New South Wales
USEPA	United States Environmental Protection Agency
VOC	Volatile Organic Compound
WWTP	Wastewater Treatment Plant

LIST OF SYMBOLS

Roman symbols

A	Surface area of the source covered by the sampling device (m^2)
C	Concentration of the solute in the medium (kg m^{-3})
$C_{G,i}$	Concentration of the solute in the gaseous interface (kg m^{-3})
$C_{L,i}$	Concentration of the solute in the liquid interface (kg m^{-3})
C_G	Concentration of the solute in the gas phase (kg m^{-3})
C_L	Concentration of the solute in the liquid phase (kg m^{-3})
d	Perpendicular distance from the first nodal point to the wall (m)
D	Molecular diffusivity of the solute in the medium ($\text{m}^2 \text{s}^{-1}$)
D_{AB}	Diffusivity of the compound A in the medium B ($\text{m}^2 \text{s}^{-1}$)
D_G	Diffusivity of the solute in the gaseous phase ($\text{m}^2 \text{s}^{-1}$)
d_G	Thickness of the gaseous film (m)
D_L	Diffusivity of the solute in the liquid phase ($\text{m}^2 \text{s}^{-1}$)
d_L	Thickness of the liquid film (m)
E	Emission rate ($\text{kg s}^{-1} \text{m}^{-2}$)
$F1, F2$	Auxiliary functions of the k - ω SST model
I	Turbulence intensity (%)
J	Mass flux of a specific solute ($\text{kg s}^{-1} \text{m}^{-2}$)
J_w	Water evaporation rate ($\text{kg s}^{-1} \text{m}^{-2}$)
J_G	Mass flux of the solute that cross the gas surface ($\text{kg s}^{-1} \text{m}^{-2}$)
J_L	Mass flux of the solute that cross the liquid surface ($\text{kg s}^{-1} \text{m}^{-2}$)
k_G	Mass transfer coefficient of the gaseous film (m s^{-1})
K_H	Dimensionless Henry's law constant
K_L	Liquid-phase overall mass transfer coefficient (m s^{-1})

k_L	Mass transfer coefficient of the liquid filme (m s^{-1})
P	Pressure ($\text{kg t}^{-2} \text{m}^{-1}$)
Q	Flow rate of the carrier gas ($\text{m}^3 \text{s}^{-1}$)
TVR	Turbulent viscosity ratio ($\text{kg t}^{-2} \text{m}^{-1}/\text{kg t}^{-2} \text{m}^{-1}$)
t	Time (s)
u	Velocity in the x direction (m s^{-1})
U	Magnitude of the velocity (m s^{-1})
u^*	Friction velocity (m s^{-1})
u_i	Velocity in i direction (m s^{-1})
v	Velocity in the y direction (m s^{-1})
w	Velocity in the z direction (m s^{-1})
y^+	Non-dimensional distance from the wall based on the influence of the shear stress

Greek symbols

$\alpha_1, \beta, \sigma_k, \gamma, \beta, \sigma_\omega$	Constants of the $\kappa - \omega$ SST model
$\beta_1, \gamma_1, \sigma_{k,1}, \sigma_{\omega,1}$	Constants of the original Wilcox $\kappa - \omega$ model
ε	Dissipation of the turbulent kinetic energy ($\text{m}^2 \text{s}^{-3}$)
η	Mass fraction of the solute in the medium (kg kg^{-1})
κ	Turbulent kinetic energy ($\text{m}^2 \text{s}^{-2}$)
μ	Dynamic viscosity ($\text{kg s}^{-2} \text{m}^{-1}$)
μ_T	Turbulent viscosity ($\text{kg s}^{-2} \text{m}^{-1}$)
ρ	Specific mass (kg m^{-3})
τ	Turbulent stress tensor ($\text{kg s}^{-2} \text{m}^{-1}$)
ν	Kinematic eddy viscosity ($\text{m}^2 \text{s}^{-2}$)
ν_T	Turbulent eddy viscosity ($\text{m}^2 \text{s}^{-2}$)

$\varphi, \varphi_1, \varphi_2$ Variable that represents any constant of the $\kappa - \omega$ SST model, original

ω Specific dissipation rate (s^{-1})

Subscript

i, j, k Indicical notation

Superscript

' Fluctuations
— Average value

LIST OF FIGURES

Figure 1 – Schematic representation of mass transfer process across liquid and gas film (SANTOS et al., 2012).	25
Figure 2 – Values of Henry constant for representative odorants and other environmentally relevant chemicals, where A, B and C indicate species where emission rate is dependent primarily on air phase turbulence, both air and liquid phase turbulence and liquid phase turbulence, respectively (HUDSON; AYOKO, 2008)	31
Figure 3 – Schmidt number/solubility diagram, including various volatile tracers, momentum, and heat for a temperature range (°C), as indicated. Filled circles refer only to a temperature of 20 °C. The regions for air-sided, mixed, and water-sided control of transfer process between the gas and liquid phase are marked. At the solid lines the transfer resistance is equal in both phases. The following dimensional transfer resistances were used: $\gamma_a = 31$; $\gamma_w = 12 Sc^{2/3}$ (smooth); $\gamma_w = 6.5 Sc^{1/2}$ (wavy surface) with $\gamma_a = Rau * a$ and $\gamma_w = Rwu * w$. (JÄHNE; HAUSSECKER, 1998)	32
Figure 4 – Schematic representation of USEPA dynamic flux chamber (Kienbusch, 1986).	35
Figure 5 – Schematic representation of USEPA dynamic flux chamber.....	41
Figure 6 – Picture of USEPA Dynamic flux hood device used in the present study.	41
Figure 7 – Schematic representation of Lung System (PRATA, Ademir Abdala, 2017).	42
Figure 8 – Fans used at Flux hood. a) 4 x 4 cm in size, 6000 rpm and 12V and b) 8 x 8 cm, 3200 rpm and 12V.....	42
Figure 9 – Fan coupled and installed to a dome-shaped topper (view from dome-shaped topper outside).	43
Figure 10 – Calibration curve after outlier test: Acetic acid.....	45
Figure 11 – Calibration curve after outlier test: Butyric acid.....	47
Figure 12 – From the top-left corner in clockwise direction: (i) outlet probe line mesh refinement and prismatic elements surrounding it, (ii) fan blades mesh refinement and growth rate observed towards the main section and (iii) near wall prismatic elements close to the side wall and gas-liquid interface at the bottom.	52
Figure 13 – Experimental and numerical results comparison for acetic acid volatilisation phenomena: (a) numerical and experimental outlet concentration ratio for No Fan 2, 5, 7 and 10 L min ⁻¹ , SFanUp and SFanDown 5 L min ⁻¹ , LFanUP for 5 L min ⁻¹ and LFanDown for 2, 5 and 10 L min ⁻¹ scenarios and (b) Fan vs. No Fan concentration ratio.	89

Figure 14 – Numerical results of near interface (0.5 mm from the interface) concentration gradient (top view) (a) No Fan 2LPM, (b) 5 LPM, (c) 7 LPM and (d) 10 LPM and (e) to (h) interface wall friction velocity values for the same scenarios as for (a) to (d).	91
Figure 15 – Numerical results of near interface (0.5 mm from the interface) concentration gradient (top view) (a) LFanDown 5LPM, (b) LFanDown 10LPM, (c) LFanUp 5LPM, (d) SFanUp 5LPM and (e) SFanDown 5LPM and (f) to (j) interface wall friction velocity values for the same scenarios as for (a) to (e).....	94
Figure 16 – Concentration distribution: (a) No Fan 5LPM, (b) LFanDown 5LPM, (c) LFanUp 5LPM, (d) SFanUp 5LPM and (e) SFanDown 5LPM.	96
Figure 17 – Turbulent kinetic energy distribution: (a) No Fan 2LPM, (b) No Fan 5LPM and (c) No Fan 10LPM.....	97
Figure 18 – Turbulent kinetic energy distribution: (a) LFanDown 2LPM, (b) LFanDown 5LPM, (c) (b) LFanDown 10LPM, (d) LFanUp 5LPM, (e) SFanUp 5LPM and (f) SFanDown 5LPM.	99
Figure 19 – Streamlines colored by concentration: (a) LFanDown 5LPM, (b) LFanUp 5LPM, (c) (b) SFanUp 5LPM and (d) SFanDown 5LPM.....	100
Figure 20 – Schematic representation of internal boundary layer (IBL) development over a liquid surface proposed by Prata et al. (2021).	109
Figure 21 – Comparison of kG values for acetic acid obtained from the original USEPA flux hood (No Fan) with inlet sweep air flow of 2, 3, 5, 7 and 10 L min ⁻¹ and those obtained using Prata-Brutsaert model proposed by Prata et al. (2021). for different wind speeds.	111
Figure 22 – The Camburi WWTP.....	116
Figure 23 – Emission rate of acetic acid (HAC) at Camburi WWTP case: Comparison between the values obtained using the kG model proposed by Prata et al. (2021) and the kG values from the flux hood with $Q = 2$ L min ⁻¹ . a) roughness 0.005 m and 260° wind direction. b) roughness 0.20 m and 345° wind direction.....	117
Figure 24 – Emission rate of acetic acid (HAC) at Camburi WWTP: Comparison between the values obtained using the kG model proposed by Prata et al. (2021) and the kG values from the flux hood with $Q = 5$ L min ⁻¹ . a) roughness 0.005 m and 260° wind direction. b) roughness 0.20 m and 345° wind direction.....	118
Figure 25 – Emission rate of acetic acid (HAC) at Camburi WWTP: Comparison between the values obtained using the kG model proposed by Prata et al. (2021) and the kG values	

from the flux hood with $Q = 10 \text{ L min}^{-1}$. a) roughness 0.005 m and 260° wind direction. b) roughness 0.20 m and 345° wind direction.....	119
Figure 26 – Emission rate of valeric acid (HAV) at Camburi WWTP: Comparison between the values obtained using the kG model proposed by Prata et al. (2021) and the kG values from the flux hood with $Q = 2 \text{ L min}^{-1}$. a) roughness 0.005 m and 260° wind direction. b) roughness 0.20 m and 345° wind direction.....	120
Figure 27 – Emission rate of valeric acid (HAV) at Camburi WWTP: Comparison between the values obtained using the kG model proposed by Prata et al. (2021) and the kG values from the flux hood with $Q = 5 \text{ L min}^{-1}$. a) roughness 0.005 m and 260° wind direction. b) roughness 0.20 m and 345° wind direction.....	121
Figure 28 – Emission rate of valeric acid (HAV) at Camburi WWTP: Comparison between the values obtained using the kG model proposed by Prata et al. (2021) and the kG values from the flux hood with $Q = 10 \text{ L min}^{-1}$. a) roughness 0.005 m and 260° wind direction. b) roughness 0.20 m and 345° wind direction.....	122
Figure 29 – Emission rate of isobutyric acid (HAI) at Camburi WWTP: Comparison between the values obtained using the kG model proposed by Prata et al. (2021) and the kG values from the flux hood with $Q = 2 \text{ L min}^{-1}$. a) roughness 0.005 m and 260° wind direction. b) roughness 0.20 m and 345° wind direction.....	123
Figure 30 – Emission rate of isobutyric acid (HAI) at Camburi WWTP: Comparison between the values obtained using the kG model proposed by Prata et al. (2021) and the kG values from the flux hood with $Q = 5 \text{ L min}^{-1}$. a) roughness 0.005 m and 260° wind direction. b) roughness 0.20 m and 345° wind direction.....	124
Figure 31 – Emission rate of isobutyric acid (HAI) at Camburi WWTP: Comparison between the values obtained using the kG model proposed by Prata et al. (2021) and the kG values from the flux hood with $Q = 10 \text{ L min}^{-1}$. a) roughness 0.005 m and 260° wind direction. b) roughness 0.20 m and 345° wind direction.....	125
Figure 32 – Emission rate of butyric acid (HAB) at Camburi WWTP: Comparison between the values obtained using the kG model proposed by Prata et al. (2021) and the kG values from the flux hood with $Q = 2 \text{ L min}^{-1}$. a) roughness 0.005 m and 260° wind direction. b) roughness 0.20 m and 345° wind direction.....	126
Figure 33 – Emission rate of butyric acid (HAB) at Camburi WWTP: Comparison between the values obtained using the kG model proposed by Prata et al. (2021) and the	

<i>kG</i> values from the flux hood with $Q = 5 \text{ L min}^{-1}$. a) roughness 0.005 m and 260° wind direction. b) roughness 0.20 m and 345° wind direction.....	127
Figure 34 –Emission rate of butyric acid (HAB) at Camburi WWTP: Comparison between the values obtained using the <i>kG</i> model proposed by Prata et al. (2021) and the <i>kG</i> values from the flux hood with $Q = 10 \text{ L min}^{-1}$. a) roughness 0.005 m and 260° wind direction. b) roughness 0.20 m and 345° wind direction.....	128
Figure 35 – Comparison of <i>kG</i> values for acetic acid (AC) obtained using the flux hood with $Q = 2 \text{ L min}^{-1}$ and different fan configurations and those obtained using the Prata-Brutsaert model proposed by Prata et al. (2021) for different wind speeds. a) roughness 0.005 m and 260° wind direction. b) roughness 0.20 m and 345° wind direction.....	131
Figure 36 – Comparison of <i>kG</i> values for acetic acid (AC) obtained using the flux hood with $Q = 5 \text{ L min}^{-1}$ and different fan configurations and those obtained using the Prata-Brutsaert model proposed by Prata et al. (2021) for different wind speeds. a) roughness 0.005 m and 260° wind direction. b) roughness 0.20 m and 345° wind direction.....	132
Figure 37 – Comparison of <i>kG</i> values for acetic acid (AC) obtained using the flux hood with $Q = 10 \text{ L min}^{-1}$ and different fan configurations and those obtained using the Prata-Brutsaert model proposed by Prata et al. (2021) for different wind speeds. a) roughness 0.005 m and 260° wind direction. b) roughness 0.20 m and 345° wind direction.....	133
Figure 38 – Comparison of <i>kG</i> values for valeric acid (HAV) obtained using the Schmidt number and the flux hood with $Q = 2 \text{ L min}^{-1}$ and different fan configurations and those obtained using the Prata-Brutsaert model proposed by Prata et al. (2021) for different wind speeds. a) roughness 0.005 m and 260° wind direction. b) roughness 0.20 m and 345° wind direction.	134
Figure 39 – Comparison of <i>kG</i> values for valeric acid (HAV) obtained using the Schmidt number and the flux hood with $Q = 5 \text{ L min}^{-1}$ and different fan configurations and those obtained using the Prata-Brutsaert model proposed by Prata et al. (2021) for different wind speeds. a) roughness 0.005 m and 260° wind direction. b) roughness 0.20 m and 345° wind direction.	135
Figure 40 – Comparison of <i>kG</i> values for valeric acid (HAV) obtained using the Schmidt number and the flux hood with $Q = 10 \text{ L min}^{-1}$ and different fan configurations and those obtained using the Prata-Brutsaert model proposed by Prata et al. (2021) for different wind speeds. a) roughness 0.005 m and 260° wind direction. b) roughness 0.20 m and 345° wind direction.	136

Figure 41 – Comparison of <i>kG</i> values for isobutyric acid (HAI) obtained using the Schmidt number and the flux hood with $Q = 2 \text{ L min}^{-1}$ and different fan configurations and those obtained using the Prata-Brutsaert model proposed by Prata et al. (2021) for different wind speeds. a) roughness 0.005 m and 260° wind direction. b) roughness 0.20 m and 345° wind direction.	137
Figure 42 – Comparison of <i>kG</i> values for isobutyric acid (HAI) obtained using the Schmidt number and the flux hood with $Q = 5 \text{ L min}^{-1}$ and different fan configurations and those obtained using the Prata-Brutsaert model proposed by Prata et al. (2021) for different wind speeds. a) roughness 0.005 m and 260° wind direction. b) roughness 0.20 m and 345° wind direction.	138
Figure 43 – Comparison of <i>kG</i> values for isobutyric acid (HAI) obtained using the Schmidt number and the flux hood with $Q = 10 \text{ L min}^{-1}$ and different fan configurations and those obtained using the Prata-Brutsaert model proposed by Prata et al. (2021) for different wind speeds. a) roughness 0.005 m and 260° wind direction. b) roughness 0.20 m and 345° wind direction.	139
Figure 44 – Comparison of <i>kG</i> values for butyric acid (HAB) obtained using the Schmidt number and the flux hood with $Q = 2 \text{ L min}^{-1}$ and different fan configurations and those obtained using the Prata-Brutsaert model proposed by Prata et al. (2021) for different wind speeds. a) roughness 0.005 m and 260° wind direction. b) roughness 0.20 m and 345° wind direction.	140
Figure 45 – Comparison of <i>kG</i> values for butyric acid (HAB) obtained using the Schmidt number and the flux hood with $Q = 5 \text{ L min}^{-1}$ and different fan configurations and those obtained using the Prata-Brutsaert model proposed by Prata et al. (2021) for different wind speeds. a) roughness 0.005 m and 260° wind direction. b) roughness 0.20 m and 345° wind direction.	141
Figure 46 – Comparison of <i>kG</i> values for butyric acid (HAB) obtained using the Schmidt number and the flux hood with $Q = 10 \text{ L min}^{-1}$ and different fan configurations and those obtained using the Prata-Brutsaert model proposed by Prata et al. (2021) for different wind speeds. a) roughness 0.005 m and 260° wind direction. b) roughness 0.20 m and 345° wind direction.	142

LIST OF TABLES

Table 1 – Details of investigated flux chamber configurations.	43
Table 2 - Summary of configuration performed and measured temperatures.....	44
Table 3 – Boundary conditions.....	53
Table 4 – Numerical Simulation tested cases	54
Table 5 – Estimating kG gas phase control from kG experimental.	113
Table 6 – Applying estimating kG in Prata-Brutsaert model.....	114

TABLE OF CONTENTS

1	INTRODUCTION.....	19
2	OBJECTIVES.....	23
3	LITERATURE REVIEW.....	24
3.1	THEORETICAL ASPECTS ON VOLATILISATION PASSIVE LIQUID SURFACES	24
3.1.1	<i>Fick's Law.....</i>	24
3.1.2	<i>The two-film theory</i>	25
3.1.3	<i>Two-resistance models</i>	27
3.1.4	<i>Henry's Law</i>	28
3.1.5	<i>The global mass transfer coefficient.....</i>	28
3.1.6	<i>Schmidt number.....</i>	30
3.2	ODOROUS COMPOUNDS EMISSION RATE: USEPA FLUX HOOD	32
4	METHODOLOGY.....	40
4.1	EXPERIMENTAL SET-UP	40
4.1.1	<i>Flux hood configuration.....</i>	40
4.1.2	<i>Volatilisation experiments: Acetic acid.....</i>	43
4.1.3	<i>Volatilisation experiments: Butyric acid</i>	46
4.1.4	<i>Emission rate and mass transfer coefficients from flux hood experiments</i>	47
4.2	NUMERICAL SIMULATION.....	48
5	RESULTS AND DISCUSSIONS	56
5.1	EFFECTS OF FAN CONFIGURATION ON THE VOLATILISATION INSIDE A FLUX HOOD.....	56
5.2	NUMERICAL INVESTIGATION OF FLUX HOOD FLUID FLOW AND MASS TRANSFER MODIFIED BY AN INTERNAL FAN	87
5.2.1	<i>Comparison between experimental and numerical estimation of outlet probe concentration</i>	88
5.2.2	<i>Interface friction velocity and near wall concentration gradient</i>	89
5.2.3	<i>Concentration distribution and turbulent kinetic energy.....</i>	94
5.3	COMPARISON OF MASS TRANSFER PARAMETERS INSIDE THE USEPA FLUX HOOD FOR TWO VOCs.....	100
5.4	EXPERIMENTAL ASSESSED EMISSION RATE RESCALING TO REAL METEOROLOGICAL AND SOURCE CONDITIONS	108
5.4.1	<i>Volatilisation model proposed by Prata-Brutsaert</i>	108
5.4.2	<i>Hypothetical scenario</i>	111
5.4.3	<i>Real wastewater treatment plant scenario</i>	112
6	CONCLUSIONS AND PERSPECTIVES.....	146
7	REFERENCES.....	149

1 INTRODUCTION

Industrial and domestic wastewater treatment plants (WWTPs) are associated with environmental impacts to air quality in neighbourhood communities. WWTPs are important sources of odorous gases to the atmosphere as nitrogen, sulphur, and volatile organic compounds (VOC). These odorous gases may cause adverse effects on human health, annoyance which can turn into complaints to authorities and price depreciation of properties. WWTPs are characterized by large areas representing fugitive sources of odorous gases. WWTPs units with passive liquid surface, for instance, primary and secondary settlement tanks, non-aerated sequencing batch reactors, equalization tanks, aerated biological filters and stabilization ponds (SANTOS et al., 2012), are potential sources of odour emissions due to volatilisation of dissolved odorants in the liquid phase driven by the interaction between the liquid-phase and the sweeping wind.

The emission from passive liquid surface is related to the phenomena occurring in the region very close to the interface. The resistance to the gaseous transport through the liquid-gas interface is limited to a very thin sublayer of each side of the interface, where the turbulence is reduced, and the processes of molecular diffusion become dominant. Resistance to mass transfer in the region close to the interface may be more important only in the liquid phase, in the gas phase or in both phases depending on the chemical properties of the substances involved (solvents and solute). Therefore, the global mass transfer coefficient is dependent on the Henry's constant of the compound of interest.

The volatilisation process can be described by a two-resistance mass transfer model, originally introduced in the framework of the two-film theory (LEWIS; WHITMAN, 1924) in which the mass flux at the liquid-gas interface is a function of the compound concentrations in the bulk liquid phase and the bulk gas phase, the liquid-film and the gas-film mass transfer coefficients (k_L and k_G) and the Henry's law coefficient (K_H). The bulk-liquid concentration can be directly measured from a liquid sample. The gas-phase concentration is commonly neglected as the passive surface is open to the atmosphere. The general approach to estimate k_L and k_G consists in deriving empirical or semi-empirical expressions based on variables relevant to the mass transfer process that can be easily measured or estimated (PRATA; SANTOS; et al., 2018). Typically, it involves at least one variable representing wind forcing and another accounting for the compound molecular diffusion. Essentially, the latter is taken as the compound molecular diffusivity or the Schmidt number and the former as the wind velocity at a certain height or the friction velocity (u^*). There are correlations to estimate the friction velocity u^* available in the literature, according to Prata

(2017), these correlations were originally developed from experimental data for wind drag over the ocean, which may present important differences in relation to the wind-wave field over WWTPs, which are relatively small liquid surfaces, with short fetch (distance along the liquid surface in the direction of the wind flow).

There are different approaches in the literature to estimate the emission rate of odorous compounds at passive liquid surfaces in WWTPs: (i) predictive emission models, (ii) reverse dispersion modelling (indirect method) and (iii) sampling with enclosure devices, such as a dynamic flux chamber or a wind tunnel (direct method).

Mathematical emission models such as WATER9 (US EPA, 2001); TOXCHEM+ (ENVIROMEGA, 2004) and Gostelow et al. (2001) are based on a mass balance for each compound in the liquid phase of the treatment facility (SANTOS et al., 2012). This mass balance includes mechanisms of compound removal from liquid phase (volatilisation, stripping, biodegradation, chemical oxidation), which result from its interaction with the reaction medium through physical, chemical and biological processes, typical of each treatment process. Despite the advantages presented by these models, such as being a relatively rapid and low-cost approach, their validity is restricted to the conditions for which they were formulated. The volatilisation removal mechanism included in the models is described by different empirical formulations for the calculations of friction velocity and mass transfer coefficients depending on the model.

Indirect methods are based on simultaneous measurements of meteorological conditions and pollutant concentration profiles across the emitted plume and on the use of atmospheric dispersion models. The dispersion models calculate concentration based on emission rate (among other parameters), in this case, a model is used in a reverse way as the emission rate is estimated based on the pollutants concentration measurements. However, the use of indirect methods can be limited by the large number of downwind measurements required (with associated costs of measurement campaigns or permanent monitoring stations) and constraints of the terrain and surrounding buildings. Because of such limitations, presently, indirect methods are rarely adopted for routine purposes.

Direct methods use devices that enclosure a minimal part of emitting surfaces and directly sample the emissions. Dynamic flux chamber (or flux hood) and portable wind tunnel are enclosure devices that can be used to monitor emission variations caused by changes in the WWTP processes. They can be an inspiration for legislators or regulators of the environment to establish standards or procedures for the estimation of the emission rates for passive liquid surfaces. These

open bottom devices are placed over the emitting surface; a sweep gas flow transports the volatilised compounds through the equipment to a sampling bag or a sorbent tube for posterior analysis, or to a gas-specific sensor for in-line analysis. There is a wide variety of configurations and operational conditions for these sampling devices as explained by Hudson and Ayoko (2008). Kienbusch (1986) was commissioned by the United States Environmental Protection Agency (USEPA) to present a standard and recommendations for the construction and operation of an emission isolation flux chamber, which became a standard technique for estimating emission rates from landfill and later adapted for liquid surfaces (EKLUND et al., 1998). It has been often referred in the literature as the “USEPA flux hood/flux chamber”.

Despite of being designed to achieve complete mixing and consequent homogeneous distribution of concentration inside the device (EKLUND, 1992), Hudson and Ayoko (2009) pointed out that the compound can accumulate (concentration build-up) inside the flux hood, affecting sampling representativeness if concentration reach values close to saturation. Parker et al. (2013) also pointed out that flux hoods operating at typical sweep air flow rates underestimates the emission rate due to restrictions in low air exchange rates. Regarding the USEPA flux hood, Prata et al., (2016) and Andreao et al. (2019) indicated that the friction velocity on the liquid surface inside the hood does not match typical values of atmospheric flow if typical sweep air flow rates are used. In addition, these authors observed that the USEPA flux hood present an issue concerning flow pattern inside in the device, the sampling probe can be exposed to clean sweep air flow causing a decrease in the concentration of the sampled gas (which would mean a negative bias in the measured emission rate).

To create turbulent conditions similar to those in the field and/or to improve mixing in the headspace, many authors have included a fan inside the flux hood (ANEJA, V. P.; CHAUHAN; WALKER, 2000; LAOR; PARKER; PAGÉ, 2014; LYMAN et al., 2018; WOODBURY B. L., PARKER D. B., EIGENBERG R. A., SPIEHS, 2011). Also, the use of an internal fan has been investigated using computational fluid dynamics to simulate the flow patterns inside the device (ANDREÃO, Willian L. et al., 2019; ECKLEY et al., 2010; PRATA et al., 2016). The use of an internal fan in the proposed USEPA flux hood has been regulated in countries like Australian and New Zealand standard AS/NZS 4323.4:2009.

Despite the practical advantages of flux hoods for field use, the appropriate flux hood operational conditions are still a matter of discussion. There is still a lack of experimental data and detailed information regarding the mass transfer phenomena occurring inside the flux hood modified by a

fan. Doubts remain concerning if the flux hood should be expected to mimic atmospheric conditions in which the real emission occurs regarding, for instance, the friction velocity for volatilisation gas-phase controlled odorous gases. Doubts also remain about the sampling recovery efficiency and in which flux hood operational conditions the odorous gas of interest accumulates in the headspace. Yet, there is a question if it is possible to have its conditions staggered to a field situation without the emission rate of the odours compound being underestimated.

The above-mentioned doubts and lacks of understanding about the flux hood operational conditions lead to the methods applied in the present thesis. Laboratory experimental and computational numerical simulations intended to investigate the USEPA flux hood operational conditions under several geometrical configurations. Laboratory experimental simulation is related to series of gas chromatography to test volatilisation rate of acetic and butyric acid solution. Emission rate and mass transfer coefficients are evaluated from flux hood experiments under different internal fan configurations. Additional investigation concerns computational fluid dynamics to explain the findings by investigating velocity and concentration distributions inside the flux hood. Worldwide, researches that estimate the volatilisation of odorous compounds from liquid surfaces have gained more attention, due precisely to the greater representativeness of the sampled data in relation to the estimation methods. The present thesis is divided into five sections: Section 2 presents the general and specific objectives, Section 3 presents the Literature Review about the theoretical aspects on volatilisation of passive liquid surfaces and odorous compounds emission rate, Section 4 details the experimental and numerical protocols, Section 5 presents the main results and discussions and Section 6 the conclusions and perspectives.

2 OBJECTIVES

The main objective of the present work is to investigate the performance of the USEPA flux hood to measure volatilisation rate of odorous compounds from passive liquid surfaces.

The present thesis has the following specific objectives:

- Assess mass transfer parameters for gas phase-controlled compound inside USEPA flux hood under various sweep air flow rates;
- Analyse the influence of different fan configurations on the measurement of emission rate of gas phase-controlled compound using a flux hood;
- Investigate flow features and mass transfer dynamics leading to the possible mechanisms underpinning the effects of different fan configurations on the measurement of emission rate of gas phase-controlled compound with the flux hood;
- Evaluate the estimation of gas-film mass transfer coefficient (k_G) for a gas phase-controlled compound based on a reference compound;
- Evaluate uncertainty implication of the presence of a fan for the scaling up of measured emission rates of gas phase-controlled compounds with the flux hood.

3 LITERATURE REVIEW

The literature review presented in this section addresses the understanding of theoretical concepts of mass transfer and operational concepts related a dynamic flux chamber (flux hood) device, that directly measure the emission rate of odorous compounds from passive liquid surfaces.

3.1 Theoretical aspects on volatilisation passive liquid surfaces

The transport of molecules from higher concentration to a lower concentration in a stagnant medium occurs by a mechanism called ‘molecular diffusion’ while in a turbulent medium the phenomenon is called ‘eddy diffusion’ or ‘turbulent diffusion’. This latter process occurs through random motion of the fluid elements and is much faster than molecular diffusion. The difference in concentrations is called the ‘concentration driving force’ in mass transfer.

If the concentration in the liquid phase is greater than the concentration of the gas phase, mass transfer occurs in the liquid-gas direction and this phenomenon is called volatilisation. However, if the concentration in the gas phase is greater than the concentration of the liquid phase, mass transfer occurs in the gas-liquid direction and the phenomenon is called solubilization. Therefore, volatilisation can be understood as the mass transport process of a particular compound which is dissolved in a liquid medium, and which is transferred to an adjacent gaseous medium i.e., a physical-chemical process resulting from the lack of equilibrium between a compound in the gaseous phase and in solution.

Volatilisation is commonly observed in wastewater treatment plants (WWTP), in units that have passive surfaces, such as sedimentation tanks, equalization tanks and stabilization ponds, characterized by the absence of an active gas flow (such as active aeration or intense bubbling) across the surface.

3.1.1 FICK'S LAW

The Fick's Law of the molecular diffusion (Equation (1)) describes the mass transfer due to molecular diffusion in both liquid and gas phases. At the gas-liquid interface, the fluxes given by the Fick's Law must be identical to to obey the the mass conservation principle.

$$J_A = -D_{AB} \frac{\partial \rho m_A}{\partial z} \quad (1)$$

where A indicates the substance that is diffused in substance B; J_A is the mass flow of substance A ($\text{kg s}^{-1} \text{m}^{-2}$); D_{AB} is the mass transfer diffusion coefficient from A to B ($\text{m}^2 \text{s}^{-1}$), the magnitude of the diffusion coefficient depends on the properties of both the constituent A being transported and the medium B; ρ represents the specific mass (kg m^{-3}); m_A is the mass fraction ($\text{kg}_A \text{kg}_{\text{Mixture}}^{-1}$). The negative sign indicates that the flow is in the opposite direction to the concentration gradient. The rate at which a solute moves at any point in any direction must therefore depend on the concentration gradient at that point and in that direction. Equation (1) can be written in terms of concentration and expressed by the ratio between the mass of substance A and the volume of the mixture ($\text{kg}_A \text{kg}_{\text{Mixture}}^{-1}$):

$$J_A = -D_{AB} \frac{\partial C_A}{\partial z} \quad (2)$$

3.1.2 THE TWO-FILM THEORY

According to the theory of the two films (LEWIS; WHITMAN, 1924; WHITMAN, 1962), adjacent to the gas-liquid interface, two thin layers (stagnated films) are formed, one in the liquid phase and the other in the gas phase (see Figure 1). A concentration gradient is assumed in each film and that within each phase there is enough agitation to eliminate the gradient, i.e., at points beyond the film, the turbulence is sufficient to eliminate the concentration gradient, so that the resistance associated with the films is the limiting factor of the mass transfer process between the phases.

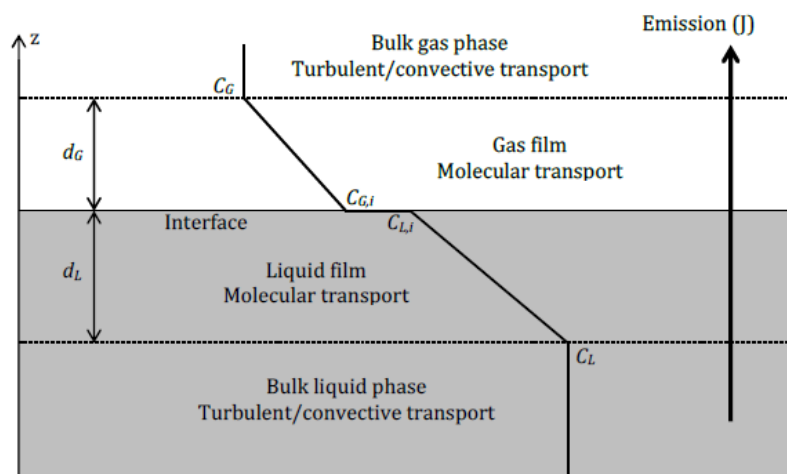


Figure 1 – Schematic representation of mass transfer process across liquid and gas film (SANTOS et al., 2012).

In this way, Equation (2) can be applied to the liquid film where molecular diffusion is said to be dominant. Since it is assumed that the films are so thin (d_L) that the concentration distribution inside them can be approximated by linear profiles, which are considered constant along the whole surface, as represented in Figure 1. Therefore, applying Equation (2) along films with linear profiles (which means that the gradient is constant), mass fluxes across the liquid film are given by Equation (3):

$$J_L = -D \frac{\Delta C_L}{\Delta Z} = -D_L \frac{(C_{L,i} - C_L)}{d_L} \quad (3)$$

where J_L is the mass flow of compound through the liquid film ($\text{kg s}^{-1} \text{ m}^{-2}$); D_L is the molecular diffusivity of the compound in the liquid phase ($\text{m}^2 \text{ s}^{-1}$); $C_{L,i}$ is the compound concentration adjacent to the gas-liquid interface (kg m^{-3}); C_L is the compound concentration in the bulk liquid phase (kg m^{-3}) and d_L is the thickness of the liquid film (m).

Analogously, for the gas phase we have:

$$J_G = -D \frac{\Delta C_G}{\Delta Z} = -D_G \frac{(C_{G,i} - C_G)}{d_G} \quad (4)$$

where J_G is the mass flow of compound through the gaseous film ($\text{kg s}^{-1} \text{ m}^{-2}$); D_G is the molecular diffusivity of the compound in the gas phase ($\text{m}^2 \text{ s}^{-1}$); $C_{G,i}$ is the compound concentration adjacent to the gas-liquid interface (kg m^{-3}); C_G is the compound concentration in the bulk gas phase (kg m^{-3}) and d_G is the thickness of the gas film (m).

Equations (3) and (4) are equivalents to model the mass transfer coefficients as $k_L = D_L/d_L$ (m s^{-1}) being the mass transfer coefficient of the liquid phase and $k_G = D_G/d_G$ (m s^{-1}) being the mass transfer coefficient of the gas phase.

The existence of stagnant films with constant physical thickness is not representative of most of the situations of interest, since the layers adjacent to the air-liquid interface of passive liquid surfaces in WWTPs are likely to be sheared turbulent boundary layers, in many cases also subjected to wave-induced stresses (air side) and macro and microscale wave breaking (DEMARS; MANSON, 2012; PEIRSON; WALKER; BANNER, 2014; PRATA; SANTOS; et al., 2018). However, given its relative simplicity, some concepts used in the two-film theory, such as the

notions of “film thickness” and “film resistances”, are incorporated in the representation of other modelling approaches for gas-liquid mass transfer, being also frequently used to report results (CHAO et al., 2005; JÄHNE; HAUSSECKER, 1998; LIMPT et al., 2005; MACKAY; YEUN, 1983; PRATA; LUCERNONI; et al., 2018).

3.1.3 TWO-RESISTANCE MODELS

Lewis and Whitman (1924) visualized that two stagnant fluid films exist on either side of the interface and mass transfer occurs through these films, in sequence, by purely molecular diffusion. Beyond these films the concentration in a phase is equal to the bulk concentration. Then, they defined the “two-film theory” despite of stagnant film does not exist. Nevertheless, the two-film theory or two-film theory has proved to be extremely useful in mass transfer modelling, analysis, and calculations.

Treybal (1981) preferred to call it the two-resistance theory because the existence of the mass transfer resistances is a physical reality but that the films is not, being just conceptual. Then, two-resistance volatilisation models are based on the assumption that the overall resistance to volatilisation or, more generally, to liquid-gas mass transfer, is composed of the resistances associated with two relatively restrict regions/layers, at the gas and liquid phases close to the interface. Such regions are normally identified as “liquid film” and “gas film”, but the films do not have to be stagnant nor is the mass transfer solely due to molecular diffusion, as originally assumed in the two-film theory. In this new context, the “films” are the conceptual layers, adjacent to the interface, which present the most important constraints to the mass transfer process. Given the concept of the film-specific mass transfer coefficients, k_L and k_G , the rate of mass transfer of a given compound across each film can be rewritten as Equations (5) and (6) (PRATA; SANTOS; et al., 2018).

$$J_L = k_L(C_L - C_{L,i}), \text{ where } k_L = \frac{D_L}{d_L} \quad (5)$$

$$J_G = k_G(C_G - C_{G,0}), \text{ where } k_G = \frac{D_G}{d_G} \quad (6)$$

3.1.4 HENRY'S LAW

Under ideal equilibrium conditions, the distribution of a compound between the liquid and gaseous phases follows a defined ratio (temperature dependent, among other factors), mathematically described by Henry's Law:

$$K_H = \frac{C_{G,i}}{C_{L,i}} \quad (7)$$

where K_H is the constant of Henry's Law in dimensionless form; $C_{G,i}$ is the concentration of the compound at the gas interface (kg m^{-3}); $C_{L,i}$ is the concentration of the compound at the liquid interface (kg m^{-3}).

This situation represents an equilibrium condition, considering the spontaneous random motion of molecules from liquid to gas direction compensates the motion from gas to liquid in the opposite direction, so that the final balance makes null. In cases where this equilibrium is not configured, an effective mass transfer between the phases is verified. This transfer occurs in the liquid-gas (volatilisation) direction, when the concentration in the liquid phase is greater than the equilibrium concentration, and in the gas-liquid (solubilisation) direction, when the concentration in the gas phase is above the equilibrium concentration. In these cases, Henry's law does not describe the relation between concentrations in the bulk of gas and liquid phases. However, it is assumed that equilibrium is reached almost-instantaneously at the gas-liquid interface, so that Henry's law (see Equation (7)) is still a valid means of relating interface concentrations (CHAO et al., 2005; JÄHNE; HAUSSECKER, 1998; PEIRSON; WALKER; BANNER, 2014).

3.1.5 THE GLOBAL MASS TRANSFER COEFFICIENT

In the absence of chemical reactions, the mass flux across the liquid film (J_L) is the same mass flux across the gas film (J_G), corresponding to the overall mass flux between phases (J), makes Equation (5) equals to Equation (6), written as Equation (8).

$$J = k_G(C_{G,i} - C_G) = k_L(C_{L,i} - C_L) \quad (8)$$

From Henry's law, $C_{G,i} = C_{L,i}K_H$ (where K_H is the non-dimensional Henry's law coefficient described in Equation (7)); substituting this in Equation (8) and rearranging, Equation (9) is obtained.

$$C_{L,i} = \frac{k_L C_L + k_G C_G}{k_G K_H + k_L} \quad (9)$$

Substituting Equation (9) back in Equation (8) and rearranging, one arrives at Equation (10):

$$J = \frac{k_L k_G}{k_G + \frac{k_L}{K_H}} \left(C_L - \frac{C_G}{K_H} \right) \quad (10)$$

Equation (10) is the classical equation for liquid-gas mass transfer in terms of the liquid-phase overall mass transfer coefficient (m s^{-1}), K_L , which can be written as:

$$J = K_L \left(C_L - \frac{C_G}{K_H} \right) \text{ where } K_L = \frac{k_L k_G}{k_G + k_L / K_H} \text{ or } \frac{1}{K_L} = \frac{1}{k_L} + \frac{1}{k_G K_H} \quad (11)$$

The Equation (11) describes both volatilisation (positive J) and solubilisation (negative J), depending on whether the difference between C_L and C_G/K_H is positive or negative. The conditions for validity of Equation (11) are generally met at the passive liquid surfaces present in WWTPs, unless the air-liquid interface is significantly covered by surface films, scums or other physical barriers (HUDSON; AYOKO, 2008b; PRATA; SANTOS; et al., 2018). The terms $1 = k_L$ and $1 = k_G K_H$ can be understood as the resistances relative to the liquid and gas films, respectively. In this perspective, $1 = k_L$ represents the overall resistance to mass transfer between the phases. Thus, the overall mass transfer coefficient becomes an important parameter that incorporates the effects of Henry's Law along with the individual mass transfers through the liquid and gas films.

It is worth noting that the values of C_L , C_G , K_H and K_L are required to solve Equation (11). In this case, it can be assumed that C_L equals $C_{L,\infty}$ for a homogeneous mixture. However, C_G can hardly be assumed equal to $C_{G,\infty}$ and a measurement in the gas phase very close to the interface must be made.

For few soluble compounds, with K_H much greater than 10^{-3} , the term $1 = k_G K_H$ becomes negligible, i.e., $K_L \approx k_L$, that is, the overall mass transfer coefficient is limited by the transport conditions in the liquid film (Liquid phase-controlled mass transfer). For very soluble compounds, with K_H significantly less than 10^{-3} , one can neglect the term $1/k_L$ in front of the term $1/k_G K_H$, that is, $K_L \approx k_G K_H$. In this case the overall mass transfer coefficient is limited by the transport conditions in the gas film (Gas phase-controlled mass transfer). For cases where the value of K_H is around 10^{-3} , none of the terms can be neglected, so that both the liquid film and the gas film conditions are significant for the final value of the overall transfer coefficient of mass (Both phase-controlled mass transfer).

Figure 2 shows schematically the values of K_H for a series of compounds of environmental importance, relating them to dominance by the conditions of the liquid phase, the gas phase or both on the mass transfer between phases, according to the case. Then, for cases where K_H values are higher, we have Liquid phase-dominated ($K_L \approx k_L$), on the other hand, for cases where K_H values are lower, we have Gas phase-dominated ($K_L \approx k_G K_H$), as example butyric and acetic acid. Sander (1999) presents a broad compilation of Henry's law coefficients for various compounds of environmental.

3.1.6 SCHMIDT NUMBER

A parameter of fundamental importance for the analysis of mass transfer at the liquid-gas interface, together with Henry's law constant, is the Schmidt number $S_c = \nu/D$ (in which ν is the kinematic molecular viscosity of the medium, units $\text{m}^2 \text{s}^{-1}$), expressing the relationship between the phenomena of momentum transfer and mass transfer by molecular diffusion, indicating the relationship between viscous forces and the phenomenon of diffusion.

Jähne and Haussecker (1998) draw attention to the fact that the exact limits of these solubility ranges determining the level of dominance by water, air or both phases are dependent on the Schmidt number and the surface roughness (see Figure 3).

It is important to note that exact limits for gas phase, liquid phase or both phase control vary with the chemical properties of each compound (diffusivity/Schmidt number) and temperature (which affects both the diffusivity and the Henry's coefficient)(HUDSON; AYOKO, 2008a; JÄHNE; HAUSSECKER, 1998).

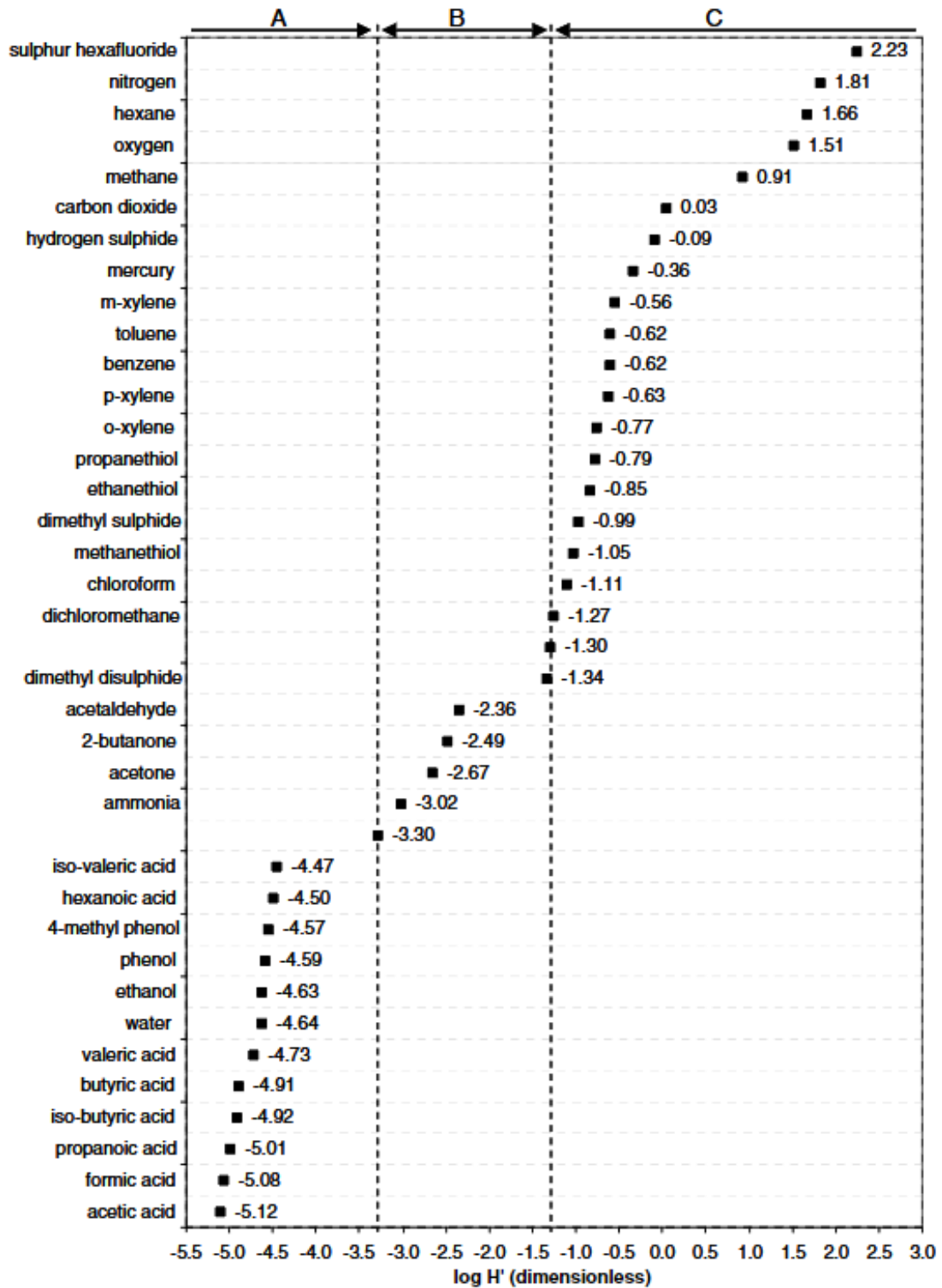


Figure 2 – Values of Henry constant for representative odorants and other environmentally relevant chemicals, where A, B and C indicate species where emission rate is dependent primarily on air phase turbulence, both air and liquid phase turbulence and liquid phase turbulence, respectively (HUDSON; AYOKO, 2008)

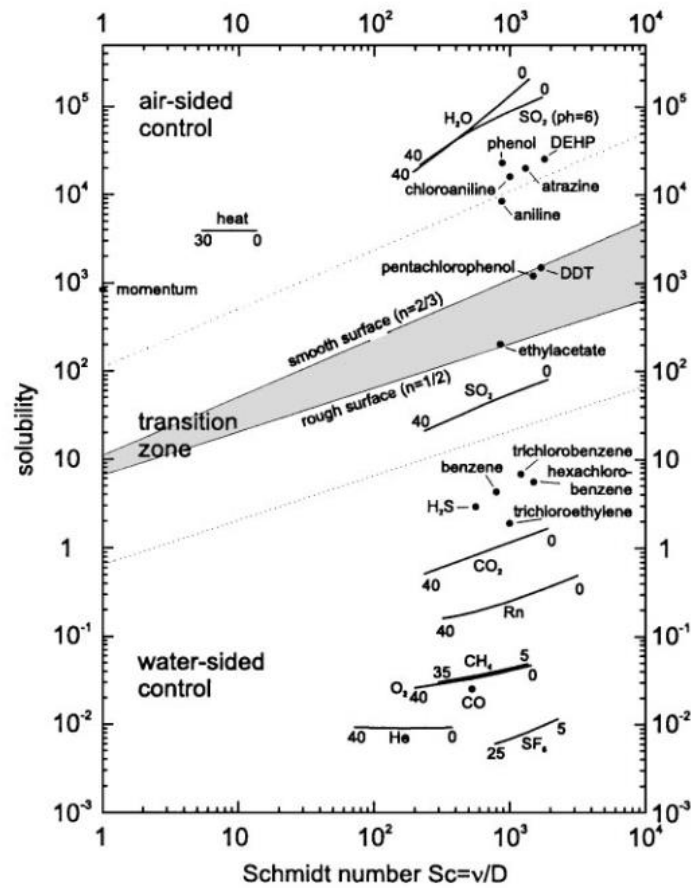


Figure 3 – Schmidt number/solubility diagram, including various volatile tracers, momentum, and heat for a temperature range ($^{\circ}\text{C}$), as indicated. Filled circles refer only to a temperature of 20°C . The regions for air-sided, mixed, and water-sided control of transfer process between the gas and liquid phase are marked. At the solid lines the transfer resistance is equal in both phases. The following dimensional transfer resistances were used: $\gamma_a = 31$; $\gamma_w = 12 S_c^{2/3}$ (smooth); $\gamma_w = 6.5 S_c^{1/2}$ (wavy surface) with $\gamma_a = R_a u_{*a}$ and $\gamma_w = R_w u_{*w}$. (JÄHNE; HAUSSECKER, 1998)

3.2 Odorous compounds emission rate: USEPA Flux hood

Estimating the emission rate of odorous compounds is the first crucial step for understanding the environmental impacts and health effects on the exposed population. The emission rate of odorous compounds from passive liquid surfaces (low level of disturbance at the air-liquid interface) will depend on the distribution of the chemical species between gas and liquid phases (Henry's Law), the concentration of the chemical species in each phase, and the mass transfer characteristics (coefficients) of the species (PARKER, D. B.; CARAWAY; et al., 2013). Wind speed has a major effect in altering the average overall mass transfer coefficient. High winds cause low resistance to mass transfer in the liquid phase with resulting high emissions (EKLUND, 1992).

Wastewater Treatment Plants (WWTPs) are characterized by large areas representing fugitive sources of odorous gases, particularly, in units that have passive liquid surfaces. Determining the odour emission rate requires knowledge of the flow rate and corresponding odour concentration. So, measuring emission from canalised sources (factory chimneys) is relatively easy because of the rejected air flow rate. Conversely, for area sources (WWTP), there is no air flow to be measured (LEYRIS et al., 2005). Furthermore, emissions from area sources are usually governed by diffusion processes, whereby a concentration gradient provides the driving force for the transfer of odorants from the soil or liquid to the air. In some cases, there may also be a significant convective element, whereby a pressure gradient provides an additional driving force. Then, special methods must be employed for emission rate measurement. There are two classes of measurement which are commonly employed (International Water Association - IWA report):

- i. Indirect measurement of emission rates using micro-meteorological methods, whereby emission rate is inferred from downwind measurements of odour concentration and wind velocity, and;
- ii. Direct measurement of emission rates from an area source using an enclosure of some sort “Hood” methods, whereby an apparatus is placed on the emission surface and air blown through it. The emission rate is then given by the air flow through the hood and the odour concentration of the exit air.

Indirect techniques such as micrometeorology do not perturb the emission process because a sampling device is not used. However, they suffer from many limitations due to the large number of samples and the extensive analysis required (LOTESORIERE et al., 2022).

At the same time, direct methods have been broadly adopted for the assessment of emissions from area sources due to being less costly and easier to handle (CAPELLI et al., 2013; HUDSON et al., 2009; PRATA; SANTOS; et al., 2018).

Due to the relative simplicity, low cost and possibility of sensory characterization of samples, direct methods have been widely used to estimate the emission rate of odorants on passive surfaces and determine its variability due to changes in WWTPs operation and atmospheric conditions. The direct assessment of odour emissions from passive liquid surfaces can be performed by using enclosed sample collection systems: (i) portable wind tunnels (JIANG; BLISS; SCHULZ, 1995; LUCERNONI et al., 2017; WANG, X.; JIANG; KAYE, 2001) and (ii) dynamic flux chamber (EKLUND, 1992; KIENBUSCH, 1986), in which the emission rate is a function of aerodynamic conditions (flushing rate) within the chamber (HUDSON et al., 2009).

These open bottom devices are placed over the emitting surface; a sweep gas flow transports the volatilised compounds through the equipment to a sampling bag or a sorbent tube for posterior analysis, or to a gas-specific sensor for in-line analysis. There is a wide variety of configurations and operational conditions for these sampling devices as explained by Hudson and Ayoko (2008b).

Direct measurement methods enclose minimal parts of the emitting surface. The calculation of odour emission rates following collection of a sample with either a wind tunnel or flux hood device involves the following equation:

$$E = \frac{C \times Q}{A} \quad (12)$$

where E [$kg \cdot s^{-1} \cdot m^{-2}$], C [$kg \cdot m^{-3}$], Q [$m^3 \cdot s^{-1}$] and A [m^2] are emission rate, gas-phase concentration of compound of interest in air, sweep flow rate of air or gas through the sampling device and surface area of source covered by the sampling device respectively.

Kienbusch (1986) presented standards and recommendations for the construction and operation of an emission insulation flux chamber (dynamic flux hood) for assessment of gaseous emissions from contaminated soils and groundwater. Later, United States Environmental Protection Agency (USEPA) became interested in this technique for estimating emission rates from hazardous wastes and funded a series of projects to develop and evaluate the flux hood method (EKLUND, 1992).

Currently the flux hood is standardized by USEPA, despite a range of different flux chamber shapes (rectangular and cylindrical) and sizes (base area and height) have been studied (GOSTELOW; PARSONS; STUETZ, 2001; HUDSON; AYOKO, 2008a; PARKER, D. B.; CARAWAY; et al., 2013).

Figure 4 shows the original schematic representation of the USEPA flux chamber and supporting equipment.

For a flux hood, odourless air is introduced into a mixed headspace above the odour-emitting surface. Air samples from the headspace are assumed to be homogeneously mixed and therefore, representative of a uniformly distributed concentration across the entire headspace. The mixing in small flux hoods is provided by the air flow patterns produced by the sweeping air system. However, in larger flux hood, the use of a small fan or an impeller is often necessary to promote the mixing inside the chamber.

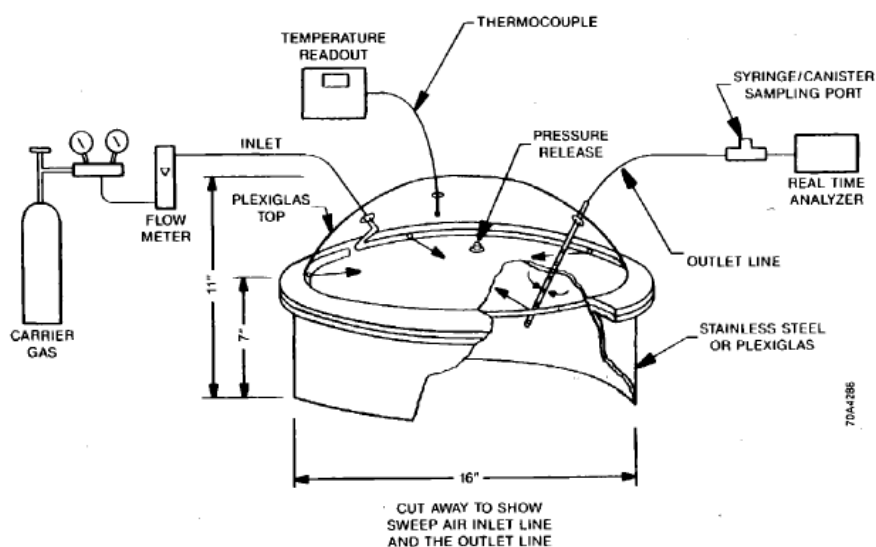


Figure 4 – Schematic representation of USEPA dynamic flux chamber (Kienbusch, 1986).

Despite of being designed to achieve complete mixing and consequent homogeneous distribution of concentration inside the device, Hudson et al. (2009) pointed out that the compound can accumulate (concentration build-up) inside the flux hood, affecting sampling representativeness if concentration reach values close to saturation. Parker et al. (2013) also pointed out that flux hoods operating at typical sweep air flow rates underestimates the emission rate due to restrictions in low air exchange rates. Regarding the USEPA flux hood, Prata et al. (2016) and Andreao et al. (2019) indicated that the friction velocity on the liquid surface inside the hood does not match typical values of atmospheric flow if typical sweep air flow rates are used. In addition, they observed that the USEPA flux hood present an issue concerning flow pattern inside in the device, the sampling probe can be exposed to clean sweep air flow causing a decrease in the concentration of the sampled gas (which would mean a negative bias in the measured emission rate).

If an internal fan is applied (at the top of the chamber), mixing is accomplished by the rotating action of the impeller, which is responsible for the flow patterns and level of shear created in the vessel. The impellers are commonly classified as axial or radial based on flow patterns, down and up or side to side, respectively.

According Prata et al. (2016) there are still unsolved issues relating to the accuracy and applicability of the USEPA dynamic flux hood. A primary concern regarding to the use of a flux hood is an artificial increase in compounds concentration (concentration build up) in the

headspace, which may occur in case of insufficient flow rate (HUDSON et al., 2009). Even when the flow rate is theoretically high, local accumulation may arise if there is not enough mixing in the air phase (EKLUND, 1992; GHOLSON et al., 1991). An increase in the headspace concentration close to the liquid surface can result in a reduction of the emission rate during the experiment and an inappropriate measurement of the local emission rate (HUDSON et al., 2009; PARKER, David et al., 2013). Experimental tracer studies have indicated that the USEPA dynamic flux hood is likely to have a generally well-mixed air phase when operated within the recommended flow rate range (EKLUND, 1992; GHOLSON et al., 1991), despite evidence of some small zones of local accumulation/stagnation (GHOLSON et al., 1991; WOODBURY B. L., PARKER D. B., EIGENBERG R. A., SPIEHS, 2011). Inaccuracies can also occur if the outlet air that is sampled is not representative of the total exiting air (GHOLSON et al., 1991). Another important point is that air flow inside the flux hood may not be able to reproduce relevant features of the atmospheric flow to which the water surface is exposed in the absence of the enclosure device. This can affect directly the mass transfer condition and strongly influence the emission rate of compounds, especially the less volatile ones.

Recently, Prata et al. (2018) assessed the mass transfer of compounds inside the USEPA flux hood. Experiments comprised the evaporation of water and the volatilisation of a range of volatile organic compounds (VOCs), i.e. acetic acid (with volatilisation dominated by conditions in the gas phase), chloroform and hydrogen sulfide (with liquid phase-dominated volatilisation) and 1-butanol (whose volatilisation was significantly dependent on both phases). They evaluated the mass transfer coefficients in the microenvironment created by the flux chamber and the effects of concentration build up in the hood's headspace. The VOCs emission rates generally increased with the sweep air flow rate, as did the mass transfer coefficients for all compounds. The emission of compounds whose volatilisation is significantly influenced by the gas phase was greatly affected by concentration build up, whereas this effect was not significant for liquid phase-controlled compounds.

Andreao et al. (2019) performed Computational Fluid Dynamics (CFD) simulations to compare the results with the laboratory experiments conducted by Prata et al. (2018), regarding air flow, acetic and hydrogen sulfide mass transfer. They evaluated the influence of inlet configurations (4, 6 and 8 inlet holes) and the internal fan flow direction on air mixing in a flux chamber. The results showed a complex flow inside the original flux chamber (4 inlet holes and no fan) and a concentration field that reaches steady state after 30 minutes. The fluid flow pattern indicates that inlet air may reach the outlet probe, forcing clean air to be collected by the probe, and, therefore,

affecting the concentration measured at the outlet. The use of an internal fan proved to produce a more complex flow inside the flux chamber with large circulations and increased turbulence and friction velocity at the liquid interface and a more uniform concentration field, and therefore, the use of a fan was recommended by authors.

Several experimental works reported the use of a fan inside of the flux chamber with a similar design of the USEPA flux chamber (PARKER, David et al., 2013; PRATA et al., 2016; WOODBURY B. L., PARKER D. B., EIGENBERG R. A., SPIEHS, 2011) and others with different dimensions (ANEJA, V. P.; CHAUHAN; WALKER, 2000; BLUNDEN; ANEJA; OVERTON, 2008; PARK; SHIN, 2001; PARKER, David et al., 2013). In any case, ideally the flux chamber must not alter the natural emission rate (GHOLSON et al., 1991). However, if it is of interest to reproduce the environmental conditions of turbulence within the chamber, the fans have been demonstrated to be appropriate devices to promote mixing of the gas phase and generate friction velocity that would be found in the field.

To create turbulent conditions similar to those in the field and/or to improve mixing in the headspace, many authors have included a fan inside the flux hood. For instance, the Australian and New Zealand standard AS/NZS 4323.4:2009 consists of a USEPA flux hood with the addition of an internal fan. Aneja et al. (2001) installed a motor driven Teflon impeller rotating at about 100 revolutions per minute inside a cylindrical flux hood, at a height of 10 cm from the measuring surface, for the purpose of generating a “continuously stirred tank reactor”. These authors stated that the impeller resulted in air velocities inside the hood between 1 and 2.5 m s⁻¹. Woodbury et al. (2011) showed that the USEPA flux hood operating at 5 L min⁻¹ behaved as a well-mixed reactor even without the installation of a fan. Parker et al. (2013) assessed the water evaporative flux inside a flux hood using a small fan (40 mm dia. and 12V), located 10 cm from the top of the dome and directing air flow upward into the dome top. They noted that water evaporative flux significantly increased with the addition of the fan. At the sweep airflow rate of 5 L min⁻¹, the water evaporative flux more than doubled due to the more disturbance in the boundary layer at the air-liquid interface. They also concluded that not only the airflow rate is an important factor, but how and where the airflow is distributed within the hood is equally important. Lyman et al. (2018) employed in their study an acrylic hemispherical dome with a diameter of 41 cm. A polystyrene foam sheet with dimensions of 3 cm × 122 cm × 122 cm with a hole cut from the center for the chamber provided for floatation, and strings attached to the chamber anchored it in place. The chamber had a fan at the top with a polyethylene blade that turned at about 100 rotations per minute to achieve uniform compounds concentration within the chamber (as in Pape et al. (2009)). They

also assessed the impact of a fan (fast enough to agitate the liquid surface) on measured fluxes of methane, non-methane hydrocarbons (C₂-C₁₁), light alcohols and carbon dioxide. They concluded that the water-air fluxes were significantly higher for ethane and propane (1.8, and 1.5 times higher, respectively) with the fan rotating at high speed, but were not significantly different for any of the other measured compounds. Tran et al. (2018) used the same flux hood modified by a fan as Lyman et al. (2018) and applied the inverse dispersion modelling technique to compare with flux hood emissions measurements of 58 organic compounds at the water ponds in the Uintah Basin. Their results suggested that the flux hood may underestimate organic compound emissions, especially alcohols, if compared with the results obtained from the inverse dispersion models technique. Andreao et al. (2019) investigated airflow and odorous compound transport inside a USEPA flux hood to determine the influence of inlet airflow rate (2, 5 and 10 L min⁻¹), inlet configurations (4, 6 and 8 inlet holes) and the inclusion of internal fan on the surface friction velocity and emission rate. Their numerical simulations showed that inlet airflow rate is less influential in promoting mixing than an internal fan, were high flow velocity and mixing within the chamber enhance the volatilisation of odorous gases and create two large circulation zones. Then, they recommended the use of a micro fan installed inside the flux hood to improve the mixing inside the chamber and produce values of friction velocity closer to those found in the atmospheric flow.

Despite its practical advantages for field use, the appropriate flux hood operational conditions is still a matter of discussion. There is still a lack of experimental data and detailed information regarding the mass transfer phenomena occurring inside the flux hood modified by a fan. Doubts remain concerning if the flux chamber should be expected to mimic atmospheric conditions in which the real emission occurs regarding, for instance, the friction velocity for volatilisation gas-phase controlled odorous gases. Doubts also remain about the sampling recovery efficiency and in which flux hood operational conditions the odorous gas of interest accumulates in the headspace (concentration build-up). Yet is that possible to have its conditions staggered to a field situation without the emission rate of the odors compound being underestimated.

The CFD simulations by Andreão et al. 2019 indicated that the use of an internal fan produced larger values of friction velocity at the liquid interface, compared to all the other configurations simulated without a fan. However, the effects of the fan inside the flux hood were only dedicated to its influence on friction velocity, *i.e.*, the mass transfer phenomena were not evaluated in the presence of an internal fan. Some experimental works were performed in field conditions exploring the use of an internal fan inside a dynamic flux chamber.

Aneja et al. (2000) and Aneja et al. (2001) installed the ventilator 10 cm above the surface with downward flow. The mixing was perfect but there was no comparison with any case without a fan and no modification of the fan configuration. Sweep air flow rates varied between 2.36 and 4.73 L min⁻¹. The fan was 20 cm in diameter and 50 RPM – more than twice the fan used in the present study with a much lower rotation. In the work carried out by Aneja et al. (2000) and Aneja et al. (2001), the emitted flux of the ammonia compound was in the order of magnitude of 10² μg s⁻¹ m⁻². The use of the fan was justified due to the need to increase the mixing inside the flux hood.

Pape et al. (2009) also used a fan, in this case with 360 revolutions per minute. There were 2 fans approximately 30 cm from the solid-gas interface. The chamber used was cylindrical. There was no comparative analysis of scenarios with and without a ventilator in the study. The compounds evaluated were evaporation of water, CO₂ and NO. Again, the fan was inserted aiming at better mixing of the emitted compounds.

Parker et al. (2013) evaluated a series of VOC and ammonia from solid-gas interface. The fan used by the authors on the flux hood was 40 mm in diameter at 10 cm from the top (which results in approximately 15 cm from the interface) – the flux hood was the same as in the present study. Parker's work also found a linear relationship between the emitted flux and the sweep air flow rate for some compounds studied (acetic, propionic, butyric and valeric acid). Sweep air flow rates ranged from 1 to 20 L min⁻¹. Parker's work showed that in the case without a fan the relationship was linear and in the case with a fan it did not follow the same relationship for the study of the evaporative flow. The fan practically doubled the emitted flow result found for the studied scenario. For the VOC study, values in the range of 3 to 13 μg s⁻¹ m⁻² were found.

Lyman et al. (2018) used a hemisphere-shaped flow chamber with a height of 20.5 cm. The fan was at the top of the flow chamber at a rotation of 100 RPM. The effect of varying fan speed was evaluated. The compounds evaluated were methane, carbon dioxide, alkanes, alkenes, aromatics, and alcohols. For some compounds evaluated by Lyman the fan effect was not relevant (methane, carbon dioxide, alkenes, aromatics, and alcohols) and for others it was (alkanes). Sweep air flow was 10 L min⁻¹. The flow results measured by Lyman for the compounds that were not influenced by the ventilator varied between 1 and 100 μg s⁻¹ m⁻² considering the different sources evaluated.

Vergote et al. (2020) inserted 4 small fans inside a cylindrical flux hood. The fans were placed on top at a distance of 30 cm from the solid-gas interface. The installation objective according to the authors was to improve the mixture. The compounds evaluated were N₂O and methane. The results found were approximately 200 μg s⁻¹ m⁻² for methane and 2 μg s⁻¹ m⁻² for N₂O.

4 METHODOLOGY

This chapter presents the methodology that will be used to achieve the specific objectives described in chapter 2. The first section (4.1) intends to present protocol and settings used in the laboratory experiments with the flux hood device. In addition, methodology for calculating the emission rate and mass transfer coefficients is showed. Following section (4.2) presents the numerical modelling methodology employed to assist in understanding mass transfer within a flux hood.

4.1 Experimental set-up

The physical-chemical experiments with the dynamic flux hood were carried out between October 2018 and April 2019 at the Odor Laboratory belonging to the School of Civil and Environmental Engineering, located at the University of New South Wales (UNSW), in Sydney, Australia. This work was partially funded by the “Coordenação de Aperfeiçoamento de Pessoal de Nível Superior – CAPES” (Edital PDSE/2018) with the concession of a scholarship.

4.1.1 FLUX HOOD CONFIGURATION

The flux hood used in this work was designed following the recommendations of Kienbusch (1986), Figure 5 and Figure 6. It was made of plexiglass® and composed of two parts, a cylindrical body 40.5 cm in diameter and 16.5 cm in height screwed to a dome-shaped top with a central height of 11.5 cm; this results in 28.5 L of internal volume and 0.12 m² of footprint area. As recommended by Kienbusch (1986) and (PRATA, Ademir A.; LUCERNONI; et al., 2018), there are four holes at the dome-shaped top, positioned equidistantly.

The sampling probe was connected to a Teflon® outlet line through a bulkhead, ¼” OD, which in turn was connected to the Nalophan® bags via “lung system”, which collected the gas from the probe.

Figure 7 shows a schematic representation of how the “lung system” works: the Nalophan® bag was attached to the drum cover and connected to the outlet tube of the Flux hood (Teflon® outlet line) via connector bulkhead. During the experiments, the Nalophan® bag was kept inside the drum and filled with samples of the gas emitted from flux hood. A second bulkhead installed on the drum cover was connected to a pump (Airchek Sampler) for air suction and vacuum formation inside the drum. Thus, gas sampling was performed by differential pressure between the drum and the Nalophan® bag connected to the flux hood.

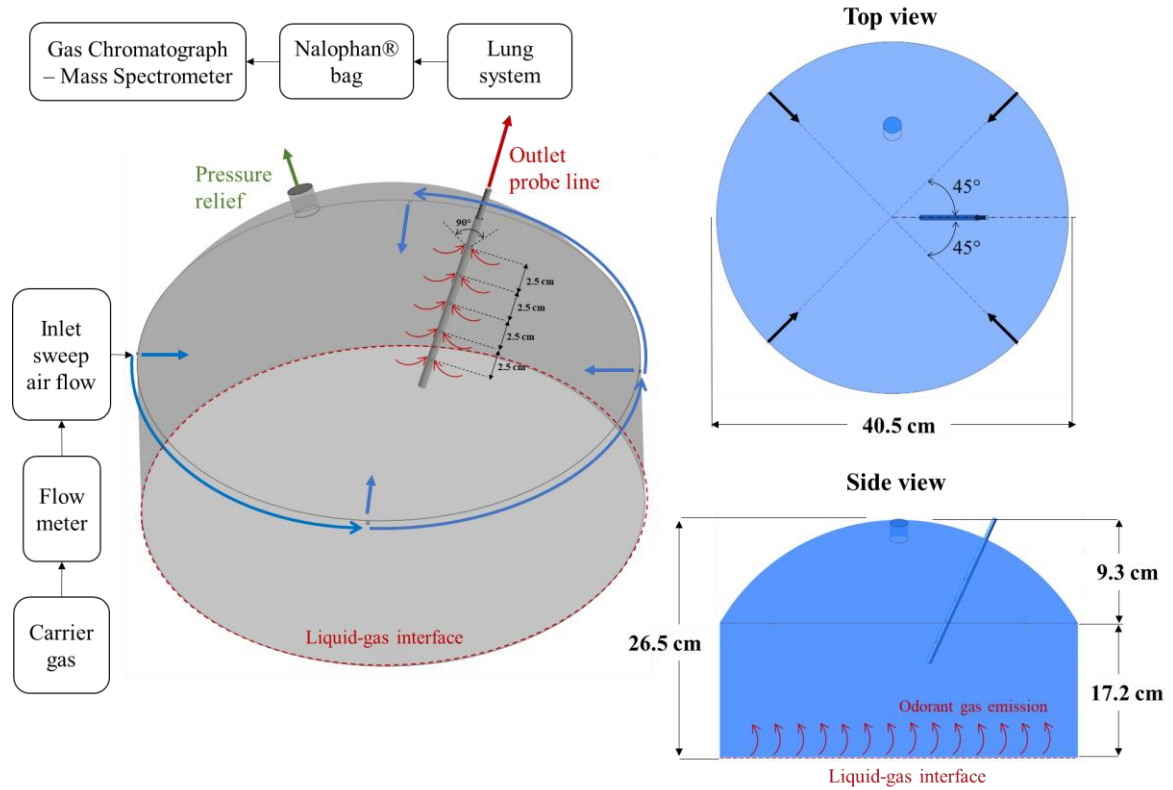


Figure 5 – Schematic representation of USEPA dynamic flux chamber.

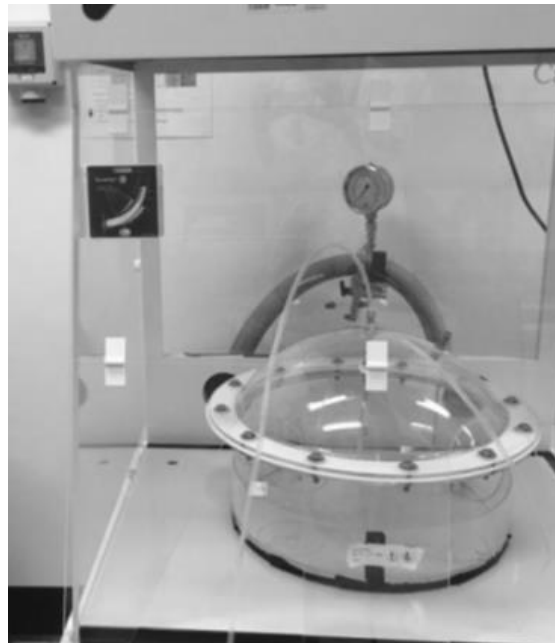


Figure 6 – Picture of USEPA Dynamic flux hood device used in the present study.

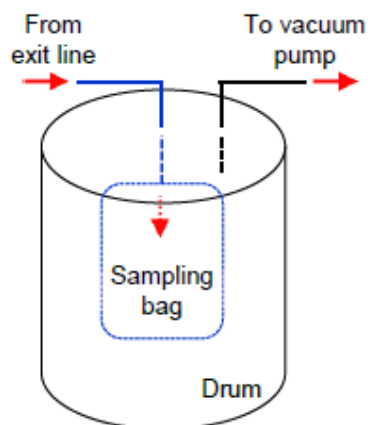


Figure 7 – Schematic representation of Lung System (PRATA, Ademir Abdala, 2017).



Figure 8 – Fans used at Flux hood. a) 4 x 4 cm in size, 6000 rpm and 12V and b) 8 x 8 cm, 3200 rpm and 12V.

For a subset of the experiments, the basic USEPA flux hood was modified by the inclusion of an internal fan (impeller), which allowed the evaluation of the effects this would have on the emission rate. Two models of fans were compared: “S” (for “small”, Figure 8a) – 4 x 4 cm in size, 6000 rpm and 12V; and “L” (for “large”, Figure 8b) – 8 x 8 cm, 3200 rpm and 12V. The fan was fixed in the hood’s headspace, 3 cm from the centre of the top, by a customised stainless-steel structure (see Figure 9), which could be installed at the dome-shaped top (and removed, for experiments without fan). Thin wires connected the internal fan to an external power point; the wires passed through the edge of the pressure equilibration hole, causing negligible reduction to the opening area. Experiments were performed with the fans rotating clockwise, which created downward flow, and

counter clockwise, which created upward flow; the direction of the flow was switched by flipping the fan before screwing to the dome. More details about configurations using internal fan are presented in Table 1



Figure 9 – Fan coupled and installed to a dome-shaped topper (view from dome-shaped topper outside).

Table 1 – Details of investigated flux chamber configurations.

Configuration	Number of inlet holes	Airflow rate at each inlet hole (kg s^{-1})	Fan dimension and rotation per minute	Impeller rotating direction
1	4	2.47×10^{-5}	$80 \times 80 \times 25$ mm 2500 rpm	Counter clockwise
2	4	2.47×10^{-5}	$80 \times 80 \times 25$ mm 2500 rpm	(flow impelled downwards)
3	4	2.47×10^{-5}	$40 \times 40 \times 10$ mm 5500 rpm	lockwise (flow impelled upwards)
4	4	2.47×10^{-5}	$40 \times 40 \times 10$ mm 5500 rpm	Counter clockwise

4.1.2 VOLATILISATION EXPERIMENTS: ACETIC ACID

Volatilisation experiments, with and without a fan, were performed in order to assess the mass transfer of acetic acid inside the flux hood, representing the behaviour of gas phase-controlled compounds (HUDSON; AYOKO, 2008b; PRATA, Ademir A.; LUCERNONI; et al., 2018). An aqueous solution was prepared by adding 1.7 L of Milli-Q® water and 40 ml of acetic acid glacial (23.53 ml/L). Inside a fume hood (Captair Gallay, Australia), the aqueous solution was transferred to a 41.0 cm diameter and 8.5 cm height cylindrical tank made of Plexiglas®, reaching approximately 1.3 cm. The flux hood was then positioned in the cylindrical tank. The sweep air feed was supplied by instrument-grade air bottles (maximum humidity content of 25 ppm). The sampling flow rate (from the sampling probe to the Nalophan® bag) was 200 mL min⁻¹, achieved by using a pump (Airchek Sampler) pre-calibrated with the lung system. Each experimental run can be divided in 2 steps, stabilisation and sampling. The run began when the sweep air and sampling flows were initiated; for experiments with the fan, the fan was also started at the same time. A period of 30 minutes was observed for stabilisation (except for Q = 2 L min⁻¹, where the stabilization was 60 min), which complies with Kienbusch's (1986) recommendation of a minimum of 4 residence times for stabilisation, which is also endorsed by (EKLUND, 1992a). After the stabilisation time, the bag in the lung system was replaced, starting then the sampling step; the sample collected during the stabilisation time was discarded. During the sampling step, two bags were sampled, each for 20 min. The temperature of the room, solution and flux hood headspace was measured with a thermometer at the beginning and end of the stabilization and sampling periods. Table 2 presents a summary of the settings adopted in each experiment and measured temperatures.

Table 2 - Summary of configuration performed and measured temperatures.

	Room temperature(°C)			Solution temperature (°C)			Headspace temperature (°C)		
	Ave	Min	Max	Ave	Min	Max	Ave	Min	Max
NoFan	18.1	17.9	18.8	19.7	18.7	20.5	18.8	18.4	19.4
SFanUp	17.8	17.5	18.0	19.2	18.1	19.9	18.7	18.2	19.0
SFanDown	18.1	18.0	18.5	19.5	18.8	20.3	19.0	18.7	19.6
LFanUp	17.9	17.9	18.1	19.5	18.7	20.0	19.6	19.1	20.0
LFanDown	17.3	17.0	18.0	19.3	18.3	20.0	19.3	19.0	20.0

For simplicity, the experiments carried out in the standard configuration are called "No Fan" and runs for Q = 2, 3, 5, 7 and 10 L min⁻¹ were performed. For experiments with a 4 x 4 cm fan, which created downward flow, and fan 4 x 4 cm, which created upward flow, are called "SFanUp" and "SFanDown", respectively. For experiments with fan 8 x 8 cm, which created downward flow,

and fan 8 x 8 cm, which created upward flow, are called “LFanUp” and “LFanDown”, respectively. Runs using an internal fan were performed for $Q = 2, 5$ and 10 L min^{-1} .

Samples from the Nalophan® bags (0.5 mL) were manually injected into a Gas Chromatograph (7890A, Agilent Technologies) coupled with a Mass Spectrometer Detector (5977B, Agilent Technologies) (GC-MSD) via a gas-tight syringe (2.5 mL SUPELCO, USA), within 30 minutes of removing the bag from the lung system. GC-MSD has been used to identify and quantify odorous compounds from gaseous samples (BARCZAK et al., 2019). Three injections were conducted for each Nalophan® bag sample totaling 6 readings on the GC-MSD for each run (three measurements for each bag). The GC-MSD was equipped with a HP-5MS 30 m x 0.25 mm x 0.25 μm column with helium as the carrier gas at the flow rate of 1.2 mL min^{-1} . The initial temperature of the GC oven was $60 \text{ }^\circ\text{C}$ for 0.1 min, increasing to $220 \text{ }^\circ\text{C}$ at $25 \text{ }^\circ\text{C min}^{-1}$, and then being held for 1 min.

To determine the concentration of acetic acid in the samples, calibration curves were previously established using gas samples at five known concentrations, produced by evaporating different amounts of pure standard solutions of the compounds into Nalophan® bags flushed with fixed volumes of sweep air (method adapted from Wang et al. (2015)). Subsequently, the known concentrations were plotted with the respective peak area obtained in the GC-MSD and a linear fit was obtained and outliers (Grubb's test) were disregarded (Figure 10).

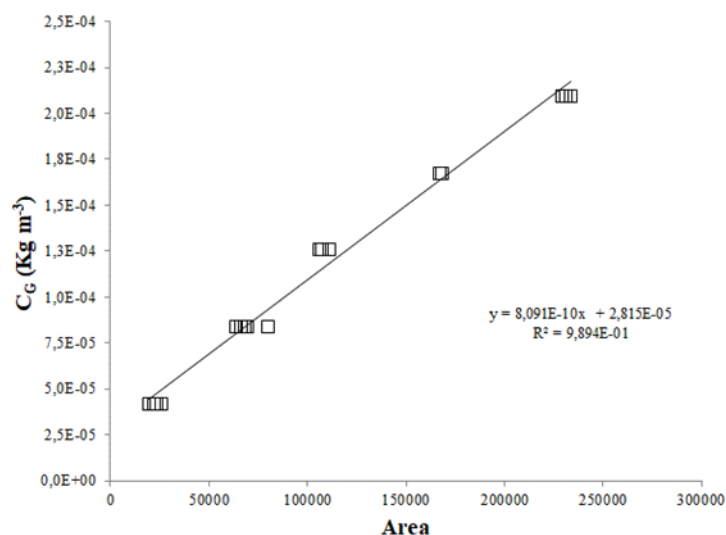


Figure 10 – Calibration curve after outlier test: Acetic acid.

Before calculating the mass transfer coefficients, statistical tests were performed to identify and exclude outliers for samples read in the GC-MSD.

For each configuration shown in Table 2, a total of 6 injections were read in the GC-MSD and the results submitted to the Grubbs's test which is based on the assumption of normality of data. Using the mean, \bar{x} , and sample standard deviation, s , of the whole set, including the suspect outlier, x_{suspect} , the distance of the outlier from the mean is calculated as a number of standard deviations:

$$G = \frac{|x_{\text{suspect}} - \bar{x}|}{s} \quad (13)$$

G can be compared to tables of critical values for G at $\alpha = 0.05$ (95% confidence interval), G_{critical} , calculated using equation below. If $G > G_{\text{critical}}$ then the suspect point is rejected.

$$G_{\text{critical}} = \frac{(n-1)}{\sqrt{n}} \sqrt{\frac{t_{(0.05/n)}^{2n-2}}{n-2 + t_{(0.05/n)}^{2n-2}}} \quad (14)$$

where t is related to t -value from t -student test and n is the number of data.

As any G suspect was higher than G_{critical} then the hypothesis that the “value is not an outlier” was accepted.

4.1.3 VOLATILISATION EXPERIMENTS: BUTYRIC ACID

Except for the sample collection, experiments to estimate the butyric acid emission rate followed similar procedures to those for acetic acid. The aqueous solution of butyric acid was obtained by mixing 0.5 mL of standard *n*-butyric acid and 1.7 L Milli-Q® water. The butyric acid aqueous solution was placed into the cylindrical tank, the flux hood was then placed over the tank and the sweep gas flow turned on. After the stabilization period, sampling was conducted with a sorbent tube connected directly to the exit of the sampling probe. The sampling pump was installed serially after sorbent tube, so as to avoid contamination of the sample. A sampling flow rate of 75 mL min⁻¹ was kept by a mass flow controller (Alicat scientific). The stabilization time was 30 min following the recommendations of Eklund (1992). After this period, five samples were collected sequentially in sorbent tubes, each tube having a sampling time of 5 min. Sample analysis was performed using GC (7890A, Agilent Technologies) - MSD (5975C, Agilent Technologies). A DB-VRX 30 m × 0.25 mm × 1.4 μm column was utilized for compound separation, with helium as the carrier gas at the flow rate of 1.2 mL min⁻¹. Sorbent tubes were loaded on an Ultra automatic

sampler (Markes International, UK) and samples were thermally desorbed using a Unity thermal desorber (TD) (Markes International, UK). The GC column temperature was initially held at 50 °C for 2 min, then raised at a rate of 15 °C/min to 200 °C, and then held for 5 min. The MSD data acquisition is set in full scan mode with a range from 35 to 325 m/z at the rate of 4 times per second.

Calibration curves for butyric acid were established using gas samples at five known volumes in duplicate, produced by evaporating different amounts of pure standard solutions of the compounds into sorbent tubes flushed with fixed volumes of sweep air. Outliers (Grubb's test) were disregarded (Figure 11). Before both sampling and calibration, the sorbent tubes were conditioned in a tube conditioner (Markes International, UK) for 30 min at a constant temperature of 300 °C so that any moisture or remaining compounds inside the tubes was evaporated.

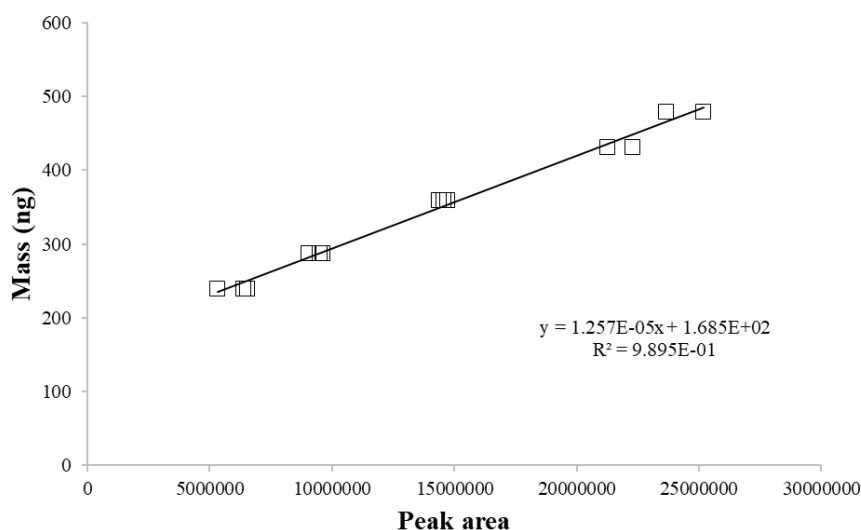


Figure 11 – Calibration curve after outlier test: Butyric acid.

Sorbent tubes were chosen for sampling after successive attempts to collect butyric acid gas samples using Nalophan® bags. GC-MSD readings showed a decay in concentrations higher than 20% for the same bag analysed, whereas this phenomenon was not observed in experiments with acetic acid in Nalophan® bags. Other sampling attempts were performed with Nalophan® bags previously conditioned with butyric acid, but the same instability was observed.

4.1.4 EMISSION RATE AND MASS TRANSFER COEFFICIENTS FROM FLUX HOOD EXPERIMENTS

Considering that the flux hood presents complete mixing of the emission and sweep gas, the concentration of the sampled gas can be approximated as the same concentration in the flux hood

headspace. Once this concentration is known, the volatilisation rate of the compounds, J ($\text{kg s}^{-1} \text{m}^{-2}$), inside the USEPA flux hood is calculated by Equation

$$J = \frac{Q \times C_m}{A} \quad (15)$$

where C_m the measured gas-phase concentrations (kg m^{-3}), obtained directly from GC-MSD readings for acetic acid samples; and A the area (m^2) of the surface enclosed by the hood (“footprint area”).

Based on the two-resistance model, it is appropriate to describe the mass transfer inside the flux hood. Then, the bulk concentration of the compounds in gas phase (C_G) is approximated by the concentration C_m sampled in the Nalophan® bags in the experiments with flux hood. The bulk liquid-phase concentration of the compounds (C_L) is known beforehand in the experiments, based on the amount of the pure compound used to prepare the aqueous solutions and the dissociation equilibrium constants (only non-dissociated acid is available for volatilisation). The values of non-dimensional Henry’s Law Coefficient (K_H) were estimated and corrected for the experimental temperatures based on Sander (2015). Using these values of K_H , C_L and C_G (C_m) together with the experimental volatilisation rate J (Equation (11)) were obtained the overall mass transfer coefficient K_L from experiments.

4.2 Numerical simulation

The fluid flow inside the flux hood was assumed isothermal (20°C), incompressible and turbulent. Clean air and the odorous compound (acetic acid) were assumed as Newtonian fluids. The variables of interest (concentration of acetic acid and flow velocity) were obtained by solving the mass, momentum, and mass of chemical specie conservation equations. To solve numerically, Reynolds Averaged Navier-Stokes (RANS) simulations for a neutral atmosphere will be performed through the $k - \omega$ Shear-Stress Transport (SST) model. The mass, *momentum* and mass chemical species of the perfect gas conservation equations described in terms of the steady state Reynolds average are, respectively:

$$\frac{\partial}{\partial x_i} (\rho \bar{u}_i) = 0 \quad (16)$$

$$\frac{\partial}{\partial x_j} (\rho \overline{u_i u_j}) = -\frac{\partial p}{\partial x_i} + \frac{\partial}{\partial x_j} \left[\mu \left(\frac{\partial \overline{u_i}}{\partial x_j} + \frac{\partial \overline{u_j}}{\partial x_i} - \frac{2}{3} \delta_{ij} \frac{\partial \overline{u_l}}{\partial x_l} \right) \right] + \frac{\partial}{\partial x_j} (-\rho \overline{u_i' u_j'}) \quad (17)$$

where ρ represents the specified mass [kg / m³], u represents the velocity components [m / s], p is the static pressure [Pa] and μ is the dynamic viscosity [Pa.s]. The overbar indicates averaged quantities.

$$\frac{\partial(\rho \overline{\omega})}{\partial t} + \frac{\partial(\overline{u_i \overline{\omega}})}{\partial x_i} + \frac{\partial(u_i' \omega')}{\partial x_i} = \frac{\partial}{\partial x_i} \left(\rho D_m \frac{\partial \overline{\omega}}{\partial x_i} \right) + M \quad (18)$$

where ω^* represents the mass fraction of the compound in [kg kg⁻¹]; M is mass source term [kg s⁻¹ m⁻³].

In the mass conservation equation for chemical species, the mathematical description represents the balance of the chemical species along a volume of differential control. The terms of the equation show, respectively, the variation with time of the chemical species in the control volume, the advective transport of the scalar, the diffusive transport of the chemical species and the term source, generation or removal of the chemical species.

These equations called Reynolds Averaged Navier-Stokes (RANS) equations lead to an extra term ($-\rho \overline{u_i' u_j'}$), called Reynolds stress tensor. After replacing all variables, there are more variables than equations to solve for the flow field and a closure problem emerges. To try to solve the closure problem Boussinesq (1877) introduced the concept of turbulent viscosity. According to Boussinesq (1877), the Reynolds tensor can be treated as in laminar flow by substituting dynamic viscosity for turbulent viscosity as shown in the Equation (19) . This analogy is accurate for many flows and simplifies the mathematical description and solution.

$$\tau_{ij} = (-\rho \overline{u_i' u_j'}) = u_t \left(\frac{\partial \overline{u_i}}{\partial x_j} + \frac{\partial \overline{u_j}}{\partial x_i} \right) \quad (19)$$

where u_t is the turbulent viscosity having the same dimensions as the dynamic viscosity.

The Reynolds Averaging procedure leads to new terms in the momentum and chemical species mass equations which were modelled using the Boussinesq analogy which, in turn, conduct to a new variable called turbulent viscosity. To determine the turbulent viscosity, a two-equation

turbulence model was employed. A large number and variety of two-equation models are available in the recent literature, *e.g.*, $k-\varepsilon$ and $k-\omega$ mainly.

Although the $k-\varepsilon$ model is a two-equation model still widely used to simulate ventilation conditions, several studies had confirmed that the SST $k-\omega$ (Shear Stress Transport) model is more appropriate to simulate a mass transfer process in aerial boundary layer (SAHA et al., 2011). This model developed by Menter (1994) results from a combination of two models, respectively for calculations in the inner boundary layer and in outside of the boundary layer. One of the advantages of the $k-\omega$ formulation is the near wall treatment for low-Reynolds number computations. Indeed, the model does not comprise the complex nonlinear wall damping functions required for the $k-\varepsilon$ model and it is therefore more correct and more consistent (RONG et al., 2011). The better performance of this model has been demonstrated in different studies. The SST model is recommended for high accuracy boundary layer simulations. For this reason, the SST model is applied in this study. Andreão et al. (2019) and Andreão and Feroni (2022) also have used $k-\omega$ SST to simulate a similar flux hood geometry.

Menter (1994) proposed a hybrid model between the most used models ($k-\varepsilon$ and $k-\omega$), the $k-\omega$ Shear-Stress Transport (SST), to predict the turbulent viscosity. The model consists of two differential equations: one for turbulent kinetic energy (k) and another for specific turbulent dissipation rate (ω). The $k-\omega$ SST combines the good performance of the $k-\omega$ formulation near the wall and the $k-\varepsilon$ away from the wall. The $k-\omega$ SST was chosen to be used in present project because it is simple and treat well the regions of the presented geometry and good results were obtained by very similar geometry and flow conditions (ANDREÃO, Willian L. et al., 2019).

The transport equations for k and ω used in the $k-\omega$ SST model for stationary conditions are:

$$\frac{\partial(\rho k \bar{u}_j)}{\partial x_j} = P_k - \beta^* \rho k \omega + \frac{\partial}{\partial x_j} \left[(\mu + \sigma_k \mu_t) \frac{\partial k}{\partial x_j} \right] \quad (20)$$

$$\begin{aligned} \frac{\partial(\rho \omega \bar{u}_j)}{\partial x_j} = & \frac{\alpha \rho}{u_t} P_k - \beta^* \rho \omega^2 + \frac{\partial}{\partial x_j} \left[(\mu + \sigma_\omega \mu_t) \frac{\partial \omega}{\partial x_j} \right] + 2(1 \\ & - F_1) \rho \sigma_{\omega 2} \frac{1}{\omega} \frac{\partial k}{\partial x_j} \frac{\partial \omega}{\partial x_j} \end{aligned} \quad (21)$$

here P_k is the production of k :

$$P_k = \min \left(2u_t \bar{S}_{ij} \frac{\partial \bar{u}_i}{\partial x_j}, 10\beta^* \rho k \omega \right) \quad (22)$$

As those differential equations that represent the problem of interest do not present analytical solutions, it is necessary to discretize the equations and propose a numerical solution. Such discretization results in a mesh that stores the address of each point at which the equations were solved. The Commercial software Ansys CFX 19.1 based on the Finite Volume Method was used. Gradients are calculated at the main points of the mesh, and the values in the interfaces are obtained by interpolation. Diffusive flows in turbulent flows are non-uniform and the representation of this variation along the nodal points is necessary. Thus, the transport of any variable between faces is calculated by interpolation methods, whose simple approach is to consider a linear profile distribution between the points.

The *Upwind interpolation scheme* has been widely used in CFD studies due to its simplicity. The use of the *Upwind* method confers a very stable discretization scheme that complies with the transportability requirement, however, the accuracy of the first-order methods can cause, in some cases, a false diffusion due to numerical errors (VERSTEEG; MALALASEKERA, 2007). Therefore, higher order scheme strains a larger number of points and reduce discretization errors, so the High-Resolution methods were used to discretize convective-diffusive flows.

Another point is that the velocity field is extremely dependent on the pressure field, which is unknown. The iterative solution strategy used is the *SIMPLEC (Semi-Implicit Method For Pressure-Linked Equations Consistent)* pressure-velocity coupling method. SIMPLEC is a modification of the SIMPLE algorithm developed by Patankar (1980) where the inconsistencies of the velocity correction equations were partially removed, eliminating the need for the pressure relaxation factor and obtaining considerable improvements in the convergence rate of the method.

A fan was inserted in the hood domain as an additional rotating domain (with interfaces set below, above and around as a cylinder encapsulating the fan blades). The computational representation of the tested flux hood was built using ANSYS Space Claim 19.1.

The commercial software Ansys Workbench 19.1 package was employed to produce the mesh. The whole control volumes distribution is a series of hybrid meshes, with prismatic elements near

walls and tetrahedral elements in the domain center. synthesizes. The choice of the hybrid mesh is to take advantage of prismatic elements, which provide controlled refinement near walls, regions of higher velocity and concentration gradients.

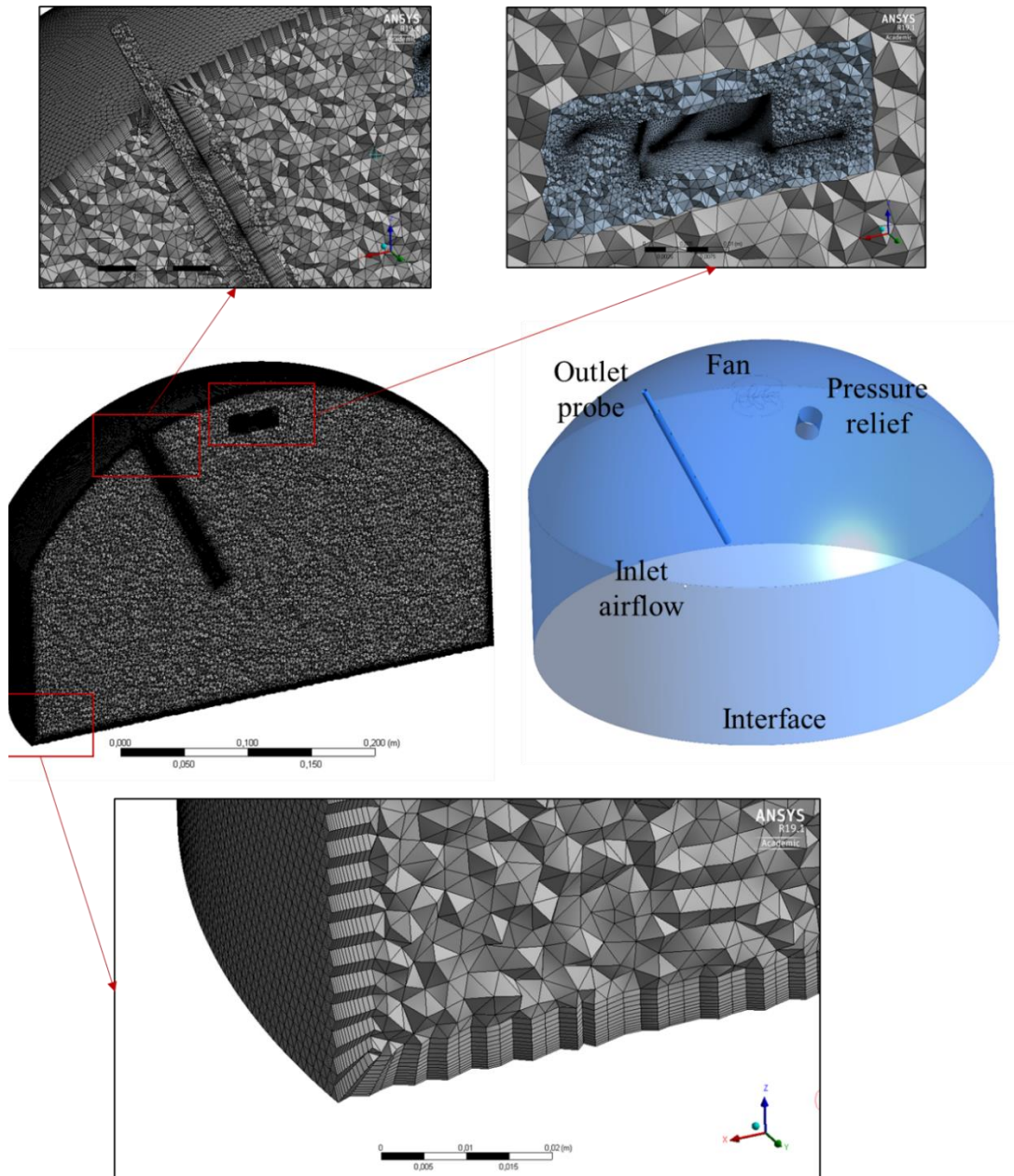


Figure 12 – From the top-left corner in clockwise direction: (i) outlet probe line mesh refinement and prismatic elements surrounding it, (ii) fan blades mesh refinement and growth rate observed towards the main section and (iii) near wall prismatic elements close to the side wall and gas-liquid interface at the bottom.

The computational domain, boundaries and mesh are presented in Figure 12. Fan and No Fan numerical configurations presented about 12 and 9 million elements, respectively. Inlet sweep air flow and outlet probe line holes are realistically matched between experiments and computational domain.

Inlet sweep air flow was set as its mass flow rate value according to the tested case assumed to be equally distributes among the four inlet orifices. The air entering the domain is considered completely clean as concentration boundary condition for the inlets. On the walls impermeability and no slip (null tangential and normal velocities) conditions were imposed. These conditions were also adopted for the liquid-gas interface, as an approximation of the resistance that the water surface imposes on the air flow. A differential pressure of 0 Pa was considered at the pressure relief boundary since there is near equilibrium with the external atmosphere.

The constant concentration defined at the interface was calculated based on Equation (23) where $C_{G,i}$ is the acetic acid concentration at the interface [kg m^{-3}], C_L is the liquid solution concentration [kg m^{-3}] and K_H is the Henry's Law Constant [-]. This equation is valid considering that the overall mass transfer coefficient is limited by the transport conditions in the gas film (as we are dealing with acetic acid). The prescribed mass flow rate for the inlet sweep air flow for the tested cases were: 2 L min^{-1} ($4.0\text{E-}05 \text{ kg s}^{-1}$), 5 L min^{-1} ($1.0\text{E-}04 \text{ kg s}^{-1}$), 7 L min^{-1} ($1.4\text{E-}04 \text{ kg s}^{-1}$) and 10 L min^{-1} ($2.0\text{E-}04 \text{ kg s}^{-1}$). For the outlet mass flow rate, it was set as $4.0\text{E-}06 \text{ kg s}^{-1}$ (200 mL L^{-1}).

$$C_{G,i}=C_L K_H = 23.53 \frac{\text{mL}}{\text{L}} * 6.75\text{E}^{-06} = 1.6\text{E}^{-04} \text{ kg.m}^{-3} \quad (23)$$

Table 3 summarizes the adopted boundary conditions for each solved equation.

Table 3 – Boundary conditions.

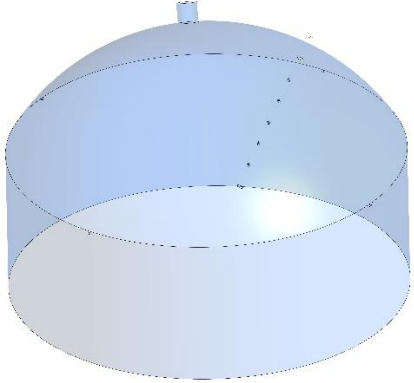
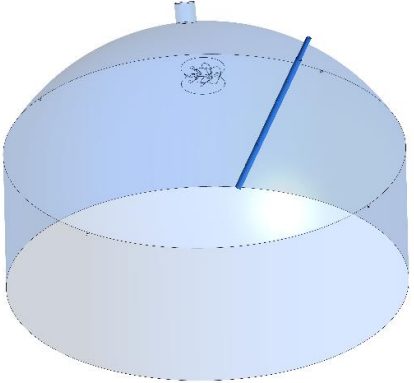
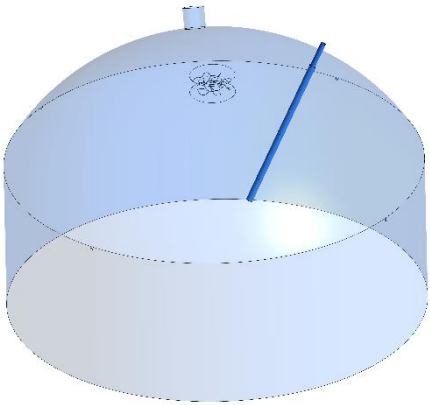
Boundary	Velocity	Turbulence	Concentration
Inlet airflow holes	Prescribed Mass Inflow Rate	$I = 5\%$	$C = 0$
Gas-liquid interface	$u_i = 0$	k and $\omega = 0$	$C_{G,i}=C_L K_H$
Outlet probe	Prescribed Mass Outflow Rate	-	-
Pressure relief	$\Delta P = 0$	$dk/dx_i = 0$ and $d\omega/dx_i = 0$	$dC/dx_i = 0$
Walls (lateral, dome, obe line and fan blades)	$u_i = 0$	k and $\omega = 0$	$dC/dx_i = 0$

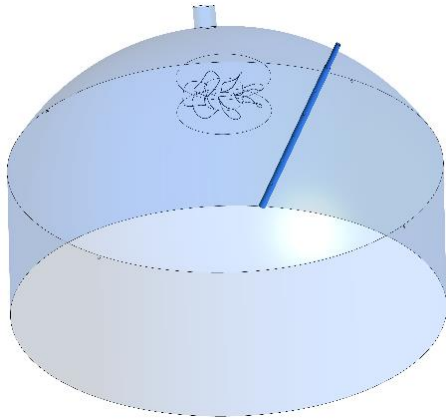
ΔP is the differential pressure with respect to atmospheric pressure [Pa]; u_i represents the air velocity inside the domain [m s^{-1}] where i varies from 1, 2 and 3, indicating the directions of the coordinate axes X, Y and Z, respectively;

T represents the air flow temperature [$^{\circ}\text{C}$]; k is the turbulent kinetic energy [$\text{m}^2 \text{s}^{-2}$] and ω is the specific dissipation rate [s^{-1}].

Table 4 presents the investigated scenarios: (i) case abbreviation and schema, (ii) presence or absence of fan, (iii) fan rotation, (iv) inlet mass flow rate and (v). For every tested case the gaseous compound is acetic acid.

Table 4 – Numerical Simulation tested cases

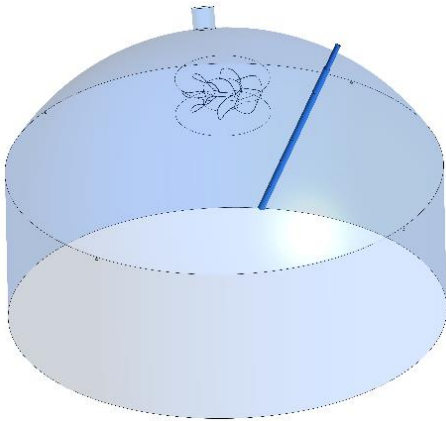
Case	Flow orientation from Fan	Fan rotation [rev min^{-1}]	Inlet sweep air flow rate [L min^{-1}]
	-	-	2, 5, 7 and 10
	Downward	6000	5
	Upward	6000	5



Upward

3200

5



Downward

3200

2, 5 and 10

5 RESULTS AND DISCUSSIONS

This Chapter presents the main results obtained in the present thesis regarding the performance of the USEPA flux hood to measure volatilisation rate of odorous compounds from passive liquid surfaces.

Section 5.1 presents the experimental and numerical results obtained for estimating the emission rate of an acetic acid solution (gas phase-controlled compound) in two central aspects: using a flux hood standard (No Fan) and a flux hood modified by an internal fan. The mass transfer parameters obtained from experiments with flux hood and numerical simulation were evaluated by combining different inlet flow rates (2, 3, 5, 7 and 10 L min⁻¹) and different settings applied through the use of two fans (large and small). The results of numerical simulations will be presented in the Section 5.2 to understand the flow inside the flux hood, as well as understanding the dynamics of mass transfer inside flux hood given the different configurations performed in the laboratory.

In Section 5.3, the k_G of two gas-phase controlled VOCs (acetic acid and butyric acid solutions) are measured using the original flux hood. The k_G result obtained for the butyric acid solution is compared with the k_G result estimated using a procedure based on Schmidt numbers from measured k_G results for acetic acid. Also in this section, the result of an investigation of butyric acid contamination inside the flux hood is presented.

Finally, in section 5.4 the bias between measured emission in laboratory and values that could be expected in the field in the absence of sampling device is presented through two case studies. Based on the results that will be presented, an assessment is made of the uncertainty implication of the presence of a fan for the scaling up of measured emission rates of gas phase-controlled compounds with the flux hood.

5.1 Effects of Fan configuration on the volatilisation inside a flux hood

In the literature review Chapter, it was established that there is a lack of information about the fluid flow and mass transfer inside the flux hood, as well as flux hood operational conditions that allows for odorous gas accumulation in the headspace. In addition, some authors have suggested the use of a fan inside the flux hood to promote greater mixing and, consequently, improve the measured emission rate. Based on that, as listed in Chapter 2, three specific objectives were established: (i) Assess mass transfer parameters for gas phase-controlled compound inside USEPA flux hood under various sweep air flow rates; (ii) Analyse the influence of different fan configurations on the measurement of emission rate of gas phase-controlled compound using a flux hood; and (iii)

Investigate flow features and mass transfer dynamics leading to the possible mechanisms underpinning the effects of different fan configurations on the measurement of emission rate of gas phase-controlled compound with the flux hood.

Thus, this Section presents the experimental results obtained regarding the emission rate of an acetic acid solution using an original flux hood and a flux hood modified by an internal fan. It also reports some results obtained using numerical simulations to support the discussions arose by the experimental results. Nevertheless, the full results obtained using numerical simulations are presented in Section 5.2. It is communicated in a form of an article to be submitted to a scientific journal for publication. The first two sections of the article presented below shows equivalent material regarding background information/state of the art and methodology already presented in Chapters 3 and 4 of this thesis, respectively. Therefore, the reader can move directly to the third section regarding the results without compromising the understanding of the thesis.

Manuscript submitted to Chemosphere

1 **The effects of flux hood internal fan configurations on the**
2 **measurement of odorous compounds emission from passive liquid**
3 **surfaces**

4
5 K. F. Cupertino^a, A. A. Prata^{b,c}, Nhat Le-Minh^b, B. Furieri^{a*}, R. Stuetz^b and J. M. Santos^a

6
7 ^aDepartamento de Engenharia Ambiental, Universidade Federal do Espírito Santo, Vitoria,
8 Brazil

9 ^bUNSW Water Research Centre, School of Civil and Environmental Engineering
10 UNSW Sydney, NSW, 2052, Australia

11 ^cPrograma de Pós-Graduação em Recurso Hídricos e Saneamento, Centro de Tecnologia,
12 Universidade Federal de Alagoas, Maceio, Brazil

13
14 ***Abstract***

15 Flux hood is a dynamic enclosure device commonly employed to measure the emission of
16 odorous compounds from liquid surfaces in wastewater treatment unities to the atmosphere.
17 An internal fan is frequently used to improve mixing inside the hood. Experimental work was
18 conducted to investigate the influence of different internal fan configurations (with different
19 size, voltage, rotation per minute and flow direction) and inlet sweep air flow rate on the
20 friction velocity on the liquid-gas interface and mass transfer coefficients of a gas-phase
21 controlled compound that impact the emission process inside the device. Computational fluid
22 dynamics was employed to explain the findings by investigating velocity and concentration
23 distributions inside the flux hood. The results showed that for all tested scenarios, the
24 emission rates and gas-phase mass transfer coefficients generally increased with the inlet
25 sweep air flow rate. In the experiments with the modified flux hood (added Fan
26 configurations), not all tested fan configurations resulted in higher emissions and mass
27 transfer coefficients inside the flux hood compared to the original USEPA flux hood (no Fan
28 configuration). The numerical simulation results showed that the increase in friction velocity
29 promoted by the fan in some regions is compensated by a smaller concentration gradient,
30 leading to only small changes in the emission rates.

31
32 ***Keywords:*** *flux hood, internal fan, odorous compound emission, passive surface*

33 **INTRODUCTION**

34

35 Odour is a complex mixture of many inorganic and organic chemicals that might cause health
36 effects like headache, nausea, hoarseness, sore throat, cough and eye, nose and throat
37 irritation, among others (Schiffman and Williams 2005; Blanes-Vidal et al. 2014); and also
38 annoyance to the nearby population leading to complaints due to malodorous (Hayes et al.
39 2014; Hayes et al. 2017). Domestic wastewater treatment plants (WWTP) are potential
40 sources of odorous gases and can be a cause of odour complaints in urban regions if they are
41 built close to residential areas or population growth occurs towards the emitting sites.
42 Common odorants emitted by these sources are nitrogen compounds, reduced sulphur
43 compounds (such as hydrogen sulphide and methyl mercaptan) and volatile organic
44 compounds (VOC, such as aldehydes and organic acids). Besides odours, WWTP are also
45 sources of greenhouse gases such as carbon dioxide, methane and nitrous oxide (Glaz et al.
46 2016; Daelman et al. 2012).

47

48 In WWTP, odour and greenhouse gases emissions can occur from liquid passive surfaces as
49 the chemical compounds are dissolved in the liquid phase and turbulent air flow sweeps the
50 liquid-air interface promoting volatilisation. These surfaces are found on primary and
51 secondary settlement tanks and stabilisation ponds; these are characterized by not having any
52 significant forced gas flow (such as mechanical or bubble aeration) across the liquid-air
53 interface (Santos et al. 2012). The term “quiescent” is also often used to refer to these
54 surfaces, but this implies an undisturbed surface, which does not commonly happen as the
55 wind is likely to disturb the water surface and generate waves (Prata et al. 2017).

56

57 Estimating the emission rate of odorous compounds is the first crucial step for understanding
58 the health effects and nuisance caused to the exposed population. The compound emission
59 rate from passive liquid surfaces can be estimated using one of the following methods:
60 predictive emission models (Santos et al. 2012; Prata et al. 2021; Pino-Herrera et al. 2022);
61 reverse dispersion modelling (indirect method) (Laura; Capelli et al. 2013; Federico
62 Lucernoni et al. 2016; Lotesoriere et al. 2022); and sampling with enclosure devices (direct
63 method) (Prata et al. 2016; 2018; Cupertino et al. 2020; Martins et al. 2018; Andreão et al.
64 2019; L. Liu et al. 2022; L Capelli et al. 2009; F. Lucernoni et al. 2017; Invernizzi et al.
65 2019).

66 Due to the relative simplicity, low cost and possibility of sensory characterization of samples,
67 direct methods have been widely used to estimate the emission rate of odorants on passive
68 surfaces and determine its variability due to changes in WWTP operation and atmospheric
69 conditions. Flux hoods (dynamic flux chambers) and portable wind tunnels are examples of
70 enclosure devices commonly employed to measure the emission of odorants and other gases
71 from WWTP (Prata et al. 2016; 2018; Moreno-Silva et al. 2020; González et al. 2021; Laura
72 Capelli et al. 2009; Y. Liu et al. 2015; Sironi et al. 2010). These open bottom devices are
73 placed over the emitting surface; a sweep gas flow transports the volatilised compounds
74 through the equipment to a sampling bag or a sorbent tube for posterior analysis, or to a gas-
75 specific sensor for in-line analysis. There is a wide variety of configurations and operational
76 conditions for these sampling devices as explained by Hudson and Ayoko (2008). Klenbusch
77 (1986) was commissioned by the United States Environmental Protection Agency (USEPA)
78 to present guidelines and recommendations for the construction and operation of an emission
79 isolation flux chamber, which became a widely adopted technique for estimating emission
80 rates from landfills and later adapted for liquid surfaces (Eklund 1992). It has been often
81 referred in the literature as the “USEPA flux hood/flux chamber”.

82

83 Hudson and Ayoko (2009) pointed out that the compound can accumulate (concentration
84 build-up) inside the flux hood, affecting sampling representativeness if concentration reach
85 values close to saturation. Parker et al. (2013) also pointed out that flux hoods operating at
86 typical sweep air flow rates underestimates the emission rate due to restrictions in low air
87 exchange rates. Prata et al. (2016) and Andreão et al. (2019) indicated that the friction
88 velocity on the liquid surface inside the USEPA flux hood does not match typical values of
89 atmospheric flow if typical sweep air flow rates are used. The flux chamber has been
90 originally designed to achieve complete mixing, i.e., homogeneous concentration distribution
91 inside the device (Gholson et al. 1991; Eklund 1992; Woodbury B. L., Parker D. B.,
92 Eigenberg R. A., Spiels 2011) in order to avoid the interference of the sampling tube location
93 inside the device in the emission rate estimation. However, Prata et al. (2016) and Andreão et
94 al. (2019) observed that the USEPA flux hood present an issue concerning flow pattern inside
95 in the device, where the sampling probe can be exposed to clean sweep air flow causing a
96 decrease in the concentration of the sampled gas (which would mean a negative bias in the
97 measured emission rate).

Manuscript submitted to Chemosphere

98 Aiming to create turbulent conditions similar to those in the field and/or to improve mixing in
99 the headspace, many authors have included a fan inside the flux hood. For instance, the
100 Australian and New Zealand standard AS/NZS 4323.4:2009 consists of a USEPA flux hood
101 with the addition of an internal fan. Aneja et al. (2000) and Aneja et al. (2001) measured
102 ammonia emissions from swine waste treatment lagoons using a cylindrical flux hood
103 (diameter ≈ 27 cm, height ≈ 42 cm) with a motor driven Teflon impeller (about 20 cm
104 diameter) rotating at about 50 revolutions per minute installed at a height of 10 cm from the
105 measuring surface. The impeller was installed with the purpose of generating a “continuously
106 stirred tank reactor”. Sweep air flow varied from 2.36 to 4.73 min L^{-1} aiming to mimic local
107 windspeed measured at 10 m. The authors performed tracer experiments to test the flow and
108 mixing characteristics of the system, concluding that the flux hood behaved as a "perfect"
109 mixer with negligible stagnancy or channelling. Woodbury et al. (2011) showed that the
110 USEPA flux hood operating from 2.5 to 7.5 L min^{-1} behaved as a well-mixed reactor without
111 and with the installation of a 12V axial-flow fan for the emission of N_2O from a soil surface.
112 Parker et al. (2013a) assessed the water evaporative flux inside a flux hood using a small fan
113 (40 mm dia. and 12V), located 10 cm from the top of the dome and directing air flow upward
114 into the dome top (same apparatus used by Woodburry et al. (2011)). They noted that water
115 evaporative flux significantly increased with the addition of the fan. For sweep airflow rate up
116 to 10 L min^{-1} , the water evaporative flux more than doubled due disturbances in the boundary
117 layer at the air-liquid interface. They also concluded that not only the airflow rate is an
118 important factor, but how and where the airflow is distributed within the hood is equally
119 important. Lyman et al. (2018) employed in their study an acrylic hemispherical dome with a
120 diameter of 41 cm and sweep air flow of 10 L min^{-1} to measure the emission rate of different
121 compounds on a produced water pond. The chamber had a fan at the top with a polyethylene
122 blade that turned at about 100 rotations per minute to achieve uniform compounds
123 concentration within the chamber. The authors tested the fan at normal and higher speed (high
124 enough to agitate the water) and found that there were no significant differences for methane,
125 carbon dioxide, alkenes, aromatics, and alcohols, but fluxes were higher for alkanes (ethane
126 and propane, respectively, 1.8 and 1.5 times higher). Tran et al. (2018) used the same flux
127 hood modified by a fan as Lyman et al. (2018) and applied the inverse dispersion modelling
128 technique to compare with flux hood emissions measurements of 58 organic compounds at a
129 produced water pond. Their results suggested that the flux hood may underestimate organic
130 compound emissions, especially alcohols, if compared with the results obtained from the

Manuscript submitted to Chemosphere

131 inverse dispersion models technique. Andreão et al. (2019) utilized the computational fluid
132 dynamics technique to investigate the flow patterns and mass transfer H₂S and acetic acid
133 inside a USEPA flux hood. The authors evaluated the influence of inlet airflow rate (2, 5 and
134 10 L min⁻¹), inlet configurations (4, 6 and 8 inlet holes) on the emission rate of and also the
135 influence of using different internal fans on the surface friction velocity. Friction velocity on
136 the interface was not significantly affected by the number of inlet holes. However, they found
137 that the inlet air can reach the probe outlet, forcing clean air to be collected by the probe,
138 affecting the idea of a well-mixed chamber. Concerning the use of fans, their numerical
139 simulations showed that inlet airflow rate increase is less influential in promoting mixing than
140 an internal fan. Also, the authors pointed out that use of a fan can help producing values of
141 friction velocity on the liquid-gas interface closer to those found in the atmospheric flow
142 which can be especially beneficial for the measurements of gas phase controlled compounds.
143 However, no attempt was made to estimate the emission rates given by the flux chamber
144 using the internal fans.

145

146 Most of the work presented in the literature is either a specific application that uses a flux
147 chamber with an internal fan aiming that it would improve mixing inside the chamber to
148 avoid bias due to the probe location or an evaluation of the influence of the sweep air flow
149 and the use of a fan on the emission rate of different compound emitted from solid or liquid
150 surfaces. However, it is rarely concerned with a comparison between flux chambers with and
151 without fans and also with different fan configurations. Less yet, how this insertion may or
152 may not modify the fluid flow and mass transfer patterns inside the chamber.

153

154 Despite the very interesting suggestion of Parker et. al (2013a) that it would be beneficial if
155 all flux chamber research results included a statement concerning the results obtained by the
156 flux chamber in use but operated in standard conditions (using dry zero-grade sweep air with
157 a standard flow rate of 1 L min⁻¹ and distilled water in a 138 mm diameter Petri dish placed
158 in the center of the apparatus) to give the evaporation rate in mm per day, the appropriate flux
159 hood operational conditions are still a matter of discussion. Even though Parker et. al (2013a)
160 also suggested years ago that all research results should include details on the chamber design
161 and operating conditions during measurement (i.e., sweep air flow rate, sweep air relative
162 humidity, source size, temperature, etc.). so that readers can make science-based comparisons
163 between research results obtained with different chamber-based methods, there is still a lack

Manuscript submitted to Chemosphere

164 of systematic laboratory experimentation regarding the mass transfer phenomena occurring
165 inside the flux hood modified by a fan, especially for the widely used USEPA flux hood.

166

167 The present work aims to investigate the influence of different fan configurations (no fan and
168 fan configurations with different size, voltage, rotation per minute and flow direction) and
169 inlet sweep air flow rate on the friction velocity at the liquid-gas interface and mass transfer
170 coefficients of a gas-phase controlled compound (represented by the acetic acid) having as a
171 basis the original USEPA flux hood design using laboratory experimental techniques and also
172 computational fluid dynamics to explain the findings by investigating velocity and
173 concentration distributions inside the flux hood.

174

175 **METHODOLOGY**

176

177 **Experimental investigation**

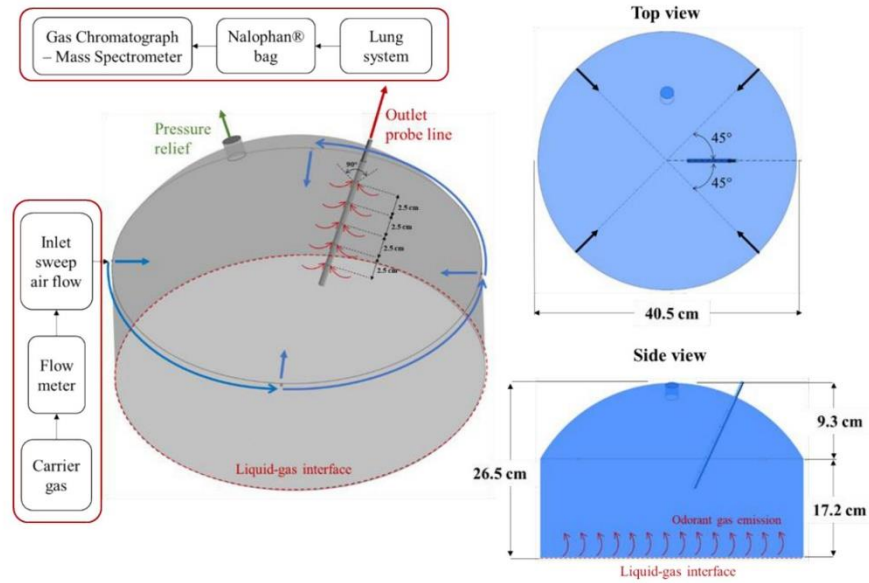
178

179 *Flux hood configuration*

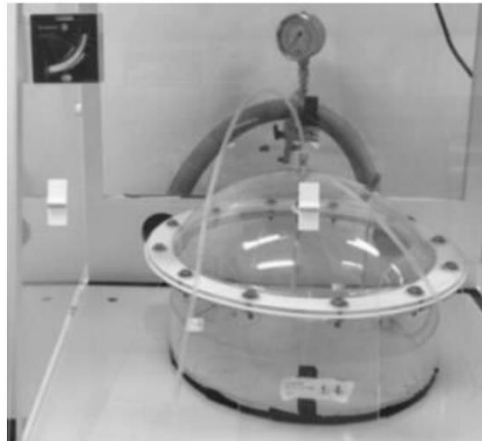
180

181 The flux hood investigated in this work was designed following the recommendations of
182 Klenbusch (1986) (Figure 1). It is composed of two parts made of Plexiglass®, a cylindrical
183 body 40.5 cm in diameter and 16.5 cm in height screwed to a dome-shaped top with a central
184 height of 11.5 cm; this design and dimensions give 28.5 L of internal volume and 0.12 m² of
185 footprint area. As recommended by Klenbusch (1986), there are four holes at the dome-
186 shaped top, positioned equidistantly, to provide the carrier gas (sweep air) at a controlled flow
187 rate. There is also a probe connected by a Teflon® outlet line, ¼" OD to a "lung system" (see
188 Prata, Lucernoni, et al. (2018), for details) used to sample the odorous gas into Nalophan®
189 bags for posterior chromatographic analysis.

190



(a)



(b)

Figure 1 – (a) Schematic representation of the flux hood proposed by Klenbusch (1986) and (b) experimental photograph of flux hood, cylindrical recipient, inlet sweep air flow line and outlet probe line.

191

192 For a subset of the experiments, the flux hood was modified by the inclusion of an internal fan

193 (impeller) for the evaluation of its effects on the measured emission rate. Two models of fan

Manuscript submitted to Chemosphere

194 were tested: “S” (for “small”, Figure 2a) – 4 x 4 cm in size, 6000 rpm and 12V; and “L” (for
195 “large”, Figure 2b) – 8 x 8 cm, 3200 rpm and 12V. The fan was fixed in the hood’s
196 headspace, 3 cm from the center of the top, by a customized stainless-steel structure (Figure
197 3) installed at the dome-shaped top (and removed, for the subset of experiments without fan).
198 Thin wires connected the internal fan to an external power supply; the wires passed through
199 the edge of the pressure equilibration hole, causing negligible reduction to the opening area.
200 Experiments were performed with the fans rotating clockwise, which created downward flow,
201 and counter clockwise, which created upward flow; the direction of the flow was switched by
202 flipping the fan before screwing to the dome.



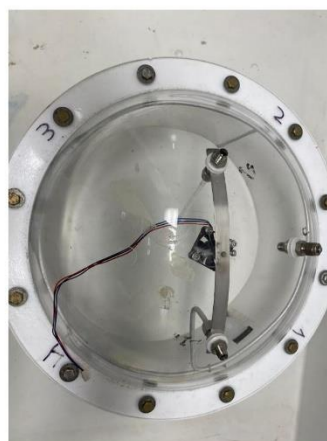
(a)



(b)

Figure 2 – Fans used at Flux hood. a) 4 x 4 cm in size, 6000 rpm and 12V and b) 8 x 8 cm, 3200 rpm and 12V.

203



(a) (b)

Figure 3 – Fan coupled and installed to a dome-shaped topper: (a) view from lateral and (b) view from dome-shaped topper inside.

204
205
206*Experimental set up*

207 Experiments, with and without a fan, were performed to assess the mass transfer of acetic acid
 208 (properties at 20°C, diffusivity in air $1.10 \times 10^{-5} \text{ m}^2 \text{ s}^{-1}$ and Schmidt number in air 1.37) inside
 209 the flux hood, representing the behaviour of gas phase-controlled compounds. For simplicity,
 210 the experiments conducted using the standard configuration are called "**No Fan**".
 211 Experiments using the 4 cm x 4 cm fan creating a downward flow and an upward flow are
 212 called, respectively, "**SFanUp**" and "**SFanDown**". Experiments using the 8 cm x 8 cm fan
 213 creating a downward flow and an upward flow are called, respectively, "**LFanUp**" and
 214 "**LFanDown**". Runs using an internal fan were performed for $Q = 2, 5$ and 10 L min^{-1} while
 215 the **No Fan** runs were performed for $Q = 2, 3, 5, 7$ and 10 L min^{-1} .

216

217 An aqueous solution was prepared by adding 1.7 L of Milli-Q® water and 40 ml of acetic
 218 acid glacial (23.53 ml/L). Inside a fume hood (Captair Gallay, Australia), the aqueous
 219 solution was transferred to a 41.0 cm diameter and 8.5 cm height cylindrical tank made of
 220 Plexiglas®, reaching approximately 1.3 cm. The flux hood was then positioned in the
 221 cylindrical tank. The sweep air was supplied by instrument-grade air bottles (maximum
 222 humidity content of 25 ppm). Each experimental run consisted of three steps: stabilisation,
 223 sampling and sample analysis. Temperature in the ambient room, aqueous solution and flux
 224 hood air headspace were measured with a thermometer at the beginning and end of the
 225 stabilization and sampling periods at each run of each experimental configuration (Table 1).

226

227 Table 1 – Averaged, minimum and maximum temperature values at each experimental configuration.

	Room temperature(°C)			Solution temperature (°C)			Headspace temperature (°C)		
	Ave	Min	Max	Ave	Min	Max	Ave	Min	Max
No Fan	18.1	17.9	18.8	19.7	18.7	20.5	18.8	18.4	19.4
SFanUp	17.8	17.5	18.0	19.2	18.1	19.9	18.7	18.2	19.0
SFanDown	18.1	18.0	18.5	19.5	18.8	20.3	19.0	18.7	19.6
LFanUp	17.9	17.9	18.1	19.5	18.7	20.0	19.6	19.1	20.0
LFanDown	17.3	17.0	18.0	19.3	18.3	20.0	19.3	19.0	20.0

228

229 *Stabilization time*

230

231 Kienbusch (1986) has recommended 4 residence times for the original USEPA flux hood to
232 reach stabilization in order to initialize any sampling procedure. Recently, Andreao et al.
233 (2019) performed numerical simulations to verify the time evolution of acetic acid
234 concentration and emission rate at outlet sampling probe from flux hood (without a fan)
235 similar to the one in this study. These authors showed that as the airflow rate increases,
236 smaller is the time for the flux hood to reach steady state. They tested inlet sweep air flow rate
237 of 2, 5 e 10 L min⁻¹ and found that the concentration distribution changed only slightly, i.e.,
238 emission rate remained constant after 30 min for sweep air flow rate of 10 L min⁻¹ to 50 min
239 for 2 L min⁻¹.

240

241 No recommendation was found in the literature regarding the stabilization time to be adopted
242 for a flux hood modified by a fan. Thus, a test with the LFanUp configuration for sweep air
243 flow of 5 L min⁻¹ was performed using two sampling strategies. Firstly, bags were used to
244 collect samples in the flux hood in different times (10, 42, 64 and 86 min). The second
245 sampling strategy used consisted of using gas-tight syringe (2.5 mL SUPELCO, USA)
246 directly on the pressure release hole at times 2, 47, 69 e 91 min. Figure 4 shows the emission
247 rate variation (ΔJ) with different time intervals (Δt) using both sampling strategies.
248 Stabilization was achieved by running the sweep air flow for 30 minutes from the instant the
249 fan was turned on, except for $Q = 2$ L min⁻¹, in which case the stabilization was achieved in
250 60 min. It is important to note that for experiments with fan, it was turned on in the beginning
251 of the stabilization period. After the stabilization period, the bag in the lung system was
252 replaced and the sample collected during the stabilization time was discarded.

253

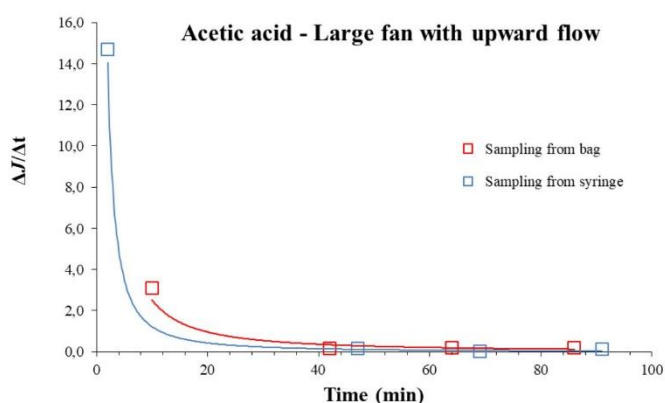


Figure 4 – Temporal variation of emission rate variation (ΔJ) with different time intervals (Δt) for the LFanUp configuration and inlet sweep air flow rate of 5 L min⁻¹. Emission rate were estimated from samples collected using bags (in red) and syringe (in blue).

254

255 *Sampling and sample analysis*

256

257 The sampling flow rate (from the sampling probe to the Nalophan® bag) was 200 mL min⁻¹.
258 During the sampling, two bags were used, each bag was filled for 20 min. Samples from the
259 Nalophan® bags (0.5 mL) were manually injected into a Gas Chromatograph (7890A, Agilent
260 Technologies) coupled with a Mass Spectrometer Detector (5977B, Agilent Technologies)
261 (GC-MSD) via a gas-tight syringe (2.5 mL SUPELCO, USA), within 30 minutes of removing
262 the bag from the lung system. Three full syringes were taken from each Nalophan® bag
263 sample totaling 6 readings on the GC-MSD for each run (three measurements for each bag).
264 The GC-MSD was equipped with a HP-5MS 30 m x 0.25 mm x 0.25 μ m column with helium
265 as the carrier gas at the flow rate of 1.2 mL min⁻¹. The initial temperature of the GC oven was
266 60 °C for 0.1 min, increasing to 220 °C at 25 °C min⁻¹, and then being held for 1 min.

267

268 Calibration curves were previously established using gas samples at five known
269 concentrations, produced by evaporating different amounts of pure standard solutions of the
270 compounds into Nalophan® bags flushed with fixed volumes of sweep air (adapted from
271 Wang et al., 2015). Subsequently, the known concentrations were plotted with the respective
272 peak area obtained in the GC-MSD, a linear fit was obtained, and outliers (Grubb's test) were
273 disregarded.

274

275 *Emission rate and mass transfer coefficients from flux hood experiments*

276

277 Assuming that the emitted gas and the sweeping air are well mixed in the flux hood, the
278 concentration of the sampled gas can be approximated as the same concentration in the flux
279 hood headspace. Then, once this concentration is determined, the volatilisation rate of the
280 compounds, J (kg s⁻¹ m⁻²) can be calculated using Equation (1).

281

$$J = \frac{Q \times C_m}{A} \quad (1)$$

282 where C_m the measured gas-phase concentrations (kg m^{-3}), obtained directly from GC-MSD
 283 readings for acetic acid samples; and A the area (m^2) of the surface enclosed by the hood
 284 (“footprint area”).

285

286 The overall mass transfer coefficient K_L from experiments was obtained using Equation 2
 287 (Santos et al., 2012). The bulk concentration of acetic acid in the gas phase (C_G) is
 288 approximated by C_m . The bulk liquid-phase concentration of acetic acid (C_L) is known
 289 beforehand in the experiments, based on the amount of the pure compound used to prepare the
 290 aqueous solutions and the dissociation equilibrium constants (only non-dissociated acid is
 291 available for volatilisation). The values of non-dimensional Henry’s Law Coefficient (K_H)
 292 were estimated and corrected for the experimental temperatures based on Sander (2015). For
 293 acetic acid, $1/(k_G K_H) \gg 1/k_L$, meaning that the gas phase resistance controls the volatilisation
 294 process and therefore that $k_G \approx K_L/K_H$.

295

$$K_L = \frac{J}{(C_L - C_m/K_H)} \quad (2)$$

296

297 Numerical simulations

298

299 Some additional and support analysis can be carried out using detailed velocity and
 300 concentration distribution inside the device. These data were produced by employing the
 301 computational fluid dynamics technique to simulate the physics involved in the fluid flow and
 302 mass transfer for the following cases: (a) No Fan and different clean air flow rates (2, 5 and
 303 10 L min^{-1}) and (b) Small Fan and flow rate of 5 L min^{-1} considering Upward and Downward
 304 flows.

305

306 The fluid flow inside the flux hood was assumed isothermal (20°C), incompressible and
 307 turbulent. The variables of interest (concentration of acetic acid and flow velocity) were
 308 obtained by solving the mass, momentum and mass of chemical specie conservation
 309 equations. Turbulence was solved using the Reynolds averaging procedure and the
 310 Boussinesq analogy to model the turbulent fluxes, $k-\omega$ SST (Shear Stress Transport) model
 311 developed by Menter (1994) was employed to determine the turbulent viscosity. $k-\omega$ SST
 312 has already been used in the works of Andreao et al. (2019) and Andreao and Feroni (2022).
 313 All equations were solved in coupled manner and considering a stationary regime.

Manuscript submitted to Chemosphere

314 Commercial software Ansys CFX 19.1 was used to solve the conservation equations based on
315 the Finite Volume Method. Ansys Workbench 19.1 package was employed to produce a
316 series of hybrid meshes, with prismatic elements near walls and tetrahedral elements in the
317 domain center are the whole control volumes distribution. Mesh sensitivity tests were
318 performed.

319

320 A fan was inserted in the hood domain as an additional rotating domain (with interfaces set
321 below, above and around as a cylinder encapsulating the fan blades). The computational
322 representation of the tested flux hood was built using ANSYS Space Claim 19.1. The
323 computational domain, boundaries and mesh are presented in Figure 5. Fan and No Fan
324 numerical configurations presented about 12 and 9 million elements, respectively. Inlet sweep
325 air flow and outlet probe line holes are realistically matched between experiments and
326 computational domain.

327

328 The prescribed mass flow rate for the inlet sweep air flow (assumed equally distributed
329 among the four inlet orifices) for the investigated scenarios were: $4.0\text{E-}05 \text{ kg s}^{-1}$ (2 L min^{-1}),
330 $1.0\text{E-}04 \text{ kg s}^{-1}$ (5 L min^{-1}) and $2.0\text{E-}04 \text{ kg s}^{-1}$ (10 L min^{-1}). For the outlet mass flow rate, it
331 was set as $4.0\text{E-}06 \text{ kg s}^{-1}$ (200 mL L^{-1}). On the walls impermeability and no slip (null
332 tangential and normal velocities) conditions were imposed. These conditions were also
333 adopted for the liquid-gas interface, as an approximation of the resistance that the water
334 surface imposes on the air flow. A differential pressure of 0 Pa was considered at the pressure
335 relief boundary since there is near equilibrium with the external atmosphere.

336

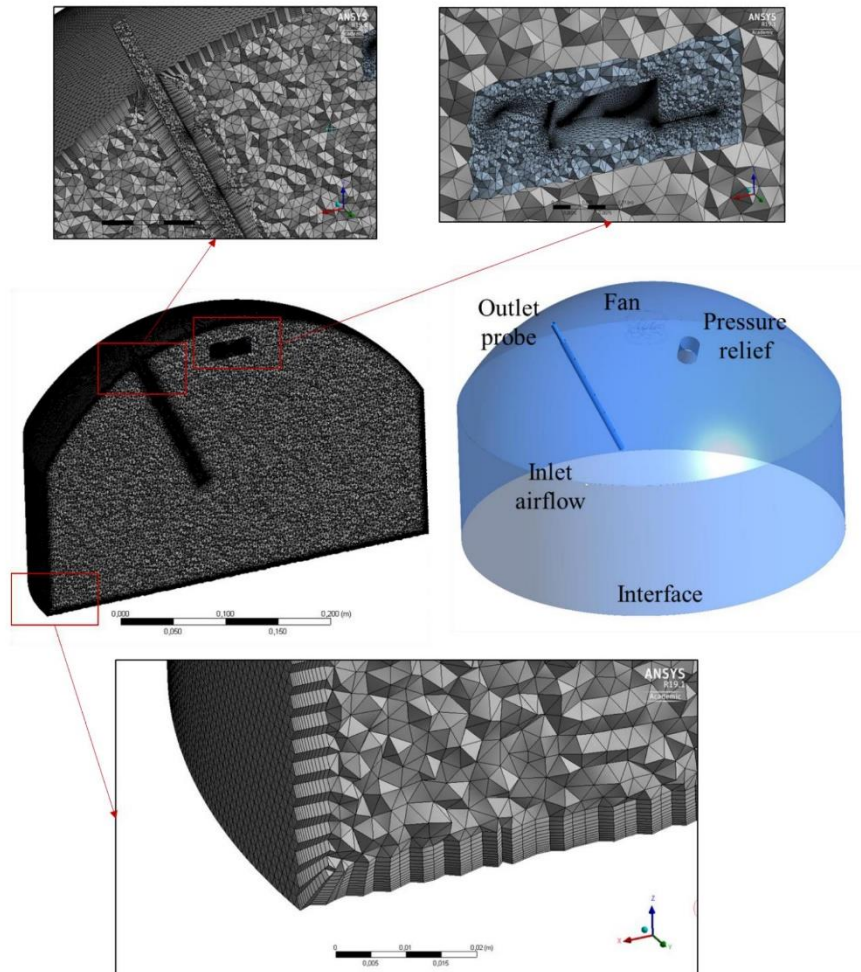


Figure 5 – Computational domain and mesh. From the top-left corner in clockwise direction: (i) outlet probe line mesh refinement and prismatic elements surrounding it, (ii) fan blades mesh refinement and growth rate observed towards the main section and (iii) near wall prismatic elements close to the side wall and gas-liquid interface at the bottom.

337

338 The constant concentration defined at the interface was calculated based on Equation (2)
 339 where $C_{G,i}$ is the acetic acid concentration at the interface [kg m^{-3}], C_L is the liquid solution
 340 concentration [kg m^{-3}] and K_H is the Henry's Law Constant [-]. This equation is valid
 341 considering that the overall mass transfer coefficient is limited by the transport conditions in

342 the gas film (as we are dealing with acetic acid). C_L was set constant, and its value (23.53
343 ml/L) was based on the experimental conditions described in Section 2.1.2.

344

$$C_{G,i} = C_L K_H = 23.53 \frac{\text{mL}}{\text{L}} * 6.75E^{-06} = 1.6E^{-04} \text{kg} \cdot \text{m}^{-3} \quad (2)$$

345

346 Table 2 summarizes the adopted boundary conditions for each solved equation.

347

348 Table 2 – Boundary conditions.

Boundary	Velocity	Turbulence	Concentration
Inlet airflow holes	Prescribed Mass Inflow Rate	$I = 5\%$	$C = 0$
Gas-liquid interface	$u_i = 0$	k and $\omega = 0$	$C_{G,i} = C_L K_H$
Outlet probe	Prescribed Mass Outflow Rate	-	-
Pressure relief	$\Delta P = 0$	$dk/dx_i = 0$ and $d\omega/dx_i = 0$	$dC/dx_i = 0$
Walls (lateral, dome, probe line and fan blades)	$u_i = 0$	k and $\omega = 0$	$dC/dx_i = 0$

349 ΔP is the differential pressure with respect to atmospheric pressure [Pa]; u_i represents the air
350 velocity inside the domain [m s^{-1}] where i varies from 1, 2 and 3, indicating the directions of
351 the coordinate axes X, Y and Z, respectively; k is the turbulent kinetic energy [$\text{m}^2 \text{s}^{-2}$] and ω
352 is the specific dissipation rate [s^{-1}].

353

354 RESULTS AND DISCUSSION

355

356 Influence of different sweep air flows and fan configurations on the emission rate and 357 mass transfer coefficients

358

359 Figure 6 presents the variation of the emission rate (J) for different sweep airflow (Q) for the
360 No Fan configuration. Estimated emission rates increased with the increase in sweep air flow
361 rate, following the same trend observed in previous studies with flux hoods (Rhoades et al.,

362 2005; Parker et al. 2013; Prata et al. 2018a). This trend can be explained by the increase in
363 friction velocity at the gas-liquid interface due to the higher inlet air flow rate through the flux
364 hood, as mass transfer resistance is gas-phase dominant for acetic acid.

365

366 A sequence of statistical tests to verify whether linear regression observed for data results in
367 Figure 6 showed to be statistically significant. Statistically significant result was obtained in
368 the T-test ($0.0019 < 0.05$) despite the fact that 7 L min^{-1} does not conform well within the
369 linear fit. The sweep air flow of 7 L min^{-1} presents the highest residual value and the highest
370 values in RStudent and DFFITS tests (10.23 and 6.11, respectively). It is worth noting that,
371 unlike the experiments performed for input airflow rates of up to 5 L min^{-1} , which were
372 performed only using a gas mass flow controller, a flow meter was used to calibrate the extra
373 flow needed to achieve the flow rates of 7 and 10 L min^{-1} , which increases the uncertainty in
374 the input airflow rate for these two cases and added to the reading sensitivity of the
375 chromatograph may have contributed to the deviation found in the standard experiments.
376 Although the statistical tests showed that linear regression was significant, a qualitative
377 analysis seems to suggest that the relationship between the emission rate and the sweep air
378 flow may not be linear inside flux chamber. This is a hypothesis put forward in this work and
379 that needs further investigation, not being the object of this study. The same discussion
380 applies to the gas-film mass transfer coefficient shown in Figure 7. Table 3 presents the
381 average, minimum and maximum of the experimental values of the overall mass transfer
382 coefficient K_L and the gas-film mass transfer coefficient k_G for all scenarios investigated in
383 this work. In order to verify the repeatability of the experiments, two runs were conducted
384 with $Q = 5 \text{ L min}^{-1}$ and the k_G variation obtained was only 6%.

385

386 Experiments using a similar flux hood (No Fan configuration) were performed earlier by
387 Prata *et al.* (2018) for nominal sweep air flow rates of 2, 5 and 10 L min^{-1} , using an acetic
388 acid solution of concentration in the liquid phase of 49.9 kg m^{-3} . Their inlet flow rates were
389 adjusted by valve rotameters and checked using a flow rate meter, in contrast to the mass flow
390 controller used in the present work. Although both studies show a similar trend of increase in
391 the emission rate and k_G with the inlet sweep air flow, the values of k_G measured by Prata et
392 al. (2018a) were consistently larger (up to an order of magnitude) than the corresponding
393 values obtained in the present study. Even if both studies used a flux hood with the same
394 geometry and adopted very similar procedures in most aspects, these differences indicate that

395 the emission of gas phase-controlled compounds inside the USEPA flux hood is sensitive to
 396 the accuracy and pattern of the controlling apparatus for the inlet sweep gas. It can be
 397 hypothesized that the use of valve rotameters and flow meters may introduce oscillations and
 398 perturbations in the sweep air flow (compared to the much more stable mass flow controller),
 399 which in turn affect the gas-side mass transfer inside the hood.
 400

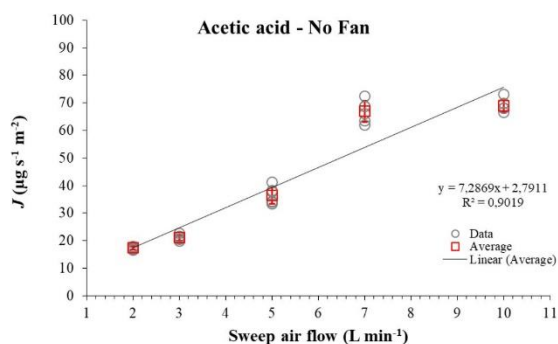


Figure 6 – Emission (J) rate varying with sweep air flow (Q) for the No Fan configuration.

401

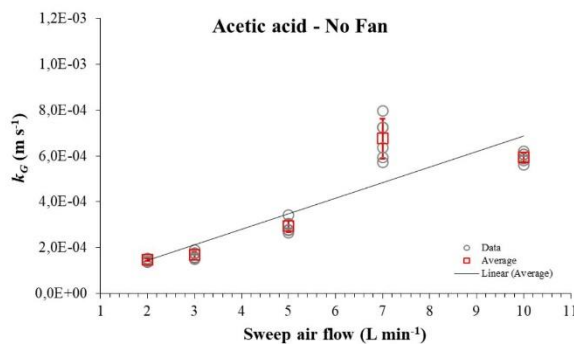


Figure 7 – Gas-film mass transfer coefficient (k_G) varying with sweep air flow (Q) for the No Fan configuration.

402

403 As observed in the experiments without a fan, the emission rates obtained in the experiments
 404 carried out with a fan also showed an increase with the inlet sweep airflow (Figure 8). The
 405 LFanUp configuration presented the highest emission averages for the sweep airflow rate of 2
 406 and 5 L min⁻¹ and the SFanUp configuration presented the highest average for 10 L min⁻¹.
 407 This initial analysis indicates that fans with upward flow, favor the emission of acetic acid
 408 solution inside the flux hood, compared to the flow directed downwards. Another behavior

409 observed for the four evaluated configurations is that the emission rate measurements present
 410 greater variability in the experiments with the sweep air flow rate of 10 L min⁻¹. The
 411 LFanDown and LFanUp configurations, for example, presented a coefficient of variation
 412 around 6.3 and 5.8%, respectively, in experiments with sweep airflow rate of 10 L min⁻¹,
 413 while the coefficient of variation in the experiments with sweep airflow of 2 L min⁻¹ were 3.2
 414 and 4.2%, respectively.

415

416 Comparing results with and without a fan, there was a small increase in the emission rate for
 417 the cases modified by a fan and carried out with the inlet sweep air flow rate of 10 L min⁻¹,
 418 mainly upward configuration (increase of 18.4% and 25.5% for large and small fan,
 419 respectively). In contrast, for the experiments with an inlet sweep air flow rate of 2 L min⁻¹, a
 420 slight decrease in the emission rate was observed, compared to the No Fan configuration. For
 421 sweep air flow rate 5 L min⁻¹, the fan blowing upwards promoted a small increase in the
 422 emission rates, while the fan with downward flow resulted in slightly lower emission. More
 423 importantly, however, is the fact that the effects of all the different fan configurations
 424 investigated, whether towards increasing or decreasing the emission rates, were overall small.
 425 This is contrary to the intuitive hypothesis that the use of a fan inside the flux hood would
 426 dramatically enhance the emission of odorants measured on liquid surfaces.

427

428 Table 3 – Emission rate and mass transfer coefficients obtained for the different configurations.

	Q (L.min ⁻¹)	J (μg s ⁻¹ m ⁻²)			K_L (10 ⁻⁹ m s ⁻¹)			k_G (10 ⁻⁴ m s ⁻¹)		
		Ave	Min	Max	Ave	Min	Max	Ave	Min	Max
No Fan	2	17.32	16.63	17.93	1.08	1.02	1.13	1.47	1.37	1.54
	3	21.07	19.76	22.58	1.20	1.09	1.34	1.68	1.49	1.90
	5	36.45	33.25	41.23	2.12	1.87	2.50	2.95	2.66	3.42
	7	66.93	62.02	72.45	4.63	4.01	5.37	6.76	5.74	7.97
	10	68.95	66.64	73.15	4.01	3.86	4.31	5.94	5.61	6.22
LFanDown	2	13.46	12.16	14.04	0.76	0.66	0.811	1.09	0.93	1.17
	5	33.11	32.03	33.66	1.89	1.79	1.95	2.80	2.61	2.94
	10	69.22	64.84	71.57	4.11	3.68	4.33	6.35	5.49	6.92
LFanUp	2	17.08	16.48	17.46	1.08	1.02	1.11	1.53	1.44	1.58
	5	43.98	42.00	47.71	2.90	2.71	3.35	4.28	4.01	5.04
	10	81.63	66.62	90.32	5.26	3.79	6.25	7.97	5.56	9.71
SFanDown	2	13.26	12.91	13.66	0.74	0.71	0.77	1.04	0.99	1.08
	5	34.33	33.45	35.16	1.99	1.90	2.07	2.94	2.75	3.11
	10	74.07	70.40	79.32	4.49	4.10	5.04	6.78	6.04	7.80
SFanUp	2	14.41	13.34	15.02	0.85	0.75	0.91	1.23	1.07	1.34
	5	37.48	35.85	39.70	2.25	2.09	2.43	3.30	3.01	3.50
	10	86.54	78.46	92.58	5.96	4.99	6.76	9.54	7.80	11.0

429

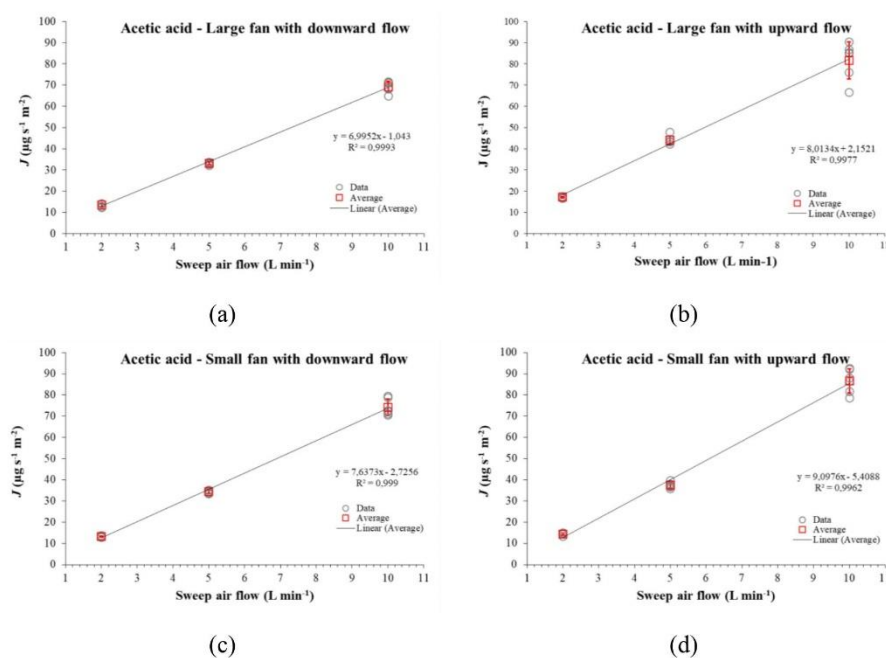


Figure 8 – Emission (J) rate varying with Sweep air flow (Q) for different configurations: a) LFanDown; b) LFanUp; c) SFanDown and d) SFanUp.

430

431 The highest and lowest gas-side mass transfer coefficient k_G was observed in the SFanUp
 432 ($1.10\text{E-}03 \text{ m}\cdot\text{s}^{-1}$) and LFanDown ($9.88\text{E-}05 \text{ m}\cdot\text{s}^{-1}$) configuration, respectively, for the sweep
 433 air flow rate of $10 \text{ L}\cdot\text{min}^{-1}$. Here, as previously seen for the emission rate, we observe larger
 434 uncertainty for the inlet sweep airflow of 10 L min^{-1} , especially for the LFanUp and SFanUp
 435 configurations.

436

437 A comparison between the average values of k_G estimated for the original USEPA flux hood
 438 (No Fan configuration) and those values obtained using the modified flux hood (including a
 439 fan) can be performed by analysing Table 3. Similar to the effect on the emission rate, the use
 440 of an internal fan does not promote an increase in the gas-film mass transfer coefficient for all
 441 configurations evaluated in the present work. Furthermore, there was no clear trend related to
 442 the size of the fan (which may be due to the fact that the smaller fan had a higher rotation
 443 speed). Summarizing, for $Q = 2 \text{ L min}^{-1}$, all fan configurations showed k_G smaller than No
 444 Fan (highest relative difference of -31.1% for SFanDown); for $Q = 5 \text{ L min}^{-1}$, the cases with
 445 fan blowing upwards had an average k_G larger than the No Fan configuration (highest for

446 LFanUp); the cases with downward flow had an average k_G smaller than the No Fan
 447 configuration (lowest for LFanDown); for $Q = 10 \text{ L min}^{-1}$, all fan configurations presented
 448 average k_G larger than the No Fan configuration (the highest being for SFanUp, with relative
 449 increase of 55.9%).

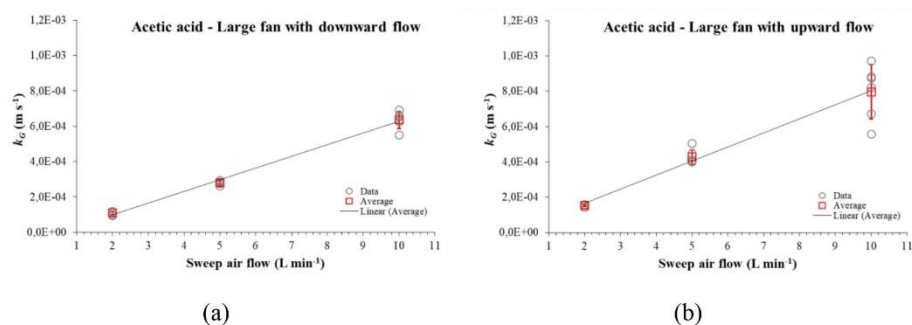
450

451 Preliminarily, an increase in the mass transfer coefficients was expected due to the increase in
 452 the friction velocity on the liquid surface promoted using the internal fan. The CFD
 453 simulations by Andreão et al. 2019 indicated that the use of an internal fan produced larger
 454 values of friction velocity at the liquid interface, compared to all the other configurations
 455 simulated without a fan. However, the effects of the fan inside the flux hood were only
 456 dedicated to its influence on friction velocity, *i.e.*, the mass transfer phenomena were not
 457 evaluated in the presence of an internal fan.

458

459 The emission rates and mass transfer coefficients for the acetic acid inside the flux hood were
 460 observed to be only slightly affected by the internal fan configuration. This seems to be, to
 461 some extent, counter-intuitive since flow velocities and turbulent friction inside the hood are
 462 estimated to be much higher with the addition of the fan. Therefore, the next section intends
 463 to explain these findings by investigating the velocity and concentration distributions inside
 464 the flux hoods obtained by the computational fluid dynamics technique.

465



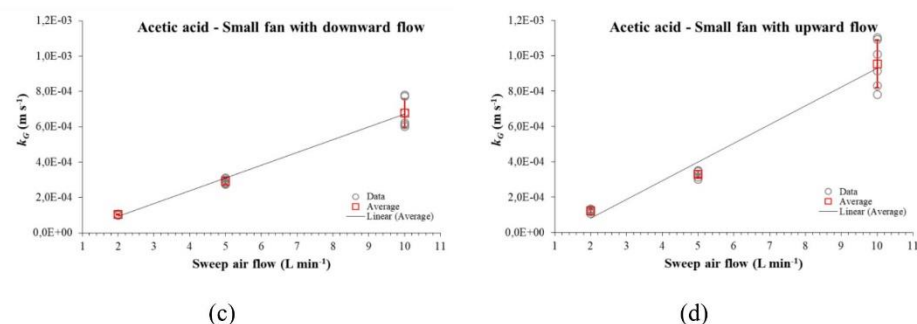


Figure 9 – Gas-film mass transfer coefficient (k_G) varying with sweep air flow (Q) for experiments modified by a fan: a) LFanDown; b) LFanUp; c) SFanDown and d) SFanUp.

466

467 **A view on the velocity and concentration distributions inside the flux hoods and their**
 468 **influence on emission rate**

469

470 Figure 10 presents a comparison between the numerical simulations results and experimental
 471 data. The concentration results obtained via GC-MS analysis were compared to the
 472 concentration calculated at the outlet probe boundary using the computational fluid dynamics
 473 technique. In summary, numerical results were about twice the experimental data for all
 474 investigated scenarios (Figure 10a). The differences found between experimental and
 475 numerical concentration results may be associated to the boundary condition set at the
 476 interface. Assuming solid and rigid conditions to represent a gas-liquid interface may
 477 intensify the simulated shear stress and consequently the mass transfer between the interface
 478 and the bulk flow. However, the same trend of the internal fan effects between numerical and
 479 experimental tests is clearly verified (Figure 10b).

480

481 In Figure 11a to Figure 11f, we observe a better mixing of acetic acid concentration in the
 482 bulk flow due to the fan, as an expected outcome of the insertion of a fan inside the flux hood.
 483 The mean bulk concentration is slightly higher for SFanUp configuration. Note that for the
 484 fan configurations, a concentration build-up is observed very near the interface at its center.
 485 This will be further discussed when analysing Figure 12.

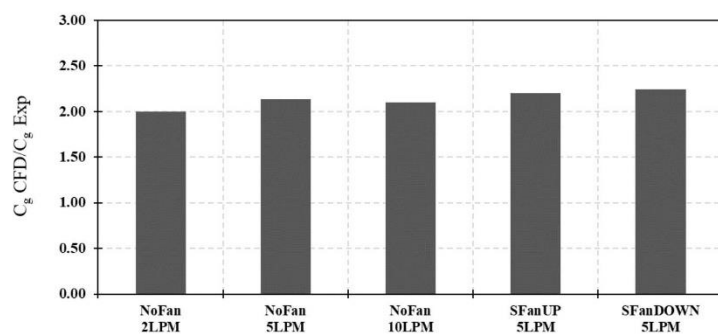
486

487 Figure 12a to Figure 12c shows top view distribution of: (i) concentration gradient at a plane
 488 parallel to and at a distance of 0.5 mm from the interface and (ii) friction velocity at interface.
 489 Concentration gradient is calculated as the difference of concentration at 0.5 mm distance and

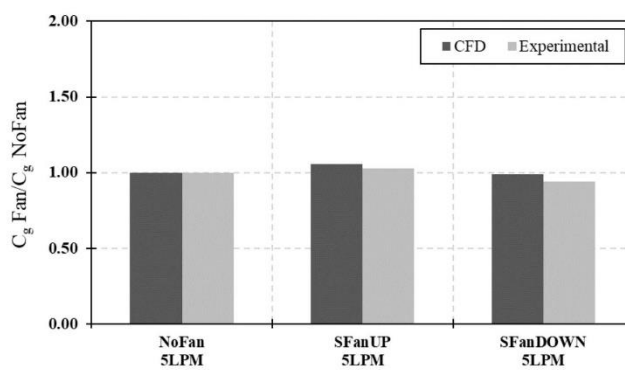
490 at the interface (constant value) divided by the distance (0.5 mm). Friction velocity is based
491 on the wall shear stress at the interface ($u^* = (\tau/\rho)$), where τ is the wall shear stress in Pa
492 and ρ is the density of the air in kg m^{-3}). The presence of an internal fan strongly modifies the
493 shear stress pattern (here discussed as the friction velocity), where the average friction
494 velocity increases by one order of magnitude. It is worth noticing that the friction velocity is a
495 key parameter to understand and to estimate volatilisation of gaseous compounds from gas-
496 liquid interfaces, and empirical models for liquid surfaces in the field have shown a nearly
497 proportional relationship between mass transfer coefficients and friction velocity (Prata et al.,
498 2018b). Due to the intensification of friction velocity, an increase of k_G and outlet
499 concentration for the fan configurations could be expected. However, similarly to the
500 experimental results, numerical simulations did not show such an increase. Exploring the
501 numerical simulation's ability to resolve in detail the velocity and concentration fields, the
502 following discussion is devoted to seeking for fluid flow structures responsible for this
503 counter-intuitive behaviour.

504 It can be seen in Figure 12 that for No Fan configuration, in general, zones of high friction
505 velocity coincide with zones of high concentration gradient, promoting a synergistic effect
506 towards high mass transfer rates. On the other hand, for SFanUP and SFanDown
507 configuration, zones of highest friction velocity presented the lowest values of concentration
508 gradient. Despite the friction velocity increased one order of magnitude (between Fan and No
509 Fan configurations), the concentration gradient did not follow the same increase. To better
510 understand the fluid flow structures responsible for these phenomena, Figure 13 highlights the
511 velocity vectors very close to the interface and, simultaneously the concentration distribution
512 at a vertical plane and friction velocity distribution at the horizontal plane. The insets in
513 Figure 13 show zoomed images of a near interface region. For the case with No Fan (Figure
514 13a), zones of highest friction velocity show a divergent flow pattern near the interface, which
515 leads to a relatively thin mass transfer boundary layer (absence of concentration build up) in
516 these zones, favouring the occurrence of mass transfer (larger friction velocity coinciding with
517 large concentration gradient). On the other hand, configurations with the fan (Figure 13b and
518 Figure 13c) indicate an accumulation of acetic acid exactly above the region of more intense
519 friction velocity, with a thickening mass transfer boundary layer resulting from convergent
520 flows in these zones. In this case, the potential increase in the emission of acetic acid due to
521 the increased friction velocity is counteracted by the smaller concentration gradient, limiting
522 the emission flux.

523



(a)



(b)

Figure 10 – Experimental and numerical results comparison for acetic acid volatilisation phenomena: (a) numerical and experimental outlet concentration ratio for No Fan 2, 5 and 10 L min⁻¹ and SFanUp and SFanDown 5 L min⁻¹ and (b) Fan vs. No Fan concentration ratio.

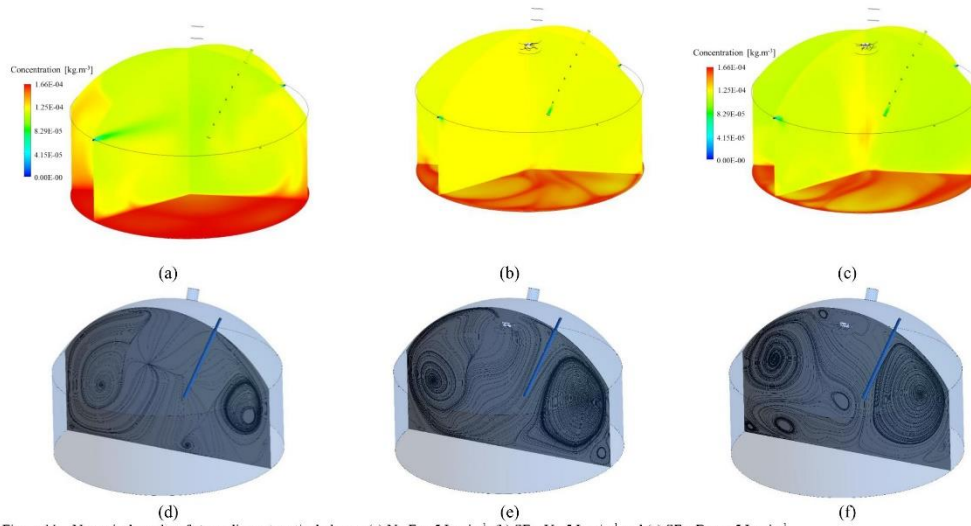


Figure 11 – Numerical results of streamlines at vertical planes: (a) No Fan 5 L min^{-1} , (b) SFanUp 5 L min^{-1} and (c) SFanDown 5 L min^{-1} .

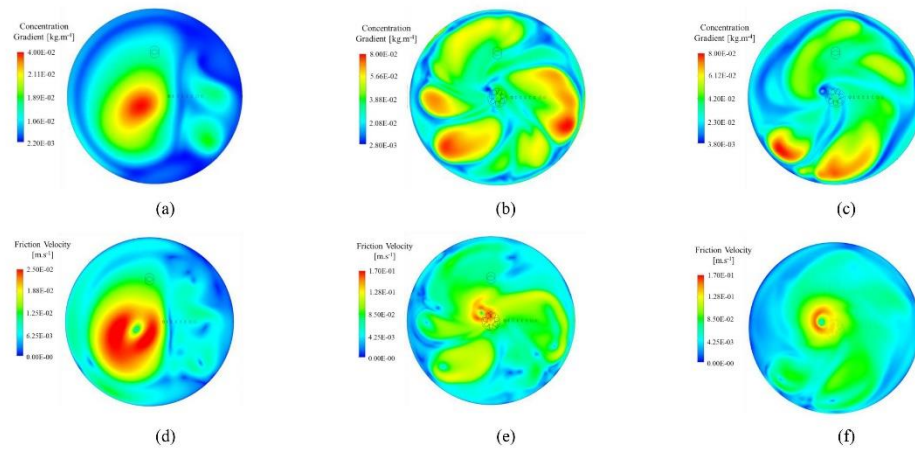


Figure 12 – Numerical results of near interface concentration gradient (a) No Fan 5 L min^{-1} , (b) SFanUp 5 L min^{-1} and (c) SFanDown 5 L min^{-1} and interface wall friction velocity (d) No Fan 5 L min^{-1} , (e) SFanUp 5 L min^{-1} and (f) SFanDown 5 L min^{-1} .

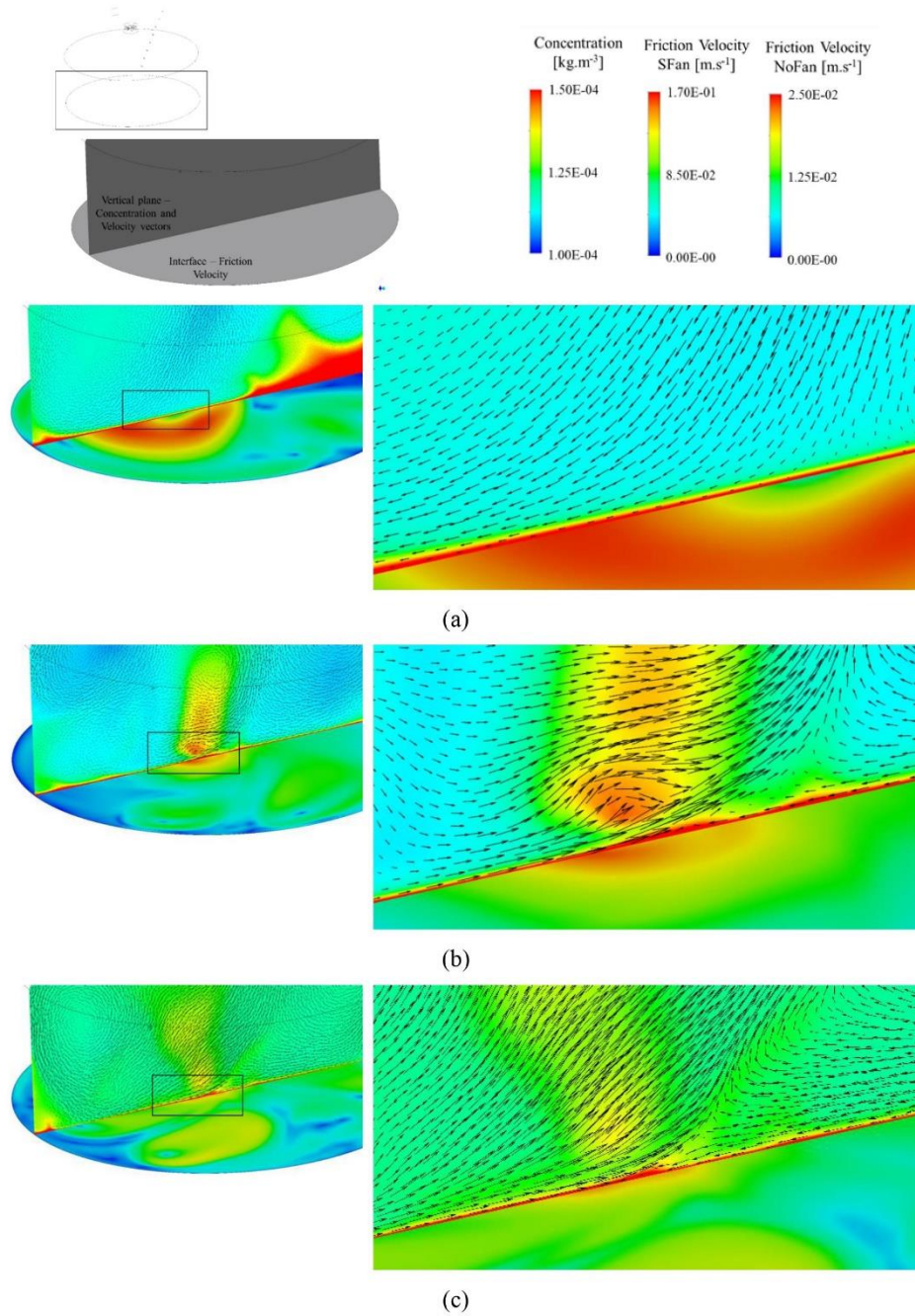


Figure 13 – Numerical results of vertical plane concentration, velocity vectors and interface wall friction velocity: (a) No Fan 5 L min⁻¹, (b) SFanUp 5 L min⁻¹ and (c) SFanDown 5 L min⁻¹.

CONCLUSIONS

Emission rates and mass transfer coefficients for an acetic acid solution were evaluated from experiments performed with the original USEPA flux hood (No Fan configuration) and the modified flux hood with different internal fan configurations. For all tested scenarios, the emission rates and gas-phase mass transfer coefficients generally increased with the inlet sweep air flow rate, showing an approximated linear trend.

In the experiments with the modified flux hood (Added Fan configurations), not all tested fan configurations resulted in higher emissions and mass transfer coefficients inside the flux hood compared to the original USEPA flux hood (no Fan configuration). For the scenarios in which the use of a fan promoted an increase or decrease in emission rate and mass transfer coefficients, the differences to the No Fan configuration were rather small.

Investigations were carried out using the computational fluid dynamics technique to understand the influence of inlet sweep air flow rate and fan configuration on emission rate. The computational simulations showed that the increase in friction velocity promoted by the fan in some regions which would increase the mass transfer coefficient is compensated by a thicker mass transfer boundary layer, with a smaller concentration gradient over the same regions, leading to only small changes in the emission rates. Further examination of the flow patterns near the liquid-gas interface inside the hood revealed these zones of high friction velocity, for the cases with the fan, have convergent flow, which favours compound accumulation, thereby reducing the concentration gradients. Thus, the computational fluid dynamics technique helped to understand why emission rates were found in the same order of magnitude with or without the use of an internal fan, which is contrary to the intuitive hypothesis that the use of a fan inside the flux hood would enhance the emission of odorants measured on liquid surfaces.

ACKNOWLEDGMENTS

The authors acknowledge the sponsorship from Coordenação de Aperfeiçoamento de Pessoal de Nível Superior (CAPES), Conselho Nacional de Desenvolvimento Científico e Tecnológico (CNPq), Fundação de Amparo à Pesquisa do Espírito Santo (FAPES) and Companhia Espírito Santense de Saneamento (CESAN), Brazil. A. Prata is a Visiting Fellow at the ARC Training Centre for the Transformation of Australia's Biosolids Resource. We are

very thankful to Rob Jenkins of WRL Workshop for the design and construction of the internal fan coupling frame.

REFERENCES

- Andréão, Willian L., Jane M. Santos, Neyval C. Reis, Ademir A. Prata, and Richard M. Stuetz. 2019. "Effects of Flux Chamber Configuration on the Sampling of Odorous Gases Emissions." *International Journal of Heat and Mass Transfer* 140: 918–30. <https://doi.org/10.1016/j.ijheatmasstransfer.2019.06.029>.
- Andréão, Willian Lemker, and Rita de Cassia Feroni. 2022. "CFD Modeling of Different Mass Transfer Coefficients on Hydrogen Sulfide Emission in a Flux Chamber." *Environmental Science and Pollution Research* 29 (10): 14961–74. <https://doi.org/10.1007/s11356-021-16855-2>.
- Aneja, V. 2001. "Measurement and Analysis of Atmospheric Ammonia Emissions from Anaerobic Lagoons." *Atmospheric Environment* 35 (11): 1949–58. [https://doi.org/10.1016/S1352-2310\(00\)00547-1](https://doi.org/10.1016/S1352-2310(00)00547-1).
- Aneja, Viney P, J P Chauhan, and J T Walker. 2000. "Characterization of Atmospheric Ammonia Emissions from Swine Waste Storage and Treatment Lagoons Hog Waste TKN of the Surface Lagoon Water Ranged from 7 to 8 PH Units , and 500 to 750 Mg N L - •, Decreased through the Fall - •) to a Minimum Flux during Th." *Journal of Geophysical Research* 105 (D9): 11535–45.
- Bazemo, Ulrich, Elena Gardner, Adrian Romero, Helene Hauduc, Ahmed Al-Omari, Imre Takacs, Sudhir Murthy, Alba Torrents, and Haydée de Clippeleir. 2021. "Investigating the Dynamics of Volatile Sulfur Compound Emission from Primary Systems at a Water Resource Recovery Facility." *Water Environment Research* 93 (2): 316–27. <https://doi.org/10.1002/wer.1417>.
- Beghi, Sandra P, Augusto C Rodrigues, Leandro M de Sá, and Jane Meri. 2012. "Estimating Hydrogen Sulphide Emissions from an Anaerobic Lagoon" 30: 91–96.
- Blanes-Vidal, Victoria, Jesper Bælum, Joel Schwartz, Per P Løfstøm, and Lars Christensen. 2014. "Respiratory and Sensory Irritation Symptoms among Residents Exposed to Low-to-Moderate Air Pollution from Biodegradable Wastes." *Journal of Exposure Science & Environmental Epidemiology* 24 (April): 388–97.
- Capelli, Laura, Selena Sironi, Renato del Rosso, and Paolo Céntola. 2009. "Predicting Odour Emissions from Wastewater Treatment Plants by Means of Odour Emission Factors." *Water Research* 43 (7): 1977–85. <https://doi.org/10.1016/j.watres.2009.01.022>.
- Cheng, Wen-hsi, Shu-kang Hsu, and Ming-shean Chou. 2008. "Volatile Organic Compound Emissions from Wastewater Treatment Plants in Taiwan : Legal Regulations and Costs of Control" 88: 1485–94. <https://doi.org/10.1016/j.jenvman.2007.07.022>.
- Daelman, Matthijs R J, Ellen M van Voorthuizen, Udo G J M van Dongen, Eveline I P Volcke, and Mark C M van Loosdrecht. 2012. "Methane Emission during Municipal Wastewater Treatment" 6. <https://doi.org/10.1016/j.watres.2012.04.024>.
- Eklund, Bart. 1992. "Practical Guidance for Flux Chamber Measurements of Fugitive Volatile Organic Emission Rates." *Journal of the Air and Waste Management Association* 42 (12): 1583–91. <https://doi.org/10.1080/10473289.1992.10467102>.
- Gholson, Alex R., John R. Albritton, R. K.M. Jayanty, Joseph E. Knoll, and M. Rodney Midgett. 1991. "Evaluation of an Enclosure Method for Measuring Emissions of Volatile Organic Compounds from Quiescent Liquid Surfaces." *Environmental Science and Technology* 25 (3): 519–24. <https://doi.org/10.1021/es00015a021>.

- Glaz, Patricia, Maciej Bartosiewicz, Isabelle Laurion, Elke S Reichwaldt, Roxane Maranger, Anas Ghadouani, and Q C Hc. 2016. "Greenhouse Gas Emissions from Waste Stabilisation Ponds in Western Australia and Quebec (Canada)." *Water Research* 101: 64–74. <https://doi.org/10.1016/j.watres.2016.05.060>.
- Gostelow, P., S. A. Parsons, and R. M. Stuetz. 2001. "Odour Measurements for Sewage Treatment Works." *Water Research* 35 (3): 579–97. [https://doi.org/10.1016/S0043-1354\(00\)00313-4](https://doi.org/10.1016/S0043-1354(00)00313-4).
- Hayes, J. E., R. J. Stevenson, and R. M. Stuetz. 2014. "The Impact of Malodour on Communities: A Review of Assessment Techniques." *Science of the Total Environment* 500–501: 395–407. <https://doi.org/10.1016/j.scitotenv.2014.09.003>.
- . 2017. "Survey of the Effect of Odour Impact on Communities." *Journal of Environmental Management* 204: 349–54. <https://doi.org/10.1016/j.jenvman.2017.09.016>.
- Hu, Lifang, Yao Du, and Yuyang Long. 2017. "Relationship between H₂S Emissions and the Migration of Sulfur-Containing Compounds in Landfill Sites." *Ecological Engineering* 106: 17–23. <https://doi.org/10.1016/j.ecoleng.2017.05.026>.
- Hudson, N., and G. A. Ayoko. 2009. "Comparison of Emission Rate Values for Odour and Odorous Chemicals Derived from Two Sampling Devices." *Atmospheric Environment* 43 (20): 3175–81. <https://doi.org/10.1016/j.atmosenv.2009.03.050>.
- Jiang, Kaiyun, Peter J. Bliss, and Terry J. Schulz. 1995. "The Development of a Sampling System for Determining Odor Emission Rates from Areal Surfaces: Part i. Aerodynamic Performance." *Journal of the Air and Waste Management Association* 45 (11): 917–22. <https://doi.org/10.1080/10473289.1995.10467424>.
- Klenbusch, M. 1986. "Measurement of Gaseous Emission Rates from Land Surfaces Using an Emission Isolation Flux Chamber." Austin, Texas.
- Lebrero, Raquel, Lynne Bouchy, Richard Stuetz, and Raúl Muñoz. 2011. *Odor Assessment and Management in Wastewater Treatment Plants: A Review. Critical Reviews in Environmental Science and Technology*. Vol. 41. <https://doi.org/10.1080/10643380903300000>.
- Liu, Lisha, Ademir Abdala Prata Junior, Ruth M. Fisher, and Richard M. Stuetz. 2022. "Measuring Volatile Emissions from Biosolids: A Critical Review on Sampling Methods." *Journal of Environmental Management* 317 (September): 115290. <https://doi.org/10.1016/j.jenvman.2022.115290>.
- Lotesoriere, Beatrice, Mario Invernizzi, Alessandra Panzitta, Giulia Uvezzi, Roberto Sozzi, Selena Sironi, and Laura Capelli. 2022. "Micrometeorological Methods for the Indirect Estimation of Odorous Emissions." *Critical Reviews in Analytical Chemistry*.
- Lyman, Seth N., Marc L. Mansfield, Huy N.Q. Tran, Jordan D. Evans, Colleen Jones, Trevor O'Neil, Ric Bowers, Ann Smith, and Cara Keslar. 2018. "Emissions of Organic Compounds from Produced Water Ponds I: Characteristics and Speciation." *Science of the Total Environment* 619–620: 896–905. <https://doi.org/10.1016/j.scitotenv.2017.11.161>.
- Menter, F. R. 1994. "Two-Equation Eddy-Viscosity Turbulence Models for Engineering Applications." *AIAA Journal* 32: 1598–1605.
- Navaratnasamy, M., J. J.R. Feddes, and I. K. Edeogu. 2004. "Comparison of Wind Tunnel and Vented Flux Chamber in Measuring Odour Emission Rates." *ASAE Annual International Meeting 2004* 51 (2001): 6181–89. <https://doi.org/10.13031/2013.17108>.
- Parker, D., Ham, J., Woodbury B., Cai, L. Spiels, M. Rhoades, M. Trabue, S., Casey, K., Todd, R., Cole, A. 2013a. "Standardization of flux chamber and wind tunnel flux measurements for quantifying volatile organic compound and ammonia emissions from

- area sources at animal feeding operations". *Atmospheric Environment* 66, 72-83. doi:10.1016/j.atmosenv.2012.03.068
- Parker, David B, Edward Caraway, Marty Rhoades, Chanci Donnell, Jan Spears, N Andy Cole, Richard W Todd, and Kenneth D Casey. 2013. "Effect of Wind Tunnel Air Velocity on VOC Flux Rates from CAFO Manure and Effect of Wind Tunnel Air Velocity on VOC Flux Rates from CAFO Manure and Wastewater," no. June 2014. <https://doi.org/10.13031/2013.25026>.
- Parker, David B., John Gilley, Bryan Woodbury, Ki Hyun Kim, Geordie Galvin, Shannon L. Bartelt-Hunt, Xu Li, and Daniel D. Snow. 2013a. "Odorous VOC Emission Following Land Application of Swine Manure Slurry." *Atmospheric Environment* 66: 91–100. <https://doi.org/10.1016/j.atmosenv.2012.01.001>.
- . 2013b. "Odorous VOC Emission Following Land Application of Swine Manure Slurry." *Atmospheric Environment* 66: 91–100. <https://doi.org/10.1016/j.atmosenv.2012.01.001>.
- Pino-Herrera, Douglas O., Yannick Fayolle, Eric D. van Hullebusch, David Huguenot, Giovanni Esposito, and Yoan Pechaud. 2022. "Surface Volatilization Modeling of (Semi-)Volatile Hydrophobic Organic Compounds: The Role of Reference Compounds." *Journal of Hazardous Materials* 424 (February): 127300. <https://doi.org/10.1016/j.jhazmat.2021.127300>.
- Prata, Ademir A., Federico Lucernoni, Jane M. Santos, Laura Capelli, Selena Sironi, Nhat Le-Minh, and Richard M. Stuetz. 2018. "Mass Transfer inside a Flux Hood for the Sampling of Gaseous Emissions from Liquid Surfaces – Experimental Assessment and Emission Rate Rescaling." *Atmospheric Environment* 179 (February): 227–38. <https://doi.org/10.1016/j.atmosenv.2018.02.029>.
- Prata, Ademir A., Jane M. Santos, Sandra P. Beghi, Isabella F. Fernandes, Lya L.C. vom Marttens, Leovegildo I. Pereira Neto, Ramon S. Martins, Neyval C. Reis, and Richard M. Stuetz. 2016. "Dynamic Flux Chamber Measurements of Hydrogen Sulfide Emission Rate from a Quiescent Surface - A Computational Evaluation." *Chemosphere* 146: 426–34. <https://doi.org/10.1016/j.chemosphere.2015.11.123>.
- Prata, Ademir A., Jane M Santos, Sandra P Beghi, Isabella F Fernandes, Lya L C Vom, Leovegildo I Pereira, Ramon S Martins, Neyval C Reis, and Richard M Stuetz. 2016. "Chemosphere Dynamic Flux Chamber Measurements of Hydrogen Sulfide Emission Rate from a Quiescent Surface: A Computational Evaluation" 146: 426–34. <https://doi.org/10.1016/j.chemosphere.2015.11.123>.
- Prata, Ademir A., Jane M. Santos, Victoria Timchenko, Neyval C. Reis, and Richard M. Stuetz. 2017. "Wind Friction Parametrisation Used in Emission Models for Wastewater Treatment Plants: A Critical Review." *Water Research* 124: 49–66. <https://doi.org/10.1016/j.watres.2017.07.030>.
- Prata, Ademir A., Jane M. Santos, Victoria Timchenko, and Richard M. Stuetz. 2018. "A Critical Review on Liquid-Gas Mass Transfer Models for Estimating Gaseous Emissions from Passive Liquid Surfaces in Wastewater Treatment Plants." *Water Research* 130 (March): 388–406. <https://doi.org/10.1016/J.WATRES.2017.12.001>.
- . 2021. "Modelling Atmospheric Emissions from Wastewater Treatment Plants: Implications of Land-to-Water Roughness Change." *Science of the Total Environment* 792 (October). <https://doi.org/10.1016/j.scitotenv.2021.148330>.
- RONG, L., P.V. NIELSEN, and G. ZHANG. 2009. "Effects of Airflow and Liquid Temperature on Ammonia Mass Transfer above an Emission Surface: Experimental Study on Emission Rate." *Bioresource Technology* 100: 4654–61.
- Saha, Chayan Kumer, Wentao Wu, Guoqiang Zhang, and Bjarne Bjerg. 2011. "Assessing Effect of Wind Tunnel Sizes on Air Velocity and Concentration Boundary Layers and on

Manuscript submitted to Chemosphere

- Ammonia Emission Estimation Using Computational Fluid Dynamics (CFD).” *Computers and Electronics in Agriculture* 78 (1): 49–60. <https://doi.org/10.1016/j.compag.2011.05.011>.
- Santos, Jane Meri, Virginie Kreim, Jean Michel Guillot, Neyval Costa Reis, Leandro Melo de Sá, and Nigel John Horan. 2012. “An Experimental Determination of the H₂S Overall Mass Transfer Coefficient from Quiescent Surfaces at Wastewater Treatment Plants.” *Atmospheric Environment* 60: 18–24. <https://doi.org/10.1016/j.atmosenv.2012.06.014>.
- Schiffman, Susan S, and C M Williams. 2005. “Science of Odor as a Potential Health Issue.” *Journal of Environmental Quality* 34 (1): 129–38. <https://doi.org/10.2134/jeq2005.0129>.
- Sironi, Selena, Laura Capelli, Paolo Céntola, Renato del Rosso, and Sauro Pierucci. 2010. “Odour Impact Assessment by Means of Dynamic Olfactometry, Dispersion Modelling and Social Participation.” *Atmospheric Environment* 44 (3): 354–60. <https://doi.org/10.1016/j.atmosenv.2009.10.029>.
- Smith, R. J., and P. J. Watts. 1994. “Determination of Odour Emission Rates from Cattle Feedlots: Part 1, A Review.” *Journal of Agricultural Engineering Research*. <https://doi.org/10.1006/jaer.1994.1014>.
- Tran, Huy N.Q., Seth N. Lyman, Marc L. Mansfield, Trevor O’Neil, Richard L. Bowers, Ann P. Smith, and Cara Keslar. 2018. “Emissions of Organic Compounds from Produced Water Ponds II: Evaluation of Flux Chamber Measurements with Inverse-Modeling Techniques.” *Journal of the Air and Waste Management Association* 68 (7): 713–24. <https://doi.org/10.1080/10962247.2018.1426654>.
- Vergote, Tine L.I., Samuel Bodé, Anke E.J. de Dobbelaere, Jeroen Buysse, Erik Meers, and Eveline I.P. Volcke. 2020. “Monitoring Methane and Nitrous Oxide Emissions from Digestate Storage Following Manure Mono-Digestion.” *Biosystems Engineering* 196 (August): 159–71. <https://doi.org/10.1016/j.biosystemseng.2020.05.011>.
- Woodbury B. L., Parker D. B., Eigenberg R. A., Spiehs, M. J. 2011. “Flow Characteristics of a Dynamic EPA Flux Chamber.” In *Annual International Meeting of the American Society of Agricultural and Biological Engineers*.

5.2 Numerical investigation of flux hood fluid flow and mass transfer modified by an internal fan

To complement the analysis presented in Section 5.1, further numerical results were explored to explain, why among the cases investigated in laboratorial experiments testing the influence of the internal fan on the concentrations in the outlet probe, the mass transfer coefficients in the gaseous phase and the emission flux rates were similar considering the experimental uncertainties.

5.2.1 COMPARISON BETWEEN EXPERIMENTAL AND NUMERICAL ESTIMATION OF OUTLET PROBE CONCENTRATION

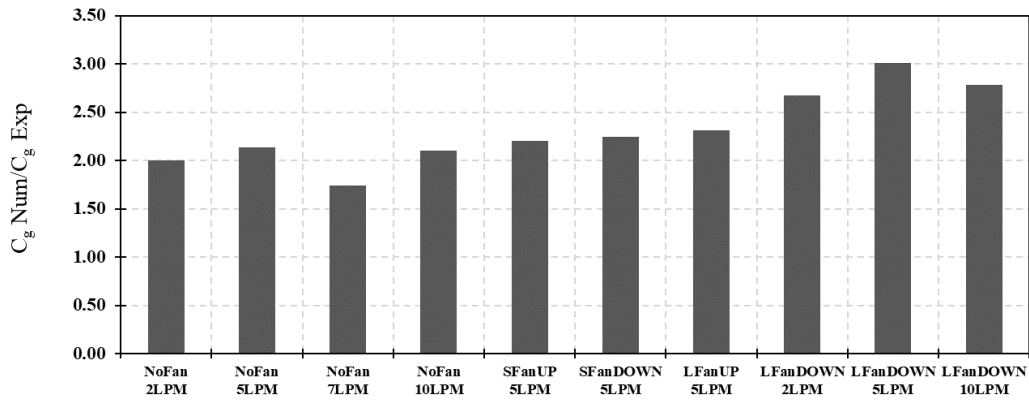
Figure 13 further extends the comparison between experimental and numerical results. We have previously analysed the No Fan scenarios for 2, 5 and 10 L min⁻¹ and the Small Fan Up and Down scenarios for 5 L min⁻¹. In addition to that, we analyze in this Section No Fan scenario for 7 L min⁻¹, Large Fan UP for 5 L min⁻¹ and Large Fan Down for 2, 5 and 10 L min⁻¹ scenarios.

Figure 13(a) data show the overestimation of the concentration obtained by numerical simulations of turbulent flow inside the flux hood. The ratios between the numerical and experimental concentrations fluctuate between approximately 1.75 and 3.00, with most cases reaching the ratio equal to 2.00. Initially analyzing cases without the fan inside, a lower ratio for flow 7 L min⁻¹ is noted. This result indicates a different trend of growth among the cases as observed in the experimental results, i.e., in the experimental results, a higher concentration was observed for the case 7 L min⁻¹ in relation to the linear adjustment with the other flows. The greatest differences observed between the numerical simulation results and the experiment were for LFanDown, considering the three flows presented.

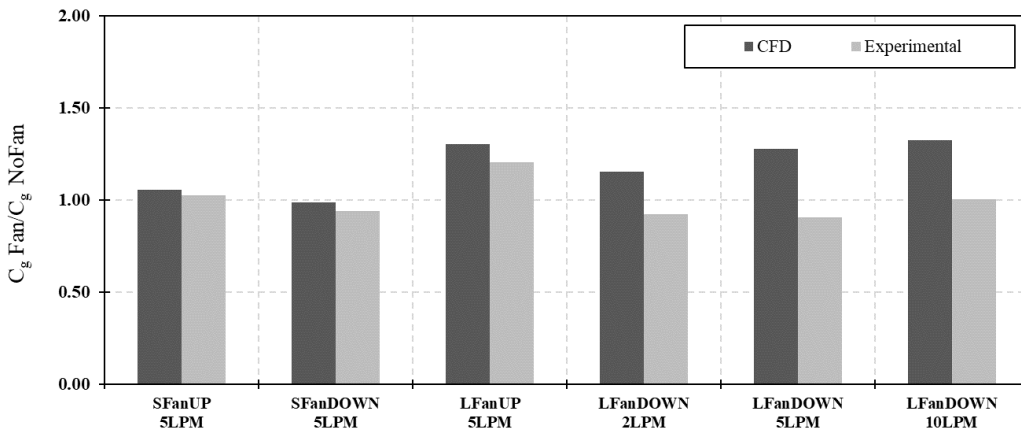
The boundary conditions for the conservation equations of momentum and mass of the compound implemented in the liquid-gas interface may be the cause for differences observed between the behaviour of the output concentration in the experiment and in the simulations. The consideration of wall and non-slip condition may be responsible for overestimating shear (and consequently, calculated friction velocity). The boundary condition for the concentration equation, i.e., estimated constant concentration based on the concentration of the compound in the liquid phase together with the effect of overestimated shear is possible cause of the higher concentration values obtained.

The data presented in Figure 13(b) is interesting from the point of view of the comparison between the cases without and with a fan. The best trends are noted for small fan cases, while

the worst compared scans were for Large Fan cases. For Large Fan cases the calculated friction velocities are the largest which can corroborate these differences.



(a)



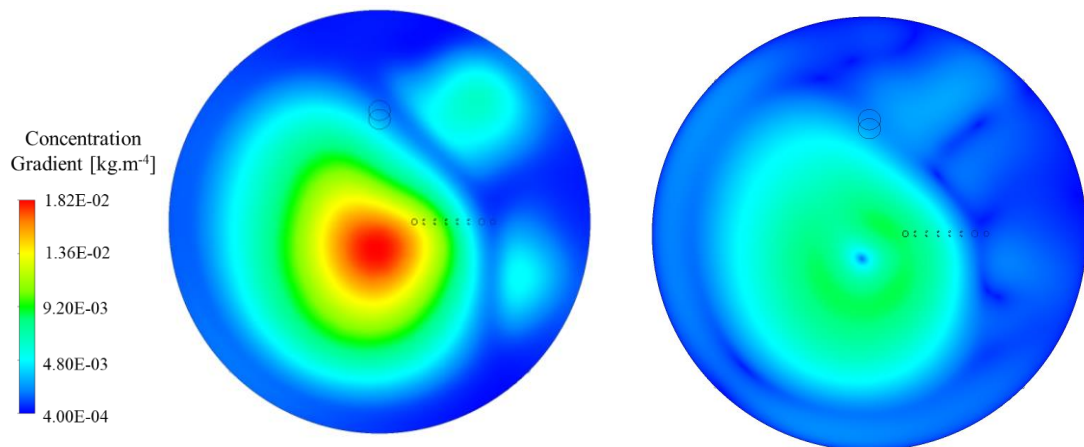
(b)

Figure 13 – Experimental and numerical results comparison for acetic acid volatilisation phenomena: (a) numerical and experimental outlet concentration ratio for No Fan 2, 5, 7 and 10 L min⁻¹, SFanUp and SFanDown 5 L min⁻¹, LFanUP for 5 L min⁻¹ and LFanDown for 2, 5 and 10 L min⁻¹ scenarios and (b) Fan vs. No Fan concentration ratio.

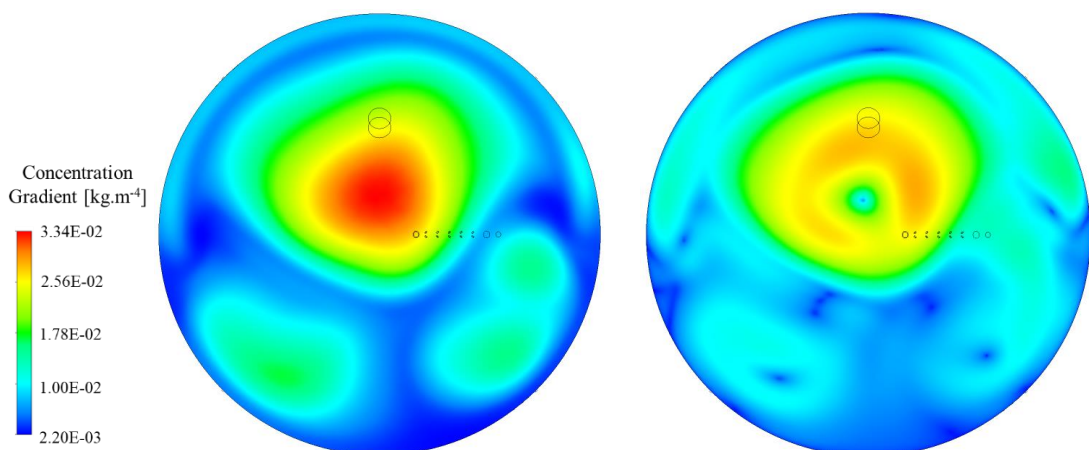
5.2.2 INTERFACE FRICTION VELOCITY AND NEAR WALL CONCENTRATION GRADIENT

Figure 14 and Figure 15 present friction velocity results at the interface and concentration gradient calculated in plane near the interface. Figure 14 presents cases without a fan and Figure 15 with fan are presented. The increase in flow rate (from 2 to 10 L min⁻¹) for No Fan cases is noticeable in the allocated friction velocity distribution at the interface (all graphics have the same color scale). The observed maximum concentration gradient increases as the sweep air

flow increases. The pattern of near-interface concentration distribution and friction velocity at the interface is quite similar between the different sweep air flows tested. The concentration of acetic acid in the outlet probe reduces slightly with increasing sweep air flow: $1.26\text{E-}04 \text{ kg m}^{-3}$ (2 L min^{-1}), $1.13\text{E-}04 \text{ kg m}^{-3}$ (5 L min^{-1}), $1.09\text{E-}04 \text{ kg m}^{-3}$ (7 L min^{-1}) and $1.06\text{E-}04 \text{ kg m}^{-3}$ (10 L min^{-1}). Even with the simultaneous increase in friction velocity and concentration gradient, the concentration of the outlet probe does not follow the observed. The influence of the increase in the volume of clean air in the headspace of the flux hood is more relevant in the result observed in the flux hood than the shear increment in the interface.



(a)



(b)

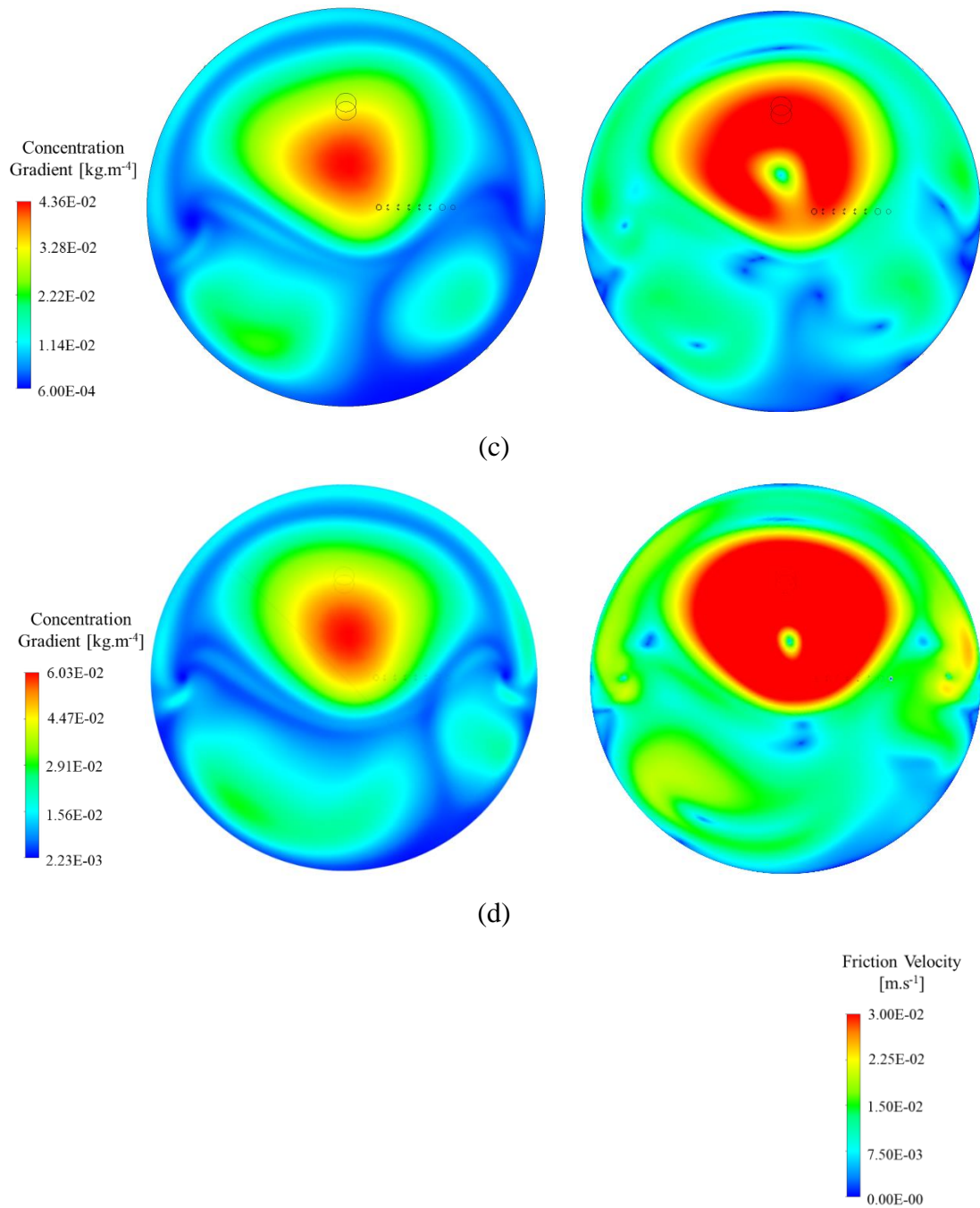
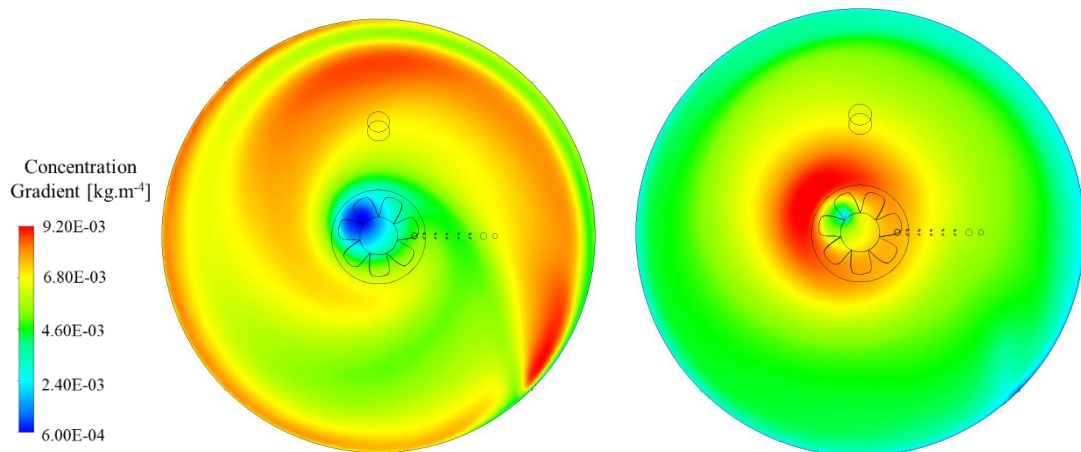


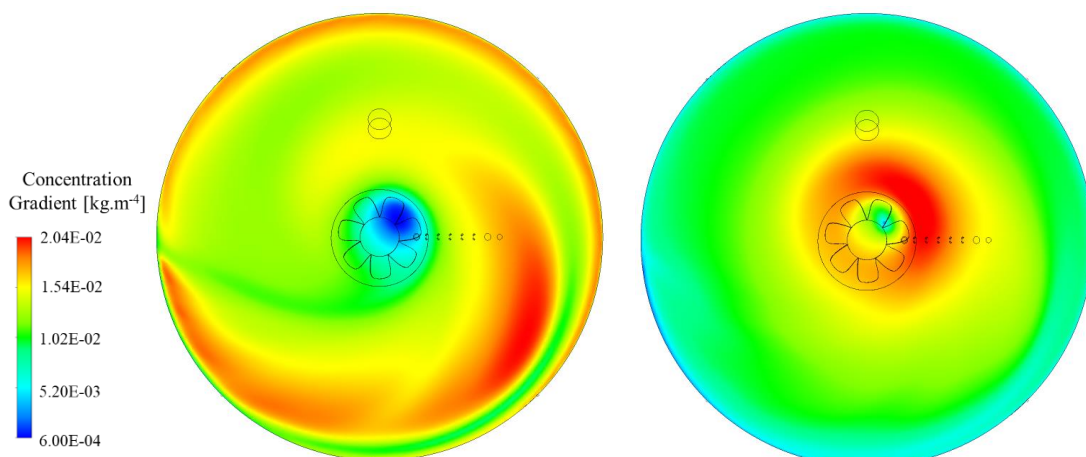
Figure 14 – Numerical results of near interface (0.5 mm from the interface) concentration gradient (top view) (a) No Fan 2LPM, (b) 5 LPM, (c) 7 LPM and (d) 10 LPM and (e) to (h) interface wall friction velocity values for the same scenarios as for (a) to (d).

To complement the result observed in the scenarios without fan and what was noticed in the experimental result we can investigate the numerical behaviour of cases with fan. Figure 15 presents the distribution results of the concentration gradient and friction velocity for the scenarios with a fan. For the LFanDown case, results are presented for two sweep air flows, 5 and 10 L min⁻¹. Differently from what was observed with the increase of sweep air flow in

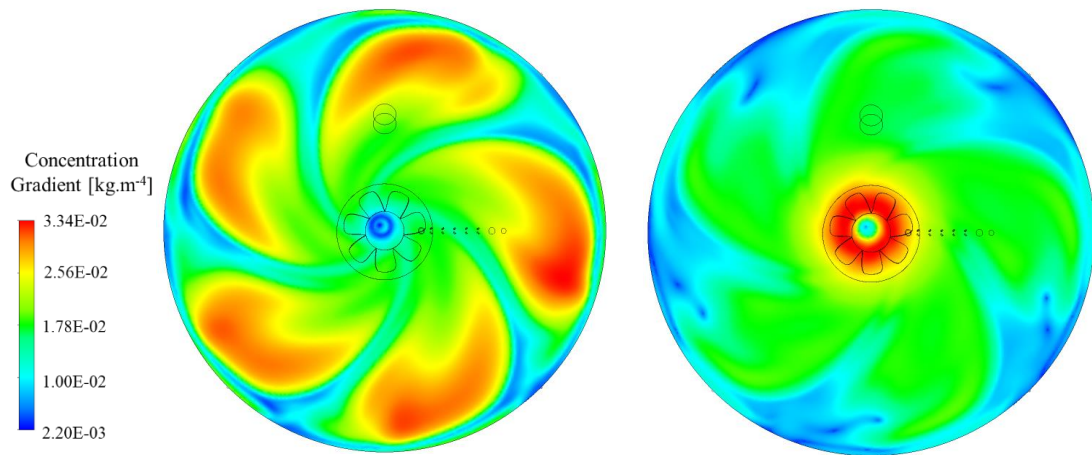
cases without a fan, the analysis of cases with fan follows another strategy of understanding. The increase in shear at the interface (quantified by the friction velocity) is spatially accompanied by regions of low concentration gradient as well as the inverse, i.e., regions with lower friction velocity are in similar regions with high concentration gradient – qualitatively observing the images shown in Figure 15. Comparing some scenarios of Figure 14 and Figure 15 we noticed that there is even a decrease in the maximum value of the concentration gradient near the interface even though it extends over a larger area. In Figure 15(c) the central part of the interface is characterized by local increase in friction velocity and low concentration gradient values.



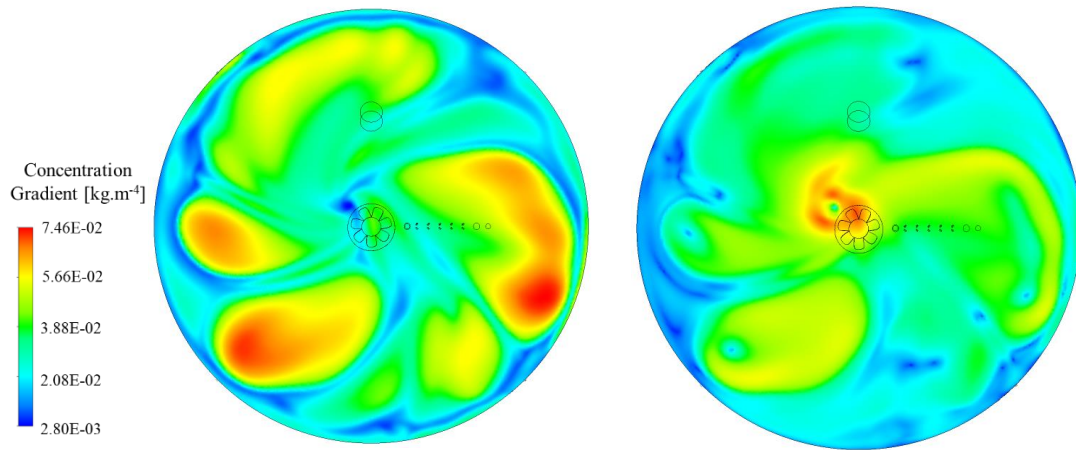
(a)



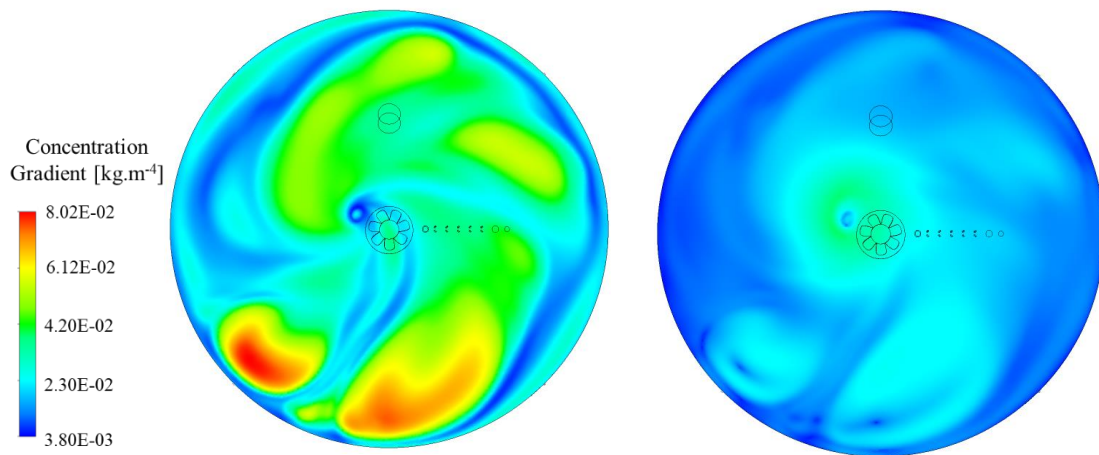
(b)



(c)



(d)



(e)

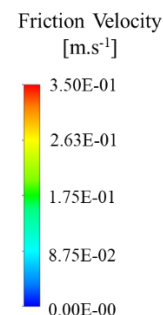


Figure 15 – Numerical results of near interface (0.5 mm from the interface) concentration gradient (top view) (a) LFanDown 5LPM, (b) LFanDown 10LPM, (c) LFanUp 5LPM, (d) SFanUp 5LPM and (e) SFanDown 5LPM and (f) to (j) interface wall friction velocity values for the same scenarios as for (a) to (e).

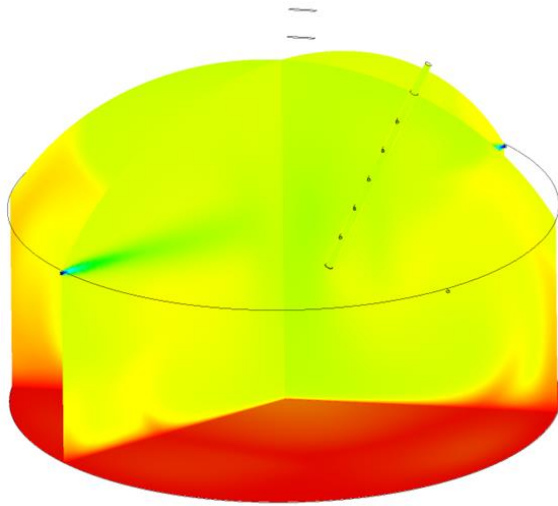
5.2.3 CONCENTRATION DISTRIBUTION AND TURBULENT KINETIC ENERGY

This section aims to investigate the 3D behaviour of flow and mass transfer in the headspace of flux hood. For this, 3 groups of results are presented: Figure 16 presents the 3D representation of the concentration distribution in three planes in the computational domain, Figure 17 and Figure 18 the distribution of turbulent kinetic energy in the domain and finally, Figure 19 lines coloured by acetic acid concentration.

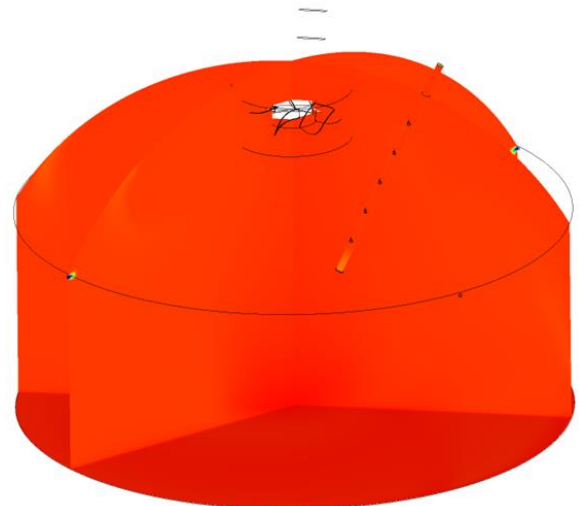
In general, the three result sets indicate the increase of the mixing in the headspace after fan insertion, regardless of size and rotation. The results of concentration distribution show the improvement of mixing efficiency if the cases without and with fan are observed. Another interesting point to note in Figure 16 is the modification of the sweep air flow pattern from the 4 holes. The No Fan flux hood features the direction of clean air flow to the central part of the headspace while the four fan cases show the vertical downward direction of this clean air. This phenomenon may favour the direction of cleaner air to the outlet probe line (see behaviour of the current lines explained in Figure 19). As a complementary result, below in Figure 19, are built streamlines coloured by the concentration of acetic acid. These streamlines were designed as those inside the domain that flows through the outlet probe line. Streamlines of Fan cases indicate, in general, a common behaviour: circular flow follows the flux hood walls (lateral and dome) and interface and spins close the center being exhausted by the outlet probe line. In that sense, clean air flow may be directed towards the suction holes.

Figure 17 and Figure 18 show turbulent kinetic energy distribution in a vertical plane evidencing the headspace of the flux hood. Initially, it is noted that the maximum observed

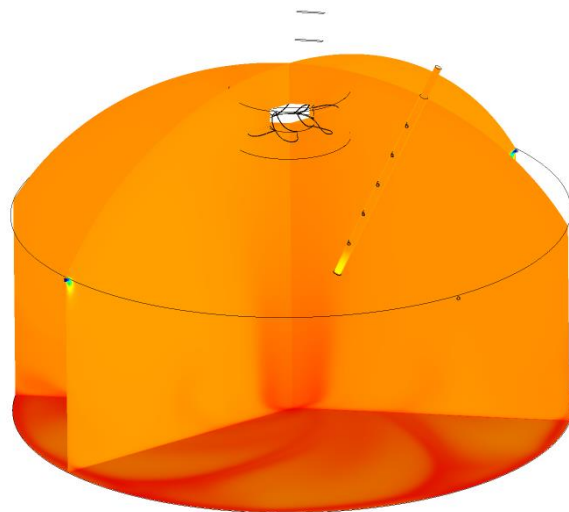
values of turbulent kinetic energy increase considerably between cases without (Figure 17) with fan (Figure 18). In addition, the distribution of turbulent kinetic energy is overall increased for the fan cases. LFanDown and LFanUp scenarios presented the highest values.



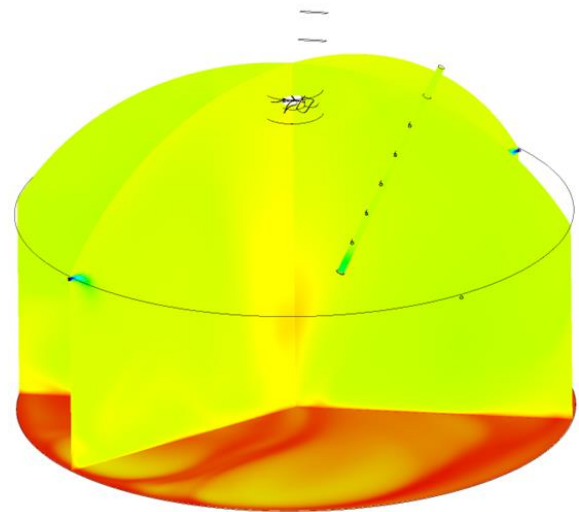
(a)



(b)



(c)



(d)

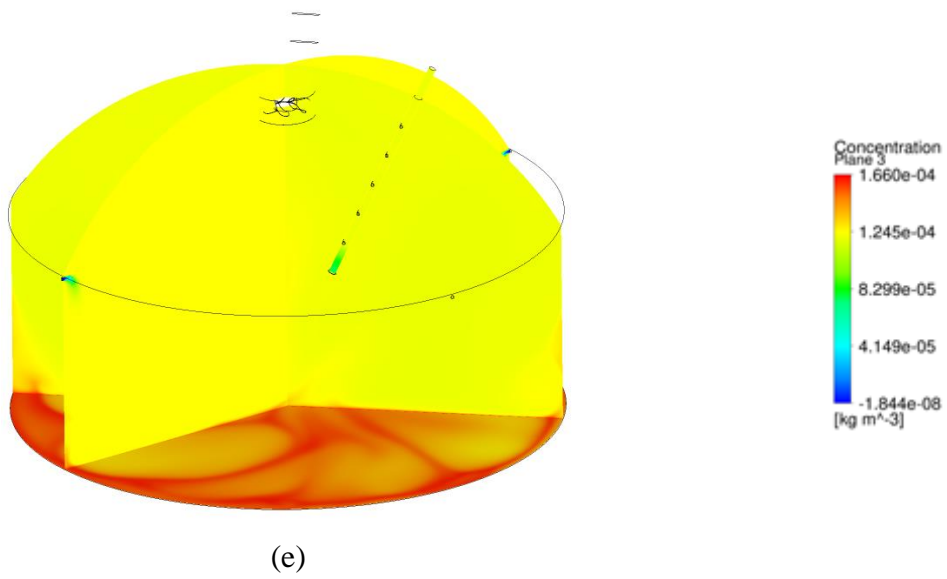
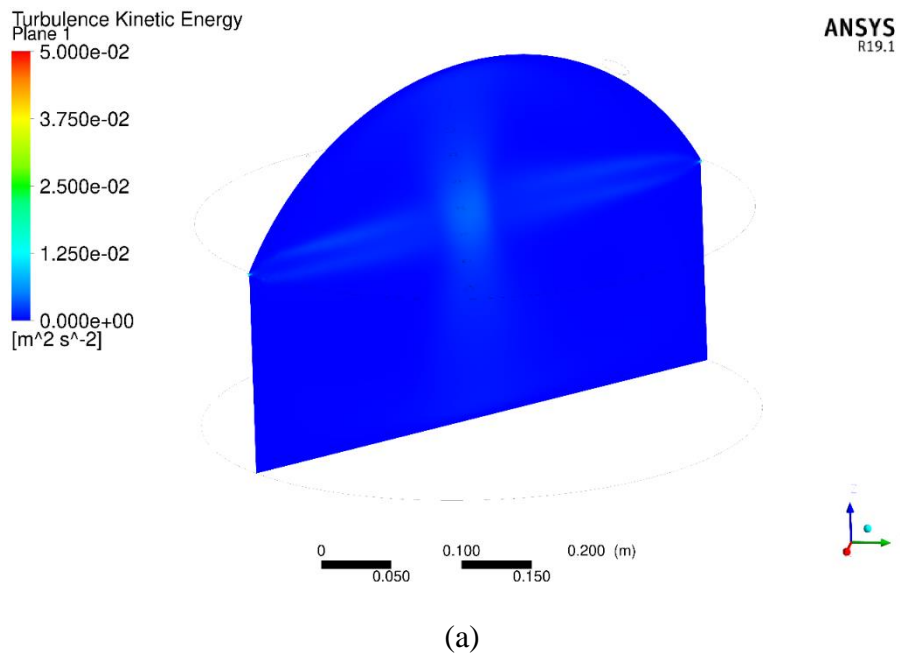
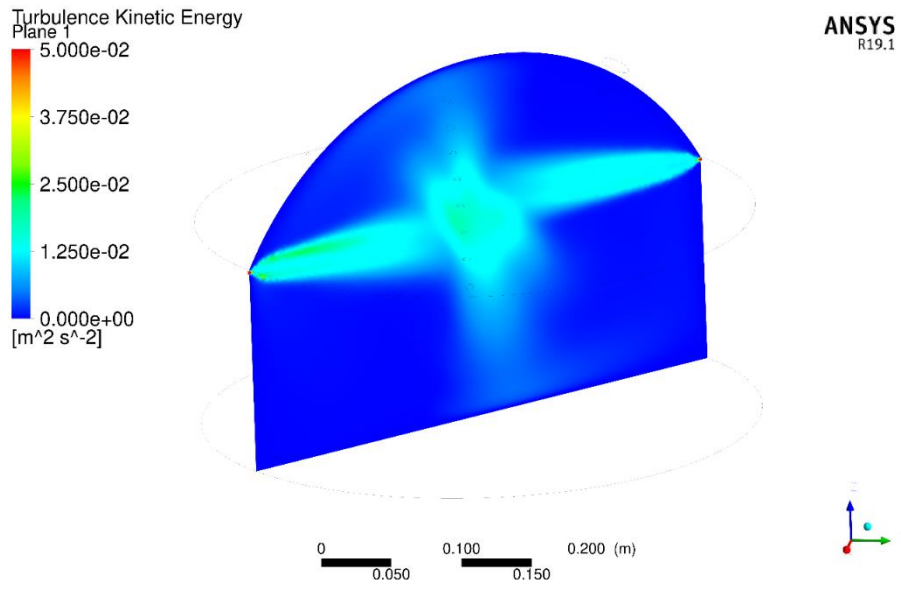
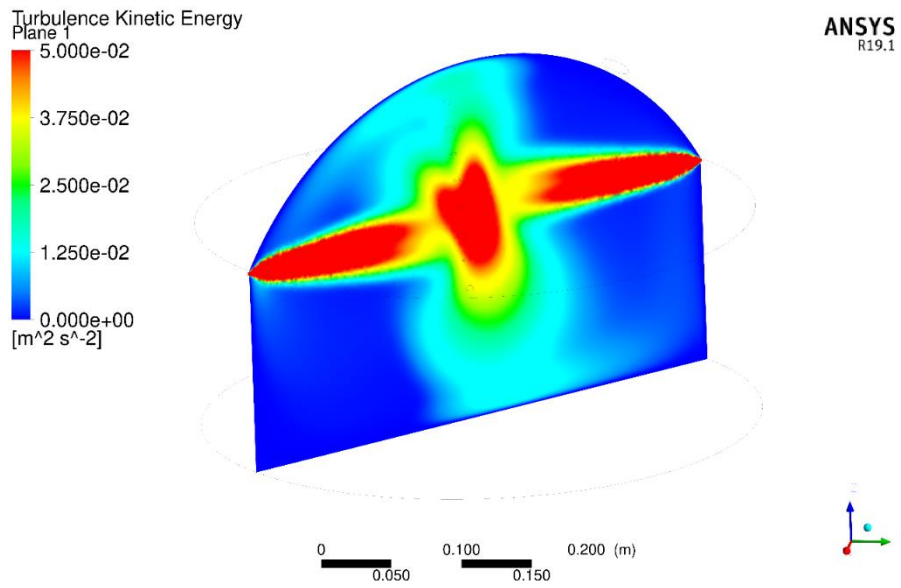


Figure 16 – Concentration distribution: (a) No Fan 5LPM, (b) LFanDown 5LPM, (c) LFanUp 5LPM, (d) SFanUp 5LPM and (e) SFanDown 5LPM.



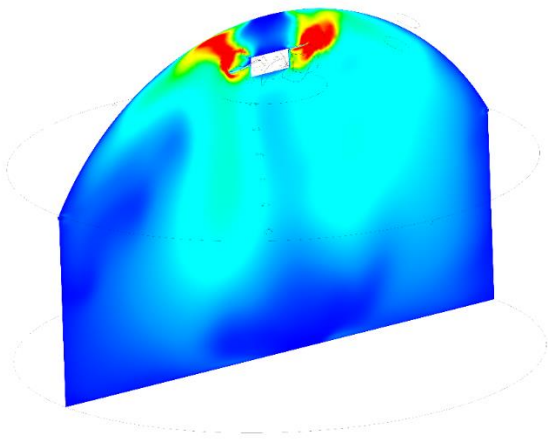


(b)

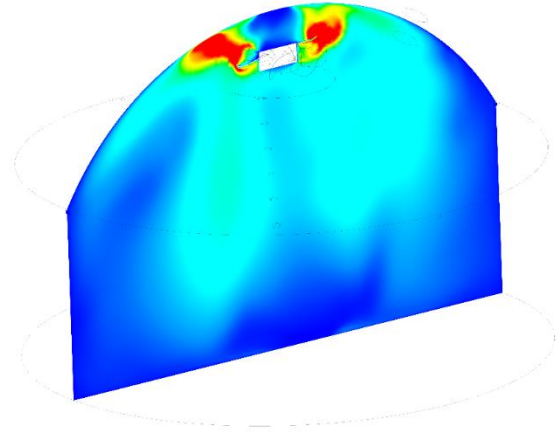


(c)

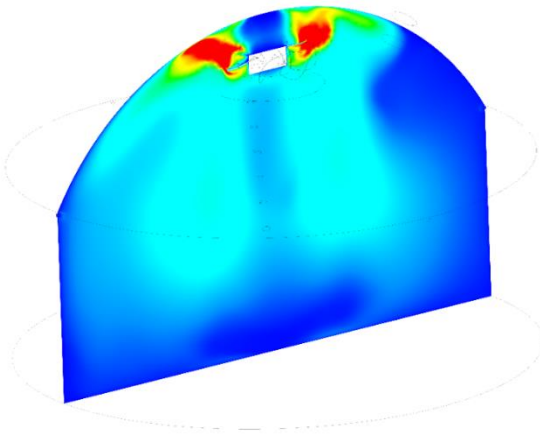
Figure 17 – Turbulent kinetic energy distribution: (a) No Fan 2LPM, (b) No Fan 5LPM and (c) No Fan 10LPM.



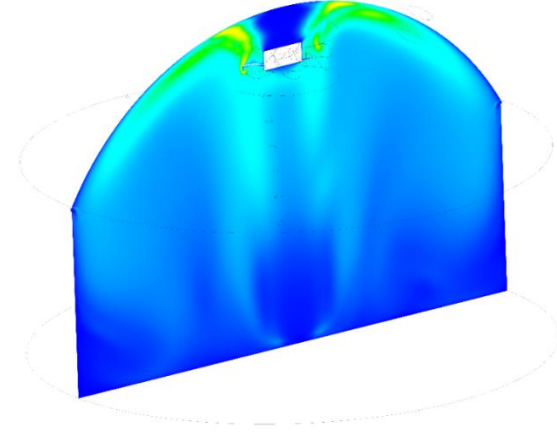
(a)



(b)



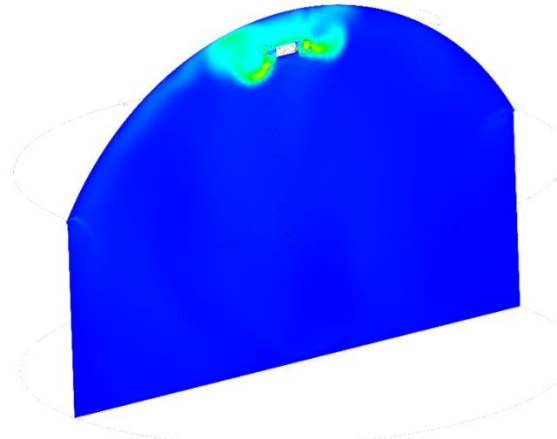
(c)



(d)



(e)



(f)

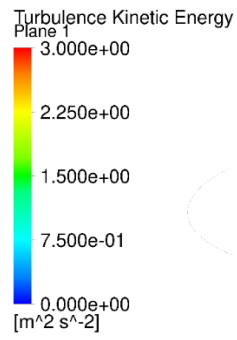
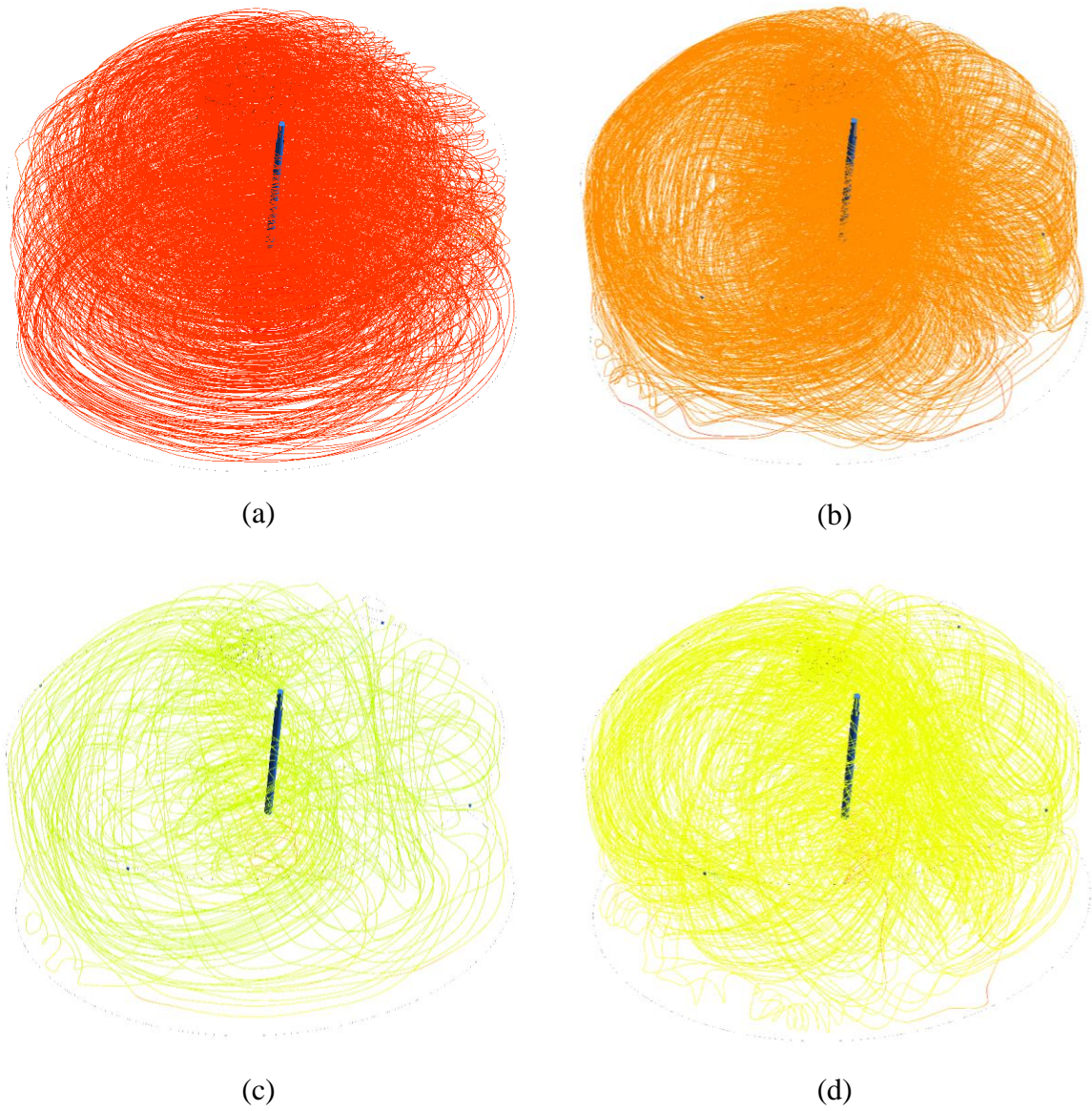


Figure 18 – Turbulent kinetic energy distribution: (a) LFanDown 2LPM, (b) LFanDown 5LPM, (c) (b) LFanDown 10LPM, (d) LFanUp 5LPM, (e) SFanUp 5LPM and (f) SFanDown 5LPM.



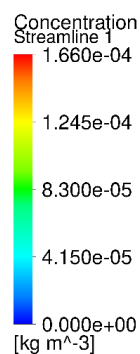


Figure 19 – Streamlines colored by concentration: (a) LFanDown 5LPM, (b) LFanUp 5LPM, (c) (b) SFanUp 5LPM and (d) SFanDown 5LPM.

5.3 Comparison of mass transfer parameters inside the USEPA flux hood for two VOCs

This section presents the evaluation of a procedure based on their Schmidt number to estimate the gas-film mass transfer coefficient (k_G) inside the original USEPA flux hood (No Fan) for a gas phase-controlled compound (acetic acid) based on a reference compound (butyric acid). This aim was listed as specific objective (iv) in Chapter 2. As it is shown and discussed in this Section, esters formation was observed in the chromatograph analysis, therefore, the explanation of this phenomenon was also included here.

It was communicated in a form of an article already published at Water Science & Technology to be submitted to a scientific journal for publication. The first two sections of the article presented below shows equivalent material regarding background information/state of the art and methodology already presented in Chapters 1 and 3 of this thesis, respectively. Therefore, the reader can move directly to the third section regarding the results without compromising the understanding of the thesis. The first two sections of the article presented below shows equivalent material regarding background information/state of the art and methodology already presented in Chapters 3 and 4 of this thesis, respectively. Therefore, the reader can move directly to the third section regarding the results without compromising the understanding of the thesis.



Comparison of mass transfer parameters inside a USEPA flux hood for two VOCs

Kamila F. Cupertino, Ademir A. Prata Jr, Nhat Le-Minh, Richard M. Stuetz and Jane M. Santos

ABSTRACT

Odororous emissions from area sources at wastewater treatment plants have become an environmental issue due to negative impacts on neighboring communities causing annoyance. Enclosure devices (such as dynamic flux chambers) have been used as direct methods to estimate area source emission rates from liquid–gas surfaces. Previously, model compounds have provided information about the internal mass transfer behavior of these sampling devices and the parameters estimated for certain model compounds that can be adapted for other compounds with similar liquid–gas partitioning properties. Acetic acid and butyric acid (both gas-phase-controlled compounds) were compared in order to assess the validity of adapting results from one compound to another. Mass transfer parameters for acetic acid and butyric acid were determined for a USEPA flux hood using a sweep air flow rate of 5 L/min. Mass transfer rates estimated for butyric acid, using the mass transfer parameters of acetic acid, were of the same order of magnitude as the experimental butyric acid mass transfer rates.

Key words | acetic acid, butyric acid, emission estimates, odorous emissions

Kamila F. Cupertino

Jane M. Santos

Departamento de Engenharia Ambiental,
Universidade Federal do Espírito Santo,
Vitória, ES,
Brazil

Ademir A. Prata Jr (corresponding author)

Nhat Le-Minh

Richard M. Stuetz

UNSW Water Research Centre, School of Civil and
Environmental Engineering,
The University of New South Wales,
Sydney, NSW 2052,
Australia
E-mail: ademir@unsw.edu.au

INTRODUCTION

Diffuse sources, such as industrial and domestic wastewater treatment plants (WWTPs), are associated with environmental impacts to air quality in neighborhood communities. They are important sources of odorous contaminants to the atmosphere such as nitrogen, sulfur and volatile organic compounds (VOCs). Their impacts include annoyance, which gives rise to complaints to authorities, adverse effects on human health and price depreciation of properties (Hayes *et al.* 2014, 2017; Brancher *et al.* 2017). Another potential environmental impact is related to greenhouse gas emissions generated from biological and chemical decomposition of organic matter.

Whereas point sources, such as stacks, can be easily subjected to periodic emission monitoring, this is not always the case for area sources. Nonetheless, the emission rate of odorous gaseous compounds shall be determined for the purpose of environmental impact assessments caused by such sources. The emission rate of compounds from passive liquid surfaces can be estimated by the use of one of the following methods (Gostelow *et al.* 2001; Hudson & Ayoko 2008a, 2008b; Prata *et al.* 2017): (i) predictive emission

models, (ii) reverse dispersion modelling (indirect method) and (iii) sampling with enclosure devices, such as a flux hood (dynamic flux chamber) or a wind tunnel (direct method).

Direct methods are characterized by the use of devices that enclose minimal parts of the emitting surfaces (enclosure devices) and directly sample the emissions. Flux hoods and portable wind tunnels are types of enclosure devices that are commonly used by environmental consulting firms, by wastewater treatment companies or by landfills to monitor variations in their process that can increase or decrease the emission of gases or odorants. In many instances, they are adopted by regulators as standards for the estimation of the emission rates in these enterprises.

Kienbusch (1986) presented standards and recommendations for the construction and operation of an emission insulation flux chamber (flux hood) for the assessment of gaseous emissions from contaminated soils. Later, the United States Environmental Protection Agency (USEPA) became interested in this technique for estimating emission rates from hazardous wastes and funded a series of projects

doi: 10.2166/wst.2020.197

to develop and evaluate the flux chamber method (Eklund 1992). This so-called USEPA flux hood is regarded as a standardized design worldwide, and has been used as a basis for other standards, such as the Australian standard AS/NZS 4323.4:2009, which adopts the same USEPA basic design, but includes an internal fan to enhance mixing.

Although it is essential to quantitatively measure the impact of a given source through the estimation of an emission rate and to assess the dispersion, monitoring emissions of atmospheric pollutants from area sources in the field presents specific difficulties and limitations. Enclosure devices require great care in their application and thorough understanding of their internal mass transfer conditions if meaningful measurements are to be obtained.

Prata *et al.* (2018a) discussed how the uncertainty in temperature at the liquid surface and other sources of inaccuracy may affect the estimation of mass transfer parameters when using the enclosure. They also proposed that having the mass transfer coefficients for a given compound, the mass transfer coefficients for another compound inside the flux hood could be estimated using appropriate powers of their Schmidt numbers. This estimate is convenient especially when, for reasons of operational limitations, the mass transfer parameters for a compound cannot be determined.

Thus, this work aims to measure experimental mass transfer parameters for acetic acid and butyric acid volatilizing from aqueous solutions inside the USEPA flux hood and to assess the validity of adapting results from one compound to another.

MATERIALS AND METHODS

The flux hood was made of Plexiglas® and followed the standard design proposed by Kienbusch (1986): a cylindrical body, with diameter of 40.5 cm and height of 17.2 cm, and a dome-shaped top whose highest part (at its central point) is 26.5 cm above the bottom. Figure 1 presents a picture of the device. At the dome-shaped top there were four equidistantly positioned holes, one of which was an opening, with diameter 2.1 cm, for pressure equilibration and balance flow release. The other three had diameter 1.3 cm and were used to fit 1/4" stainless steel bulkheads with the following purposes: one connected the sweep gas feed line to the internal inlet distribution tube; another connected the internal sampling probe to the outer sampling line; and the other was kept capped during the time of the runs. The sweep gas distribution tube was made of stainless



Figure 1 | USEPA flux hood.

steel, 1/4" OD, and fixed to the cylindrical body internal wall, at the height where the dome meets the body. It contained four equidistant inlet orifices, positioned horizontally (so as to produce horizontal inlet jets), the one closest to the inlet bulkhead connection having diameter 2.0 mm, and the other three, diameter 2.4 mm. The sampling probe consisted of a 6'-long tube, capped at the tip, perforated with two rows of holes, each row containing five holes with diameter 2.4 mm. The holes were separated 1' from each other along the tube length and positioned orthogonally in the radial direction. A Teflon® outlet line, 1/4" OD, connected to the sampling probe via one of the bulkheads, conveyed the sampled flow to Nalophan® bags (for the runs with acetic acid solution), which were filled using a 'lung system' as detailed in the work of Prata *et al.* (2018a). Sorbent tubes were used for the runs with butyric acid solution. The sweep air feed line, connecting the supplying gas bottle to the inlet distribution tube, was also Teflon® tubing, 1/4" OD.

The basic operation of the flux hood system was conducted according to the standard sampling procedure described by Kienbusch (1986), observing the additional recommendations of Eklund (1992) concerning sampling on liquid surfaces. The sweep air feed was supplied by instrument-grade air bottles and the flow rate of 5 L min⁻¹ was adjusted by a mass flow controller (Alicat Scientific, 5 SLPM).

Volatilization of acetic acid

The flux hood was used to estimate the emission rate of acetic acid from an aqueous solution. Quantities of 1.7 L of Milli-Q® water and 40 mL of acetic acid glacial were mixed in an Erlenmeyer, which was sealed to avoid volatilization losses during the transport to the room where the flux hood experiments took place. The solution was

transferred to a cylindrical tank made of Plexiglas[®], with diameter 41.0 cm and height 8.5 cm; the depth of the liquid in the tank was approximately 1.3 cm. The flux hood was then placed over the tank and sweep air flow was started. The pump (Airchek Sampler) from the lung system was turned on with a pre-calibrated flow rate of approximately 200 mL min⁻¹ for Nalophan[®] bag sampling. During the experiment, the room, solution and flux hood interior temperatures were systematically measured with a thermometer, varying from 18.0 to 20.5 °C, respectively. The stabilization time was 30 min, following the recommendations of Eklund (1992). After this period, two samples were collected sequentially in Nalophan[®] bags, each being sampled for 20 min.

After removal of the Nalophan[®] bag from the lung system, a 0.5 mL sample was taken using a gas-tight syringe (2.5 mL SUPELCO, USA) and manually injected into the Gas Chromatograph coupled with a Mass Spectrometer Detector – GC (7890A, Agilent Technologies)–MSD (5977B, Agilent Technologies). Three injections were conducted for each Nalophan[®] bag sample. All samples were injected into the GC–MSD within 30 min after Nalophan[®] bag withdrawal from the lung system.

The GC–MSD was equipped with an HP-5MS 30 m × 0.25 mm × 0.25 μm column with helium as the carrier gas at a flow rate of 1.2 mL min⁻¹. The initial temperature of the GC oven was 60 °C for 0.1 min, increasing to 220 °C at 25 °C min⁻¹, and then being held for 1 min.

Calibration curves for acetic acid were established using gas samples at five known concentrations, produced by evaporating different amounts of pure standard solutions of the compounds into Nalophan[®] bags flushed with fixed volumes of sweep air as performed by Prata *et al.* (2018a).

Volatilization of butyric acid

Except for the sample collection, experiments to estimate the butyric acid emission rate followed similar procedures to those for acetic acid. The aqueous solution of butyric acid was obtained by mixing 0.5 mL of standard n-butyric acid and 1.7 L Milli-Q[®] water. The butyric acid aqueous solution was placed into the cylindrical tank, the flux hood was then placed over the tank and the sweep gas flow turned on. After the stabilization period, sampling was conducted with a sorbent tube connected directly to the exit of the sampling probe. The sampling pump was installed serially after the sorbent tube, so as to avoid contamination of the sample. A sampling flow rate of 75 mL min⁻¹ was kept by a mass flow controller (Alicat Scientific). The stabilization time was 30 min, following the recommendations of Eklund

(1992). After this period, five samples were collected sequentially in sorbent tubes, each tube having a sampling time of 5 min. Sample analysis was performed using GC (7890A, Agilent Technologies)–MSD (5975C, Agilent Technologies). A DB-VRX 30 m × 0.25 mm × 1.4 μm column was utilized for compound separation, with helium as the carrier gas at a flow rate of 1.2 mL min⁻¹. Sorbent tubes were loaded on an Ultra automatic sampler (Markes International, UK) and samples were thermally desorbed using a Unity thermal desorber (TD) (Markes International, UK). The GC column temperature was initially held at 50 °C for 2 min, then raised at a rate of 15 °C min⁻¹ to 200 °C, and then held for 5 min. The MSD data acquisition was set in full scan mode with a range from 35 to 325 m/z at a rate of four times per second.

Calibration curves for butyric acid were established using gas samples at five known volumes in duplicate, produced by evaporating different amounts of pure standard solutions of the compounds into sorbent tubes flushed with fixed volumes of sweep air. Before both sampling and calibration, the sorbent tubes were conditioned in a tube conditioner (Markes International, UK) for 30 min at a constant temperature of 50 °C so that any moisture or remaining compounds inside the tubes were evaporated.

Sorbent tubes were chosen for sampling after successive attempts to collect butyric acid gas samples using Nalophan[®] bags. GC–MSD readings showed a decay in concentrations higher than 20% for the same bag analysed, whereas this phenomenon was not observed in experiments with acetic acid in Nalophan[®] bags. Other sampling attempts were performed with Nalophan[®] bags previously conditioned with butyric acid, but the same instability was observed.

Emission rates and mass transfer coefficients from experiment results

The volatilization rate of the compounds, J (kg s⁻¹ m⁻²), inside the USEPA flux hood is calculated by Equation (1) (Kienbusch 1986). C_m is the measured gas-phase concentration (kg m⁻³), obtained directly from GC–MSD readings for acetic acid samples and calculated for butyric acid samples (mass obtained (kg) in chromatograph-reading versus sampled volume (m³)); Q is the sweep air flow rate (m³ s⁻¹) and A is the area (m²) of the surface enclosed by the hood ('footprint area'):

$$J = \frac{QC_m}{A} \quad (1)$$

The two-resistance model describes emission of compounds from the liquid phase to the gas phase inside the flux hood (see Prata *et al.* 2018a, 2018b). Based on this consideration, it is appropriate to describe the mass transfer conditions in the gas side by means of the gas-side mass transfer coefficient k_G (m s^{-1}), so that the mass flux (J_G) of a given compound through the region of major resistance in the gas phase ('gas film') can be expressed by Equation (2):

$$J_G = k_G(C_{G,i} - C_G) \quad (2)$$

where $C_{G,i}$ is the concentration of the compound immediately at the interface with the liquid phase and C_G is the concentration of the compound in the bulk gas. Analogously, the liquid-side mass transfer coefficient k_L (m s^{-1}) can be defined, and the mass flux (J_L) of a given compound through the region of major resistance in the liquid phase ('liquid film') expressed by Equation (3):

$$J_L = k_L(C_L - C_{L,i}) \quad (3)$$

where C_L is the concentration of the compound in the bulk liquid and $C_{L,i}$ is the concentration of the compound immediately at the interface with the gas phase.

Considering that the mass flux across the liquid film (J_L) is the same mass flux across the gas film (J_G), and assuming that at the interface between the liquid and gas phases the concentrations of compounds are in equilibrium and can be related by Henry's Law ($C_{G,i} = C_{L,i} K_H$, where K_H is the non-dimensional Henry's Law coefficient), Equation (4) can be obtained, in terms of the liquid-phase overall mass transfer coefficient (K_L) (see Prata *et al.* (2018b) for derivation and further comments):

$$J = K_L \left(C_L - \frac{C_G}{K_H} \right) \quad (4a)$$

$$\frac{1}{K_L} = \frac{1}{k_L} + \frac{1}{k_G K_H} \quad (4b)$$

Assuming complete mixing in the headspace of the flux hood, the concentration of the compounds in the bulk of the gas phase C_G can be approximated by the concentration C_m sampled in the Nalophan[®] bags in the experiments with acetic acid and estimated for butyric acid (mass obtained (kg) in chromatograph-reading versus sampled volume (m^3)). The bulk liquid-phase concentration of the compounds C_L is known beforehand in the experiments, based on the amount of the pure compound used to prepare

the aqueous solutions and the dissociation equilibrium constants (only non-dissociated acid is available for volatilization). The values of the compound's K_H corrected for the experimental temperatures are taken from the literature (Sander 2015). Using these values of K_H , C_L and C_G (C_m) together with the experimental volatilization rate J (calculated via Equation (1)), Equation (4) can be solved for the experimental overall mass transfer coefficient K_L .

If an organic compound is highly volatile ($1/k_L \gg 1/(k_G K_H)$) the liquid-phase resistance controls the volatilization process, and therefore the experimental K_L will represent an approximation of its liquid-side mass transfer coefficient, that is $k_L \approx K_L$. In contrast, acetic acid and butyric acid present $1/(k_G K_H) \gg 1/k_L$, meaning that their volatilization will be gas-phase-controlled and $k_G \approx K_L/K_H$. In other words, the experiments with a highly volatile compound provide experimental values for its k_L , and the experiments with a poorly volatile compound allow its k_G to be assessed.

Having k_G for a given compound, say $k_{G,1}$, Prata *et al.* (2018a) propose that the gas-side mass transfer coefficient $k_{G,2}$ for another compound inside the flux hood can be estimated using appropriate powers of their Schmidt numbers, as in Equation (5):

$$k_{G,2} = k_{G,1} \left(\frac{Sc_{G,2}}{Sc_{G,1}} \right)^{-2/3} \quad (5)$$

where $Sc_{G,1}$ is the Schmidt number in the gas phase of the compound for which k_G is known, and $Sc_{G,2}$ is the Schmidt number in the gas phase of the compound for which k_G is unknown.

RESULTS AND DISCUSSION

Volatilization rate and mass transfer coefficients of VOCs inside the flux hood

Table 1 presents the variation of the volatilization rates J of the VOCs for the sweep air flow rate ($Q = 5 \text{ L min}^{-1}$) including average, minimum and maximum of the experimental values of the overall mass transfer coefficient K_L and the gas-side mass transfer coefficient k_G for acetic and butyric acid (gas-phase-controlled volatilization for all compounds) obtained through Equation (4a) and considering $k_G \approx K_L/K_H$.

The library search (score >80%) provided by GC-MSD identified other compounds grouped with butyric acid:

(i) butyric acid, propyl ester; (ii) butyric acid, 2-methylpropyl ester; and (iii) butyric acid, butyl ester, that were not detected in the runs for the calibration curve. The areas detected for these compounds were of the same order of magnitude as the 'pure' butyric acid compound. This loss of butyric acid concomitantly with ester formation leads to an underestimation of the emission rate calculated in Equation (1), if concentration estimates for C_m are considered only based on the 'pure' butyric acid.

Through Equation (5), the gas-side mass transfer coefficient (k_G) of butyric acid was estimated using the experimental data (k_G) of acetic acid obtained here and presented in Table 1. The estimated gas-side mass transfer coefficient for butyric acid was $3.247 \times 10^{-4} \text{ m s}^{-1}$, i.e., about 14% larger than the one obtained experimentally ($2.843 \times 10^{-4} \text{ m s}^{-1}$). If the sum of the concentrations of butyric acid and compounds grouped with butyric acid (butyric acid, propyl ester; butyric acid, 2-methylpropyl ester; and butyric acid, butyl ester) was considered for obtaining k_G , the average obtained experimentally from Equation (4a) ($3.217 \times 10^{-4} \text{ m s}^{-1}$) would be 13% larger than the average shown in Table 1 ($2.843 \times 10^{-4} \text{ m s}^{-1}$), and closer to the estimated value (1% difference).

The results discussed above indicate that some reaction with ester formation could be occurring inside the flux hood, which may impair the accuracy of the mass transfer coefficient measurement for butyric acid. A background analysis, where the sampling procedure was performed with only Milli-Q® water in the cylindrical tank and samples were collected in sorbent tubes, did not find any significant background contaminant that could be involved in the formation of the esters. Considering this, tests were performed in order to inhibit the ester formation detected in the samples collected in the flux hood experiments, described as follows.

Tests for inhibition of the formation of butyric acid ester

The proposed tests differ in some aspects from the methodology initially performed for the acetic and butyric acid experiments. The direct dumping of the aqueous solutions

into the Plexiglas® cylindrical base was avoided because it was hypothesized that ester formation would be occurring between the aqueous butyric acid solution and some contaminant or component of the Plexiglas®. Plexiglas® is a plastic material made from polymers of methyl methacrylate, an ester of methacrylic acid. To avoid hypothetical contamination, ten Petri dishes were placed inside the cylindrical base to avoid direct contact of the aqueous solution with the Plexiglas®, as shown in Figure 2. The sum of the surface area of the Petri dishes was 0.7 m^2 and was considered in the volatilization rate calculations (Equation (1)). The average ambient temperature of the six experiments was $22.3 \text{ }^\circ\text{C}$ and the average temperature of the aqueous solution was $21.8 \text{ }^\circ\text{C}$. Table 2 summarizes the configurations adopted in the six experiments performed to inhibit ester formation.

In Experiment 1, the aqueous solution was placed directly into the Petri dishes and experimental settings were maintained. Experiment 2 was conducted considering the hypothesis of ester formation through the butyric acid reaction with some contaminant present in the Milli-Q® water. Thus, in this test, Milli-Q® water was replaced by tap water.

Experiment 3 was performed with Milli-Q® water, however the carrier gas used was replaced by nitrogen (instrument grade). Both pure air and nitrogen are recommended as sweep air by Eklund (1992).

In Experiment 4, air was used as carrier gas and Milli-Q® water for the butyric acid aqueous solution. In this test, the pH of the butyric acid aqueous solution was



Figure 2 | Petri dishes inside cylindrical base.

Table 1 | Emission rate and mass transfer parameters estimated for acetic acid and butyric acid through flux hood experiments

	J ($\mu\text{g s}^{-1} \text{ m}^{-2}$)			K_L (10^{-9} m s^{-1})			k_G (10^{-4} m s^{-1})		
	Average	Min	Max	Average	Min	Max	Average	Min	Max
Acetic acid	44.297	39.956	50.429	2.895	2.415	3.628	4.083	3.305	5.241
Butyric acid	0.316	0.311	0.321	1.694	1.662	1.734	2.843	2.789	2.910

Table 2 | Test configurations performed to inhibit ester formation

Experiment	Type of water		Carrier gas			Stabilization time	
	Milli-Q	Tap water	Air	Nitrogen	Addition of H ₂ SO ₄	30 min	60 min
1 Air, Milli-Q®	X		X			X	
2 Air, Tap water		X	X			X	
3 N ₂ , Milli-Q®	X			X		X	
4 Air, Milli-Q®, H ₂ SO ₄	X		X		X	X	
5 N ₂ , Milli-Q®, H ₂ SO ₄ , 30'	X			X	X	X	
6 N ₂ , Milli-Q®, H ₂ SO ₄ , 60'	X			X	X		X

modified by adding approximately 1 mL of sulfuric acid (H₂SO₄). After the addition of H₂SO₄, the pH of the mixture reduced on average from 3.55 to 1.85.

In Experiment 5, approximately 1 mL of H₂SO₄ was also added to the aqueous solution, prepared with Milli-Q® water, and nitrogen was used as the carrier gas. The liquid phase of the butyric acid aqueous solution was also sampled and analysed during this experiment to verify if ester formation was occurring in the liquid phase rather than in the gas phase. In this test, four samples of the liquid phase were collected at times 20, 50, 80 and 120 min after the initial time of the experiment; 10 mL of the liquid phase was sampled with a syringe and mixed in 100 mL of Milli-Q® water. Again with the use of a syringe, 15 µL of this mixture was injected into the calibration rig for sorbent tube preparation and flushed with nitrogen for 30 min. No ester was detected in the four samples from the liquid phase. The gas-phase samples were also collected, following the same methodology used in the other experiments, ester formation being observed in these samples. This is strong evidence that the esters were being formed in the gas phase.

In Experiment 6, there was a change from the methodology, with samples being collected after waiting 60 min of stabilization time, instead of the 30 min proposed by

Eklund (1992). Table 3 presents the experimental k_G results for the six tests performed inside the flux hood. The average emission rate (J) and overall mass transfer coefficient (K_L) obtained for the six experiments were $0.546 \mu\text{g s}^{-1} \text{m}^{-2}$ and 2.719m s^{-1} , respectively.

A last test was performed (Experiment 7) where the concentration of butyric acid in the solution was doubled (1 mL of pure butyric acid in 1.7 L Milli-Q® water, that is, 0.588mL L^{-1}). As in experiments 4, 5 and 6, about 1 mL of H₂SO₄ was added to the aqueous solution to lower the pH of the solution. With the same flow rate of 5L min^{-1} , nitrogen was used as sweep air. The prepared aqueous solution was immediately placed into the Petri dishes. The experimental average for k_G was $4.087 \times 10^{-4} \text{m s}^{-1}$, but ester compounds grouped with butyric acid were detected. These results indicate that even by doubling the initial concentration of the aqueous solution, ester formation in the gas phase was not inhibited.

CONCLUSIONS

Flux hood experiments were performed to estimate the mass transfer parameters of acetic acid and butyric acid

Table 3 | Emission rate and mass transfer parameters estimated from tests for inhibition of the formation of butyric acid esters

	$J (\mu\text{g s}^{-1} \text{m}^{-2})$			$K_L (10^{-9} \text{m s}^{-1})$			$k_G (10^{-4} \text{m s}^{-1})$		
	Average	Min	Max	Average	Min	Max	Average	Min	Max
1 Air, Milli-Q®	0.518	0.517	0.519	2.639	2.632	2.645	3.916	3.907	3.925
2 Air, Tap water	0.519	0.519	0.520	2.646	2.644	2.649	3.927	3.923	3.931
3 N ₂ , Milli-Q®	0.546	0.530	0.569	2.813	2.703	2.977	4.090	3.930	4.328
4 Air, Milli-Q®, H ₂ SO ₄	0.550	0.535	0.561	2.781	2.669	2.857	4.864	4.668	4.997
5 N ₂ , Milli-Q®, H ₂ SO ₄ , 30'	0.547	0.533	0.567	2.526	2.442	2.645	3.457	3.441	3.619
6 N ₂ , Milli-Q®, H ₂ SO ₄ , 60'	0.598	0.591	0.607	2.906	2.853	2.960	4.225	4.149	4.304

(both compounds having their volatilization controlled by the gas phase) from aqueous solutions inside the flux hood and to assess the validity of adapting results from one compound to another via Equation (5). Mass transfer parameters for acetic acid could be successfully measured. Mass transfer rates estimated for butyric acid, using the mass transfer parameters of acetic acid, were of the same order of magnitude as the experimental butyric acid mass transfer rates. This indicates an overall successful application of Equation (5), despite the fact that the results for butyric acid indicated the presence of esters in addition to butyric acid, which compromised the precise estimation of the mass transfer parameters for butyric acid.

Additional tests were performed to investigate the ester formation and the possibility of inhibiting it: replacement of Milli-Q® water with tap water; replacement of air as a carrier gas by nitrogen; and change in pH of aqueous butyric acid solution with approximately 1 mL of H₂SO₄. Although some combinations contributed to an increase in the mass transfer coefficient k_G , ester formation was still detected in all tests. Liquid-phase samples were collected during an experiment with the flux hood and no ester formation was identified in them, revealing that the ester formation was occurring in the gas phase. We recommend further research to explore this phenomenon in more detail.

ACKNOWLEDGEMENTS

The authors acknowledge the sponsorship from Coordenação de Aperfeiçoamento de Pessoal de Nível Superior (CAPES), Conselho Nacional de Desenvolvimento Científico e Tecnológico (CNPq), Fundação de Amparo à Pesquisa do Espírito Santo (FAPES) and Companhia Espírito Santense de Saneamento (CESAN), Brazil.

REFERENCES

- AS/NZS 4323.4:2009 2009 *Stationary Source Emissions Method 4: Area Source Sampling – Flux Chamber Technique*. Australia/New Zealand Standards.
- Brancher, M., Griffiths, K. D., Franco, D. & Lisboa, H. M. 2017 A review of odour impact criteria in selected countries around the world. *Chemosphere* **168**, 1531–1570.
- Eklund, B. 1992 Practical guidance for flux chamber measurements of fugitive volatile organic emission rates. *Journal of the Air & Waste Management Association* **42** (12), 1583–1591.
- Gostelow, P., Parsons, S. A. & Stuetz, R. M. 2001 Odour measurements for sewage treatment works. *Water Research* **35** (5), 579–597.
- Hayes, J. E., Stevenson, R. J. & Stuetz, R. M. 2014 The impact of malodour on communities: a review of assessment techniques. *Science of the Total Environment* **500–501**, 395–407.
- Hayes, J. E., Stevenson, R. J. & Stuetz, R. M. 2017 Survey of the effect of odour impact on communities. *Journal of Environmental Management* **204**, 349–354.
- Hudson, N. & Ayoko, G. A. 2008a Odour sampling 1: physical chemistry considerations. *Bioresource Technology* **99** (10), 3982–3992.
- Hudson, N. & Ayoko, G. A. 2008b Odour sampling 2: comparison of physical and aerodynamic characteristics of sampling devices: a review. *Bioresource Technology* **99** (10), 3993–4007.
- Kienbusch, M. 1986. *Measurement of Gaseous Emission Rates from Land Surfaces Using an Emission Isolation Flux Chamber*. EPA/600/8-86/008, US Environmental Protection Agency, Washington, DC, USA.
- Prata Jr, A. A., Santos, J. M., Timchenko, V., Reis Jr, N. C. & Stuetz, R. M. 2017 Wind friction parametrisation used in emission models for wastewater treatment plants: a critical review. *Water Research* **124**, 49–66.
- Prata Jr, A. A., Lucernoni, F., Santos, J. M., Capelli, L., Sironi, S., Le-Minh, N. & Stuetz, R. M. 2018a Mass transfer inside a flux hood for the sampling of gaseous emissions from liquid surfaces – experimental assessment and emission rate rescaling. *Atmospheric Environment* **179**, 227–238.
- Prata Jr, A. A., Santos, J. M., Timchenko, V. & Stuetz, R. M. 2018b A critical review on liquid–gas mass transfer models for estimating gaseous emissions from passive liquid surfaces in wastewater treatment plants. *Water Research* **130**, 388–406.
- Sander, R. 2015 Compilation of Henry's law constants (version 4.0) for water as solvent. *Atmospheric Chemistry and Physics* **15**, 4399–4981.

First received 18 December 2019; accepted in revised form 11 April 2020. Available online 24 April 2020

5.4 Experimental assessed emission rate rescaling to real meteorological and source conditions

In the literature review Chapter, it was stated that doubts remain concerning if the flux hood should be expected to mimic atmospheric conditions (i.e., conditions in which the real emission occurs) regarding friction velocity for volatilisation gas-phase controlled odorous gases and if it is possible to have the measured emission staggered to a field situation. Based on that, as listed in Chapter 2, one specific objective was established: (v) Evaluate uncertainty implication of the presence of a fan for the scaling up of measured emission rates of gas phase-controlled compounds with the flux hood.

The bias between measured emission in laboratory and values that could be expected in the field in the absence of sampling device were evaluated by comparing the values of mass transfer obtained experimentally with the values obtained from the volatilisation model proposed by Prata-Brutsaert (PRATA et al., 2021) a hypothetical case and a real wastewater treatment plant (WWTP).

Before proceeding with the evaluation, a brief report on the Prata-Brutsaert model is presented, as well as the description of the two investigated scenarios.

5.4.1 VOLATILISATION MODEL PROPOSED BY PRATA-BRUTSAERT

According to Prata et al. (2021), although wind friction velocity (u^*) is a critical variable for a more robust and physically based modelling of k_G and k_L , u^* itself is not routinely measured in most practical applications of emission models for WWTP. Therefore, u^* must in turn be estimated, which is normally done by using correlations between u^* and the wind speed at a reference height.

A compiled of correlations to parametrize u^* was evaluated in Prata et al. (2017) showing that it tended to overestimate u^* . Besides, other aspect related to the parametrisation of wind friction used in emission models for WWTP comes up with the fact that the meteorological records of the reference wind speed are normally for the wind over land (typically at a height of 10 m). However, as illustrated by Prata et al. (2021), an internal boundary layer (IBL) occurs due to the difference in roughness between the land and the liquid surface (as illustrated in the Figure 20), and the friction velocity over the liquid surface is not in direct equilibrium with the reference wind velocity (JÓZSA; MILICI; NAPOLI, 2007).

Thereby, the Prata-Brutsaert model incorporated the IBL development in combination with the parametrisation of u^* for the specific case of WWTP and similar water bodies assessing their effect

for a range of fetch sizes and wind speeds. Being z_{0U} , X and U_{10} roughness parameter, total fetch and the wind speed at $Z_{ref} = 10m$, respectively; for $0.005 m \leq z_{0U} \leq 0.20 m$; $50 m \leq X \leq 300 m$; and $1 m s^{-1} \leq U_{10} \leq 20 m s^{-1}$, the u_*^{Ch-RC} can be approximated by Equation (24):

$$u_*^{Ch-RC} \approx A_0 U_{10}^b X^c \quad (24)$$

where:

$$A_0 = -0.052 z_{0U}^{0.066} \quad (25)$$

$$b = 1.24 + 4.1 \times 10^{-3} \ln(z_{0U}) \quad (26)$$

$$c = 0.5 z_{0U}^{0.38} \quad (27)$$

u_*^{Ch-RC} indicates the use of Charnock's relation to parametrise the downwind roughness parameter (z_{0D}) over the liquid surface and the consideration of roughness change (“RC”) and IBL development in calculating the fetch-averaged u^* as the wind blows from land to water.

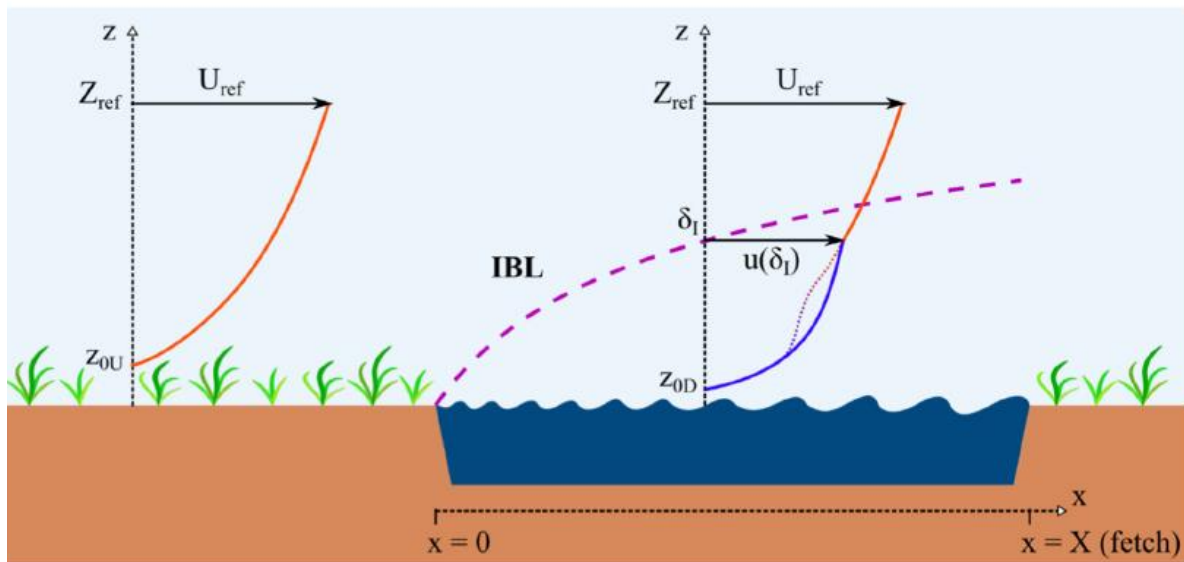


Figure 20 – Schematic representation of internal boundary layer (IBL) development over a liquid surface proposed by Prata et al. (2021).

According to Prata et al. (2021), the model of Brutsaert (1975) considers a well-developed, steady-state, two-dimensional turbulent wind boundary layer over a smooth flat surface. In this model,

the inner part of the turbulent boundary layer is divided in two sublayers: the so-called “interfacial sublayer”, which is the combination of the viscous and buffer sublayers, spanning from the surface ($z = 0$) to a height $z = z_s$; and the classical dynamic (logarithmic) sublayer, above $z = z_s$. Brutsaert (1975) proposes the value $z_s = 30\nu_G/u^*$ for the limit of the interfacial sublayer, being ν_G air viscosity. Based on this construction, the total resistance to mass transfer in the gas phase (R_G), between the surface ($z = 0$) and the top of the mass transfer boundary layer (height $z = \delta_M$, varying with the fetch), k_G (here denominated $k_{G,field}$) is given by the sum of two resistances in series: the resistance R_S , between $z = 0$ and z_s ; and the resistance R_M , between z_s and δ_M , as presented in equation (28), which can be defined as Prata-Brutsaert approach (it is detailed in supplementary material (SM) of Prata et al., (2021)Prata et al., (2021)).

$$k_{G,field} = \frac{1}{R_G} = \frac{1}{R_S} + \frac{1}{R_M} \quad (28)$$

Brutsaert (1975) derives the following expression for the resistance R_S :

$$R_S = \frac{13.6 Sc_G^{2/3}}{u^*} \quad (29)$$

And the resistance R_M is given by equation (30):

$$R_M = Sc_t \frac{1}{ku^*} \ln \left(\frac{\delta_M}{z_s} \right) \quad (30)$$

where Sc_t is the turbulent Schmidt number.

According to Prata et al. (2021) in the original model developed by Brutsaert (1975), the mass transfer boundary layer was assumed completely developed, thus the concentration was a function of height alone (that is, the concentration will be constant for a constant height). Nevertheless, for the liquid surfaces in WWTP, whose maximum fetch rarely exceeds a few hundred meters, this assumption is not valid, and a growing mass transfer boundary layer must be considered. In this sense, the application of equations (28), (29) and (30) to calculate $k_{G,field}$ requires the knowledge of the local values of u^* and δ_M along the emitting surface. Then, Prata et al. (2018) suggested that a fetch-averaged $\delta_{M,ave}$, which would produce an approximated “average” k_G for the surface

as presented in equation (31). This parametrization for the fetch-averaged δ_M (with $Sc_t=0.8$ and $k=0.4$) were shown to be very close to a data set of experimental k_G values for water evaporation in wind-wave tanks.

$$\frac{\delta_{M,ave}}{X} = 0.751 Re_*^{-0.236} X_*^{-0.138} \quad (31)$$

where $Re_* = u_* X / \nu_G$ is a fetch Reynolds number and $X_* = Xg/u_*^2$ is a non-dimensional fetch, being u_* also fetch-averaged.

5.4.2 HYPOTHETICAL SCENARIO

The hypothetical scenario is a medium-sized WWTP surrounded by with grass on the ground. The roughness parameter (z_{0U}) was chosen to be 0.005 m and total fetch (X) was chosen to be 50 m. The wind speed at $Z_{ref} = 10 \text{ m}$ (U_{10}) was varied from 1 m s^{-1} to 20 m s^{-1} to guarantee the applicability range of the Prata-Brutsaert model.

The k_G experimental results for acetic acid presented in Section 5.1 for the original USEPA flux hood with inlet sweep air flow of 2, 3, 5, 7 and 10 L min^{-1} were compared with the Prata-Brutsaert approach (equation (28)), as shown in Figure 21.

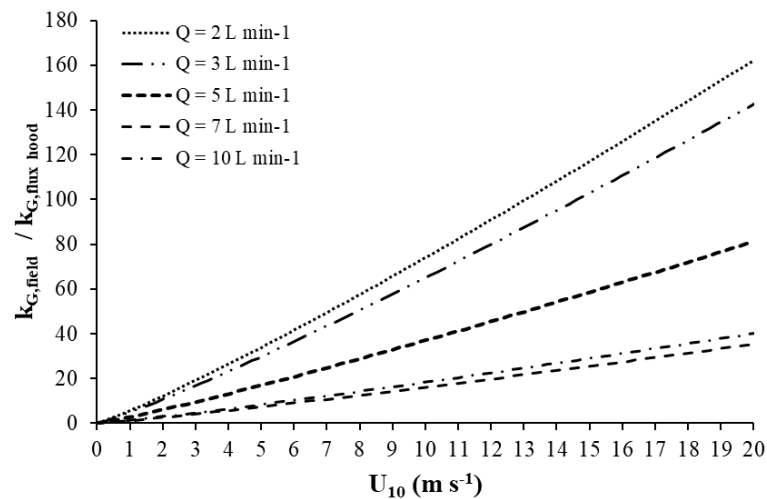


Figure 21 – Comparison of k_G values for acetic acid obtained from the original USEPA flux hood (No Fan) with inlet sweep air flow of 2, 3, 5, 7 and 10 L min^{-1} and those obtained using Prata-Brutsaert model proposed by Prata et al. (2021). for different wind speeds.

The k_G experimental data were closer to the Prata-Brutsaert model in the inlet sweep air flow 7 and 10 L m^{-1} configuration, coinciding with the highest inlet flows used in the experiments and the highest emission rates. Furthermore, this bias was on the order of up to 40 times at wind speeds close to 20 $m s^{-1}$. The bias for low wind situation (up to 2.5 $m s^{-1}$) was around 4 times.

On the other hand, the lowest flow chosen for inlet sweep air flow in the laboratory experiments ($Q = 2 L min^{-1}$) coincided for higher bias reaching 160 times for wind speed up to 20 $m s^{-1}$. Even in low wind condition, it is observed that the Prata-Brutsaert model to estimate k_G is on the order of 16 times greater when compared to the experimental data using flux hood device.

5.4.3 REAL WASTEWATER TREATMENT PLANT SCENARIO

Camburi WWTP is located in southeastern Brazil and is composed of three sequential ponds, as shown in Figure 22. Approximately, they form a rectangular geometric figure measuring 300 x 176 m with an average depth of 3.00 m. One of the ponds is aerated with surface aerators and the other two are stabilization ponds. The aerated pond may present bubbling due to aeration, which can significantly affect emission rates of volatile compounds (GRANT et al., 2013), however, all three ponds are considered in the present study as stabilization ponds.

Meteorological data (wind speed, direction, and average temperature) from the year 2020 were collected at Vitória Airport, which is located about one kilometre from the ponds. Two wind directions were chosen for the application of the Prata-Brutsaert model: 260° and 345°.

For the scenario in which wind direction is 260°, there is a potential impact in the neighborhood close to the WWTP (see their proximity in Figure 22), although it is not a wind direction that occurs very often in the region (see wind rose in Figure 22). A roughness of 0.005m was adopted for this wind direction due to low grass and free area used for landing and take-off of planes in the local airport.

For the scenario in which wind direction is 345°, the impact due to the emission in this wind direction is especially focused on the beach, which is in the southernmost part of the evaluated region (see Figure 22). A roughness of 0.20 m was adopted for this wind direction due to the large trees of the Atlantic Forest confined in a preservation area and located north of the WWTP.

In addition to acetic acid, using the same procedure proposed by Prata et al. (2018) presented in Section 5.3, the gas phase mass transfer coefficient values were also estimated for the compounds valeric acid, isobutyric acid and butyric acid using appropriate powers of their Schmidt numbers.

It is also worth mentioning that all these volatile compounds are gas phase control, which is one of the criteria for applying the methodology considering mass transfer parameters obtained from flux hood to the acetic acid compound.

Table 5 presents the average k_G obtained in the experiments carried out with the flux hood (see Section 5.1) for the acetic acid compound, it also presents the k_G estimated from the experimental k_G value of acetic acid, for the other compounds. It is important to note that the gas phase mass transfer coefficient varies with Q and experimental configuration, although it remains in the same order of magnitude.

The Schmidt numbers for pentanoic (valeric) acid, isobutyric acid and butyric acid presented in Table 5 were estimated by Sander (1999). Table 6 presents other parameters adopted and applied in the Prata-Brutsaert model to estimate the emission rate (here referred to as J_{mod}). Henry's law coefficient (K_H) was obtained with the same procedure described in Section 5.1, whereas the concentrations of the compounds in the liquid phase (C_L) were adopted based on the typical concentrations of these compounds in a WWTP (CHANTARASUKON; TUKKEEREE; ROHRER, 2016). The ambient temperature of 20°C was also adopted as a typical average obtained throughout 2020.

Table 5 – Estimating k_G gas phase control from k_G experimental.

Q	Experimental configuration	Acetic acid		Pentanoic acid (Valeric acid)		Isobutyric acid		Butyric acid	
		Sc_{G1}	k_{G1} (E-04)	Sc_{G2}	k_{G2} (E-04)	Sc_{G3}	k_{G3} (E-04)	Sc_{G4}	k_{G4} (E-04)
2	NoFan	1.37	1.40	1.98	1.15	1.79	1.23	1.94	1.17
2	LFanDown	1.37	1.09	1.98	0.85	1.79	0.91	1.94	0.87
2	LFanUp	1.37	1.53	1.98	1.20	1.79	1.28	1.94	1.21
2	SFanDown	1.37	1.04	1.98	0.82	1.79	0.87	1.94	0.83
2	SFanUp	1.37	1.23	1.98	0.96	1.79	1.03	1.94	0.98
5	NoFan	1.37	2.95	1.98	2.31	1.79	2.47	1.94	2.34
5	LFanDown	1.37	2.80	1.98	2.19	1.79	2.35	1.94	2.22
5	LFanUp	1.37	4.2	1.98	3.35	1.79	3.59	1.94	3.40
5	SFanDown	1.37	2.94	1.98	2.30	1.79	2.46	1.94	2.33
5	SFanUp	1.37	3.30	1.98	2.59	1.79	2.76	1.94	2.62
10	NoFan	1.37	5.94	1.98	4.65	1.79	4.98	1.94	4.71
10	LFanDown	1.37	6.35	1.98	4.97	1.79	5.32	1.94	5.04
10	LFanUp	1.37	7.97	1.98	6.24	1.79	6.68	1.94	6.33
10	SFanDown	1.37	6.78	1.98	5.31	1.79	5.68	1.94	5.38
10	SFanUp	1.37	9.54	1.98	7.47	1.79	7.99	1.94	7.57

Table 6 – Applying estimating k_G in Prata-Brutsaert model.

Temperature	Acetic acid		Pentanoic acid (Valeric acid)		Isobutyric acid		Butyric acid	
	K_H	C_L	K_H	C_L	K_H	C_L	K_H	C_L
	(E-05)	(Kg m ³)	(E-05)	(Kg m ³)	(E-05)	(Kg m ³)	(E-05)	(Kg m ³)
20°C	0.7194	0.0499	1.2021	0.0060	2.8473	0.0016	0.5816	0.0019

Figure 23, Figure 24 and Figure 25 present the comparing between the emission rate of the acetic acid obtained by using k_G from the Prata-Brutsaert model and the emission rates estimated using the flux hood device (with different configurations No Fan, LFanDown, LFanUp, SFanDown and SFanUp) with $Q = 2, 5$ and 10 L min^{-1} , respectively.

Analysing the inlet air flows, as the inlet flow increases, the emission rates obtained in the laboratory and the emission rates expected in the field approaches, especially for the LFanUp configuration. This behaviour is expected, since, due to the build-up concentration, the flux hood tends to underestimate the emission rate of the compound dominated by the gas phase for lower air flow rate. The increase in Q directly reflects the emission rate inside the flux hood. The LFanUp configuration (large fan installed inside the flux hood with rotation in the upwind direction) also favours mixing inside the camera, as discussed in Section 5.1, presenting a bias up to five times if compared to the expected emission rate in field.

Still analysing Figure 23, Figure 24 and Figure 25 for the acetic acid compound, it is observed that the bias between J_{mod}/J_{hood} is smaller for the configuration with 260° wind direction and roughness 0.005 m . Although the wind speed in the 345° wind direction is higher in relation to the wind speed in the 260° wind direction, when evaluating the wind rose, it is worth remembering that the Prata-Brutseart model takes into account in its parameterization that an internal boundary layer (IBL) occurs due to the difference in roughness between the land and the liquid surface (as illustrated in Figure 20), and the friction velocity over the liquid surface is not in direct equilibrium with the reference wind speed. Thus, if we adopt a 0.005 m roughness due to the background airstrip at Camburi WWTP, it has difference related to reduced liquid surface, implying in higher acetic acid emission rates in the 260° wind direction and 0.005 m roughness.

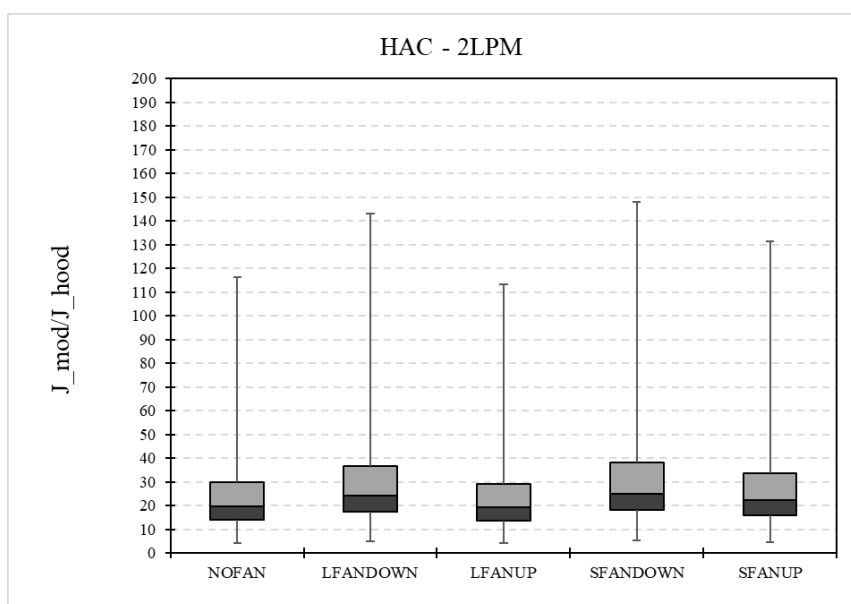
A similar behaviour was observed for the valeric acid compound (Figure 26, Figure 27 Figure 28); for the isobutyric acid compound (Figure 29, Figure 30 Figure 31) and for the butyric acid compound (Figure 32, Figure 33 and Figure 34). The SFanUp configuration estimated from tests carried out with the flux hood for the acetic acid compound (considering 260° wind direction and

inlet sweep air flow of 10 L min⁻¹) presented a median of 0.92 in relation to the Prata-Brutseart model. Similar results were observed for other compounds evaluated. On the other hand, the acetic acid compound presented the largest bias in relation to the Prata-Brutseart model in the SfanDown configuration (considering 345° wind direction and inlet sweep air flow of 2 L min⁻¹).



Figure 22 – The Camburi WWTP.

(a)



(b)

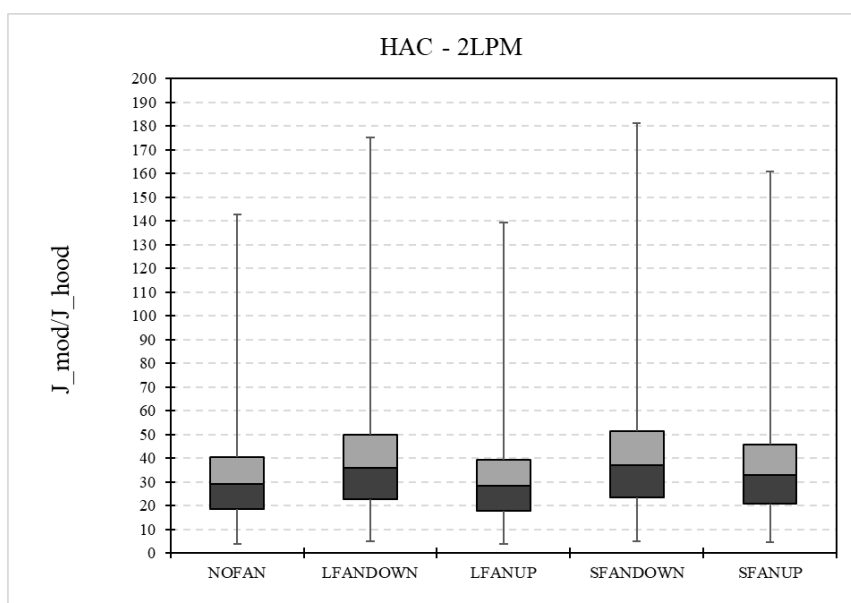
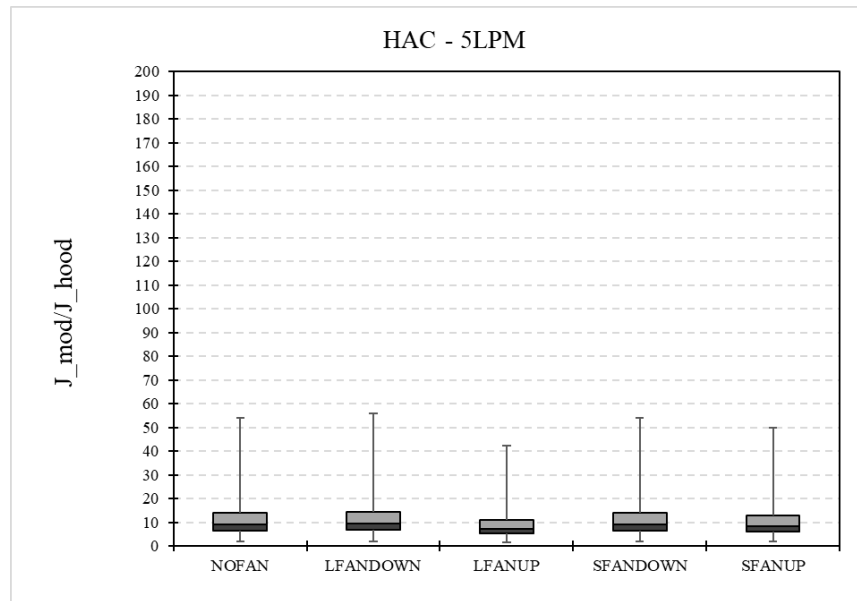


Figure 23 – Emission rate of acetic acid (HAC) at Camburi WWTP case: Comparison between the values obtained using the k_G model proposed by Prata et al. (2021) and the k_G values from the flux hood with $Q = 2 \text{ L min}^{-1}$. a) roughness 0.005 m and 260° wind direction. b) roughness 0.20 m and 345° wind direction.

(a)



(b)

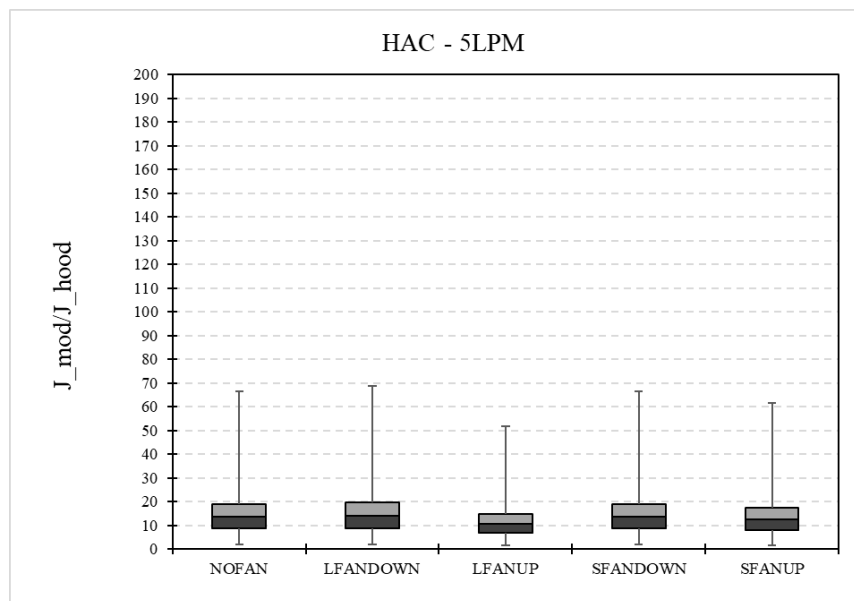
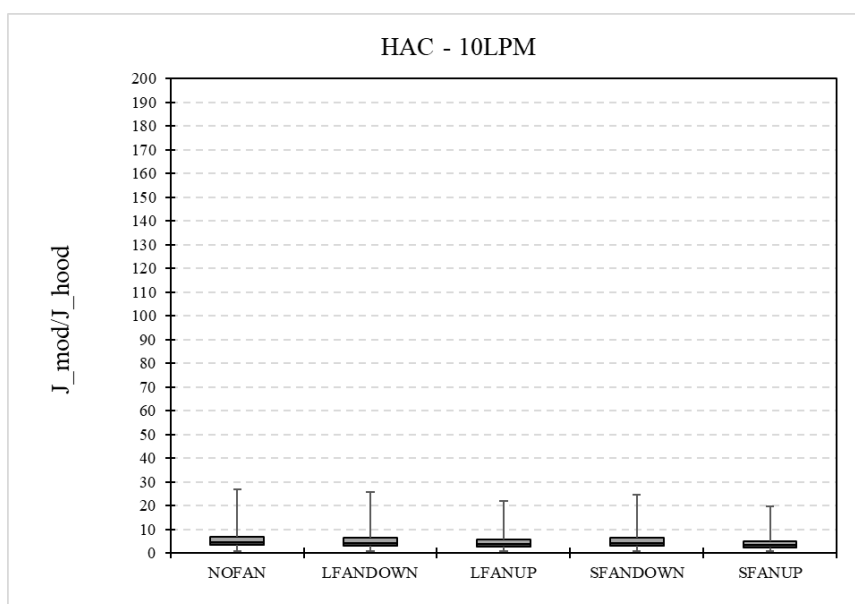


Figure 24 – Emission rate of acetic acid (HAC) at Camburi WWTP: Comparison between the values obtained using the k_G model proposed by Prata et al. (2021) and the k_G values from the flux hood with $Q = 5 \text{ L min}^{-1}$. a) roughness 0.005 m and 260° wind direction. b) roughness 0.20 m and 345° wind direction.

(a)



(b)

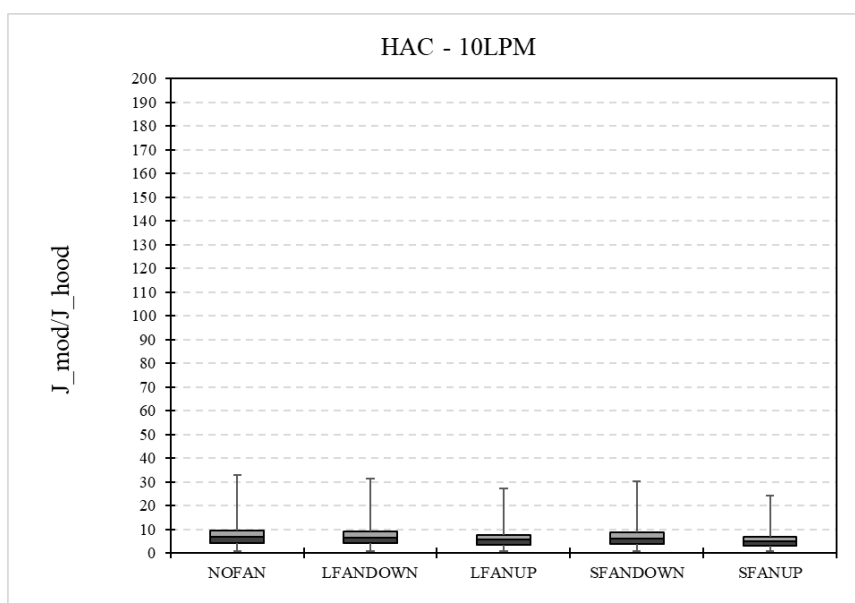
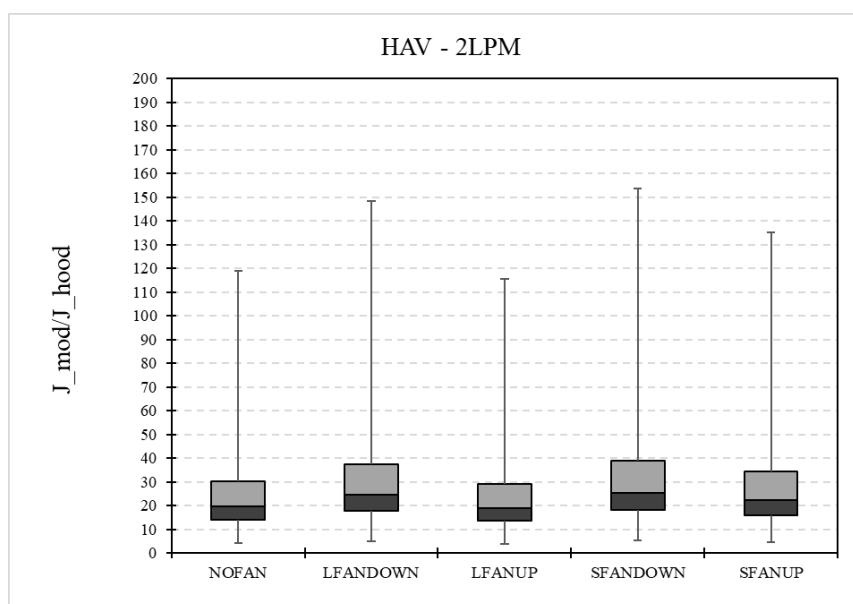


Figure 25 – Emission rate of acetic acid (HAC) at Camburi WWTP: Comparison between the values obtained using the k_G model proposed by Prata et al. (2021) and the k_G values from the flux hood with $Q = 10 \text{ L min}^{-1}$. a) roughness 0.005 m and 260° wind direction. b) roughness 0.20 m and 345° wind direction.

(a)



(b)

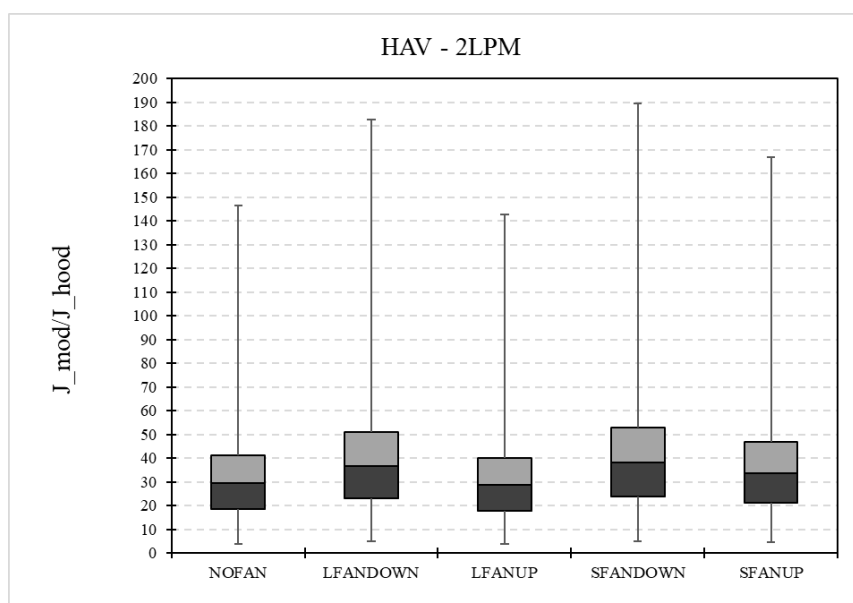
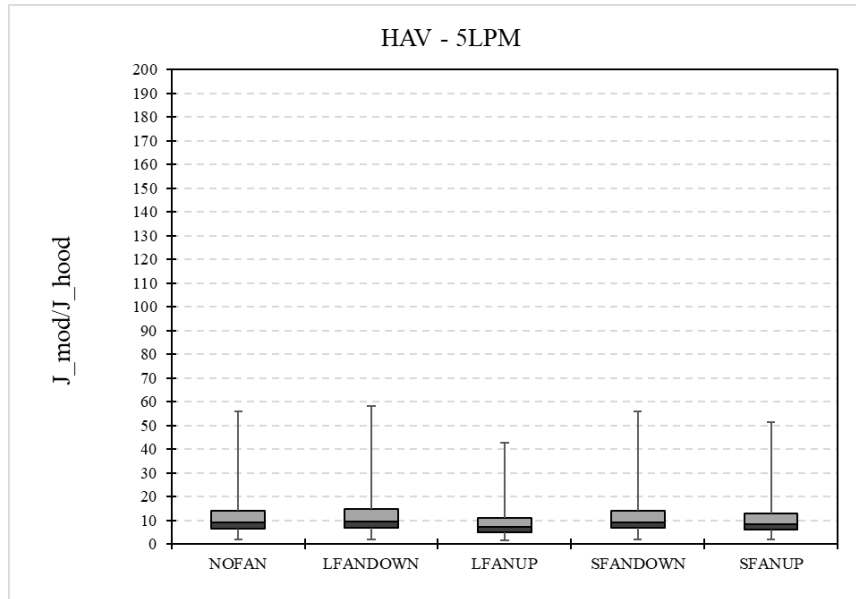


Figure 26 – Emission rate of valeric acid (HAV) at Camburi WWTP: Comparison between the values obtained using the k_G model proposed by Prata et al. (2021) and the k_G values from the flux hood with $Q = 2 \text{ L min}^{-1}$. a) roughness 0.005 m and 260° wind direction. b) roughness 0.20 m and 345° wind direction.

(a)



(b)

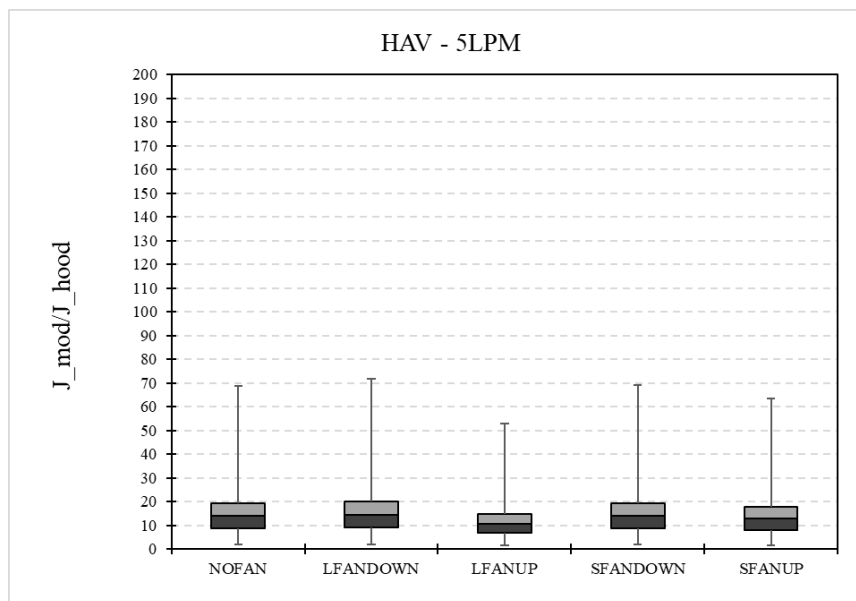
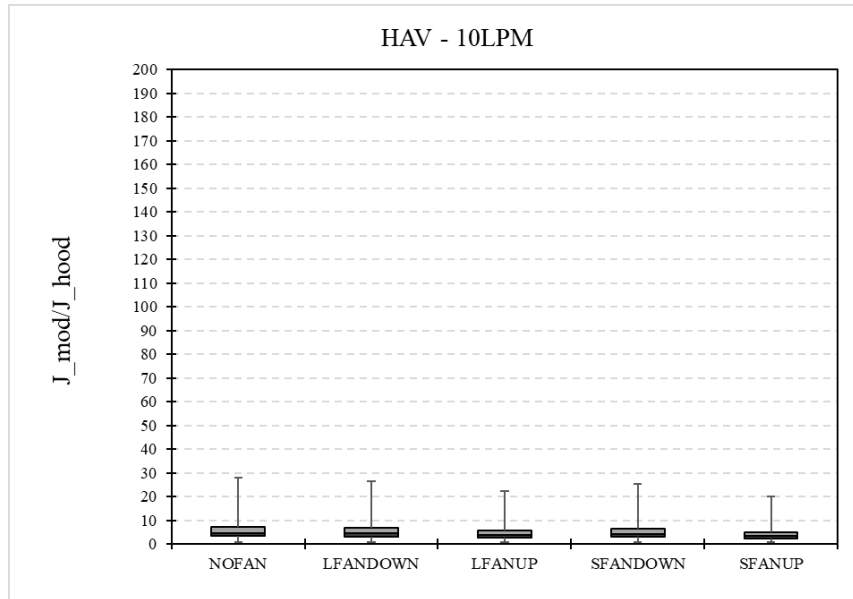


Figure 27 – Emission rate of valeric acid (HAV) at Camburi WWTP: Comparison between the values obtained using the k_G model proposed by Prata et al. (2021) and the k_G values from the flux hood with $Q = 5$ $L \text{ min}^{-1}$. a) roughness 0.005 m and 260° wind direction. b) roughness 0.20 m and 345° wind direction.

(a)



(b)

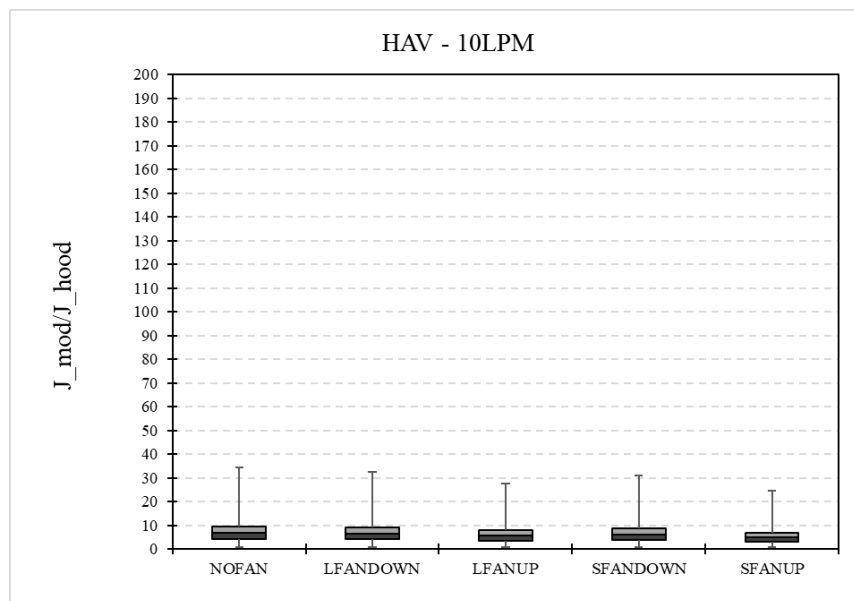
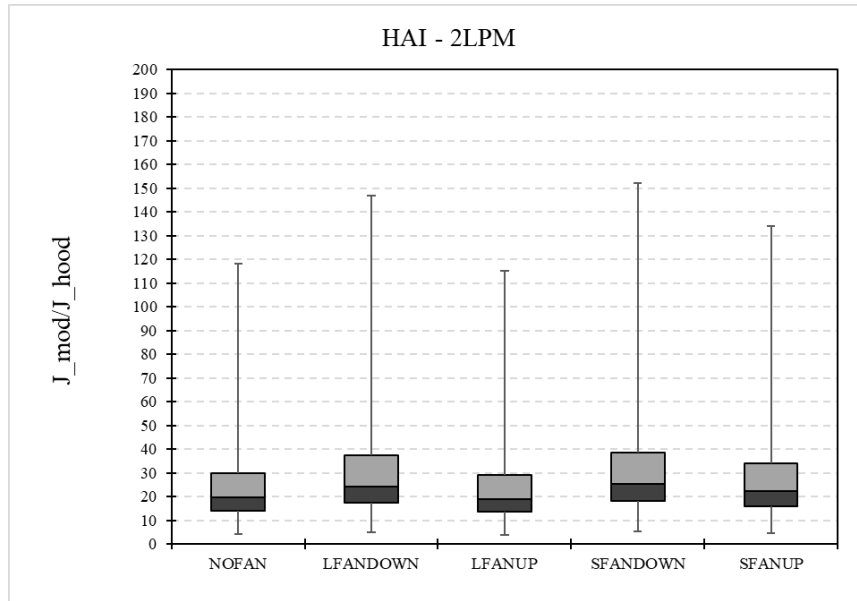


Figure 28 – Emission rate of valeric acid (HAV) at Camburi WWTP: Comparison between the values obtained using the k_G model proposed by Prata et al. (2021) and the k_G values from the flux hood with $Q = 10 \text{ L min}^{-1}$.

a) roughness 0.005 m and 260° wind direction. b) roughness 0.20 m and 345° wind direction.

(a)



(b)

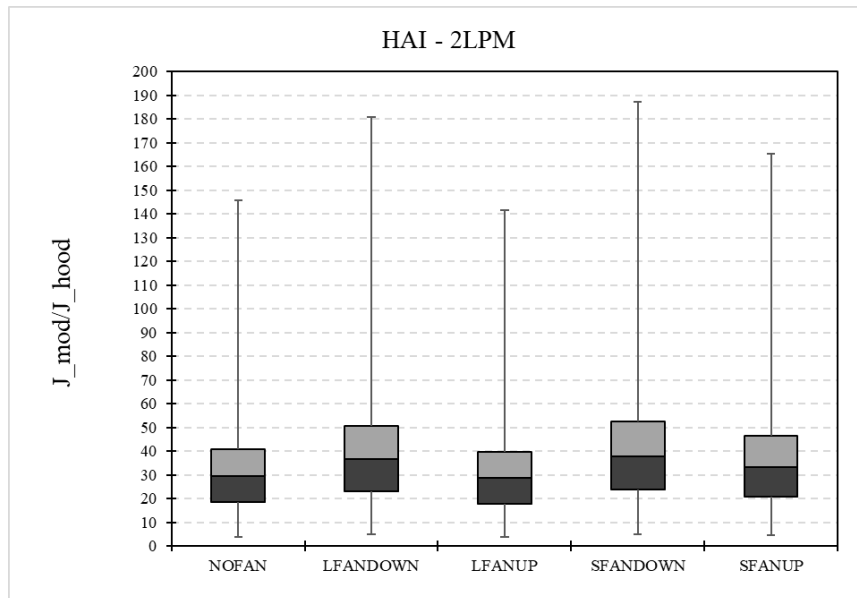
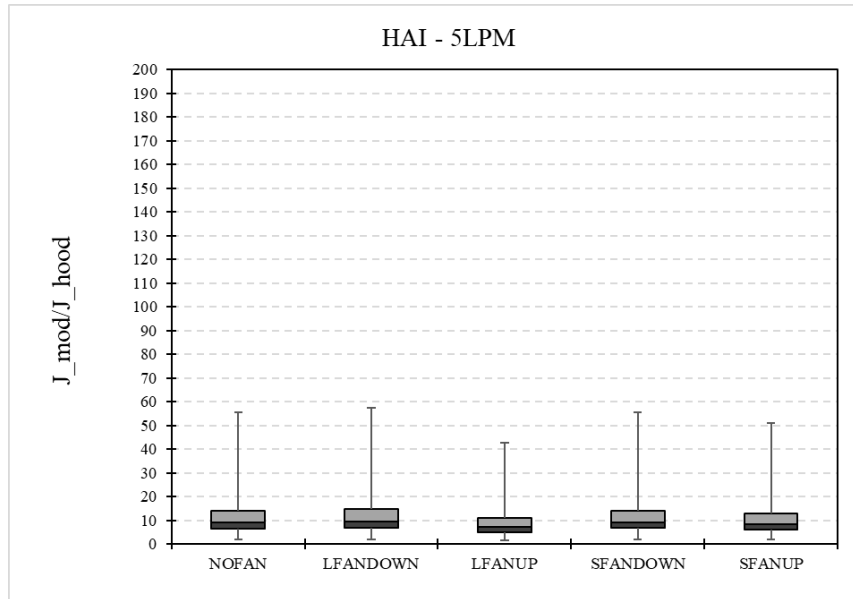


Figure 29 – Emission rate of isobutyric acid (HAI) at Camburi WWTP: Comparison between the values obtained using the k_G model proposed by Prata et al. (2021) and the k_G values from the flux hood with $Q = 2 \text{ L min}^{-1}$. a) roughness 0.005 m and 260° wind direction. b) roughness 0.20 m and 345° wind direction.

(a)



(b)

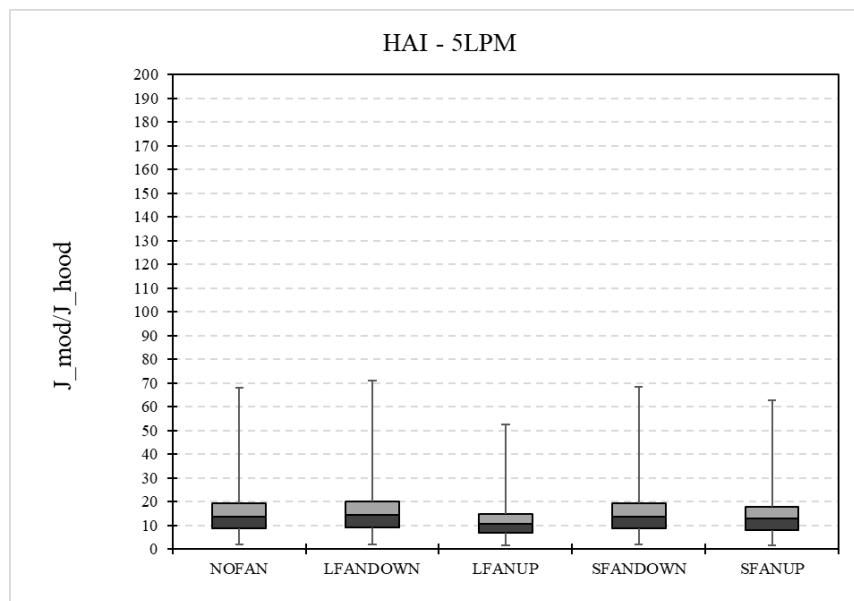
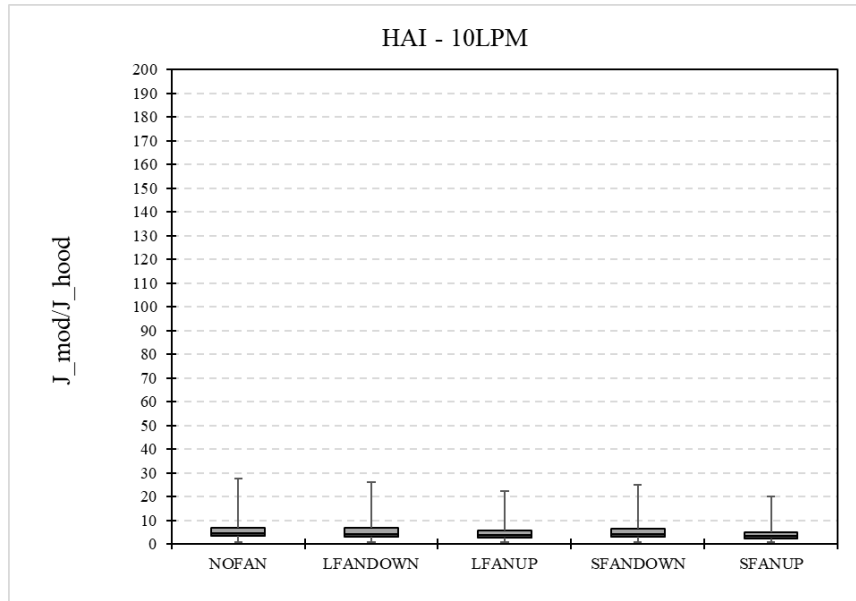


Figure 30 – Emission rate of isobutyric acid (HAI) at Camburi WWTP: Comparison between the values obtained using the k_G model proposed by Prata et al. (2021) and the k_G values from the flux hood with $Q = 5 \text{ L min}^{-1}$. a) roughness 0.005 m and 260° wind direction. b) roughness 0.20 m and 345° wind direction.

(a)



(b)

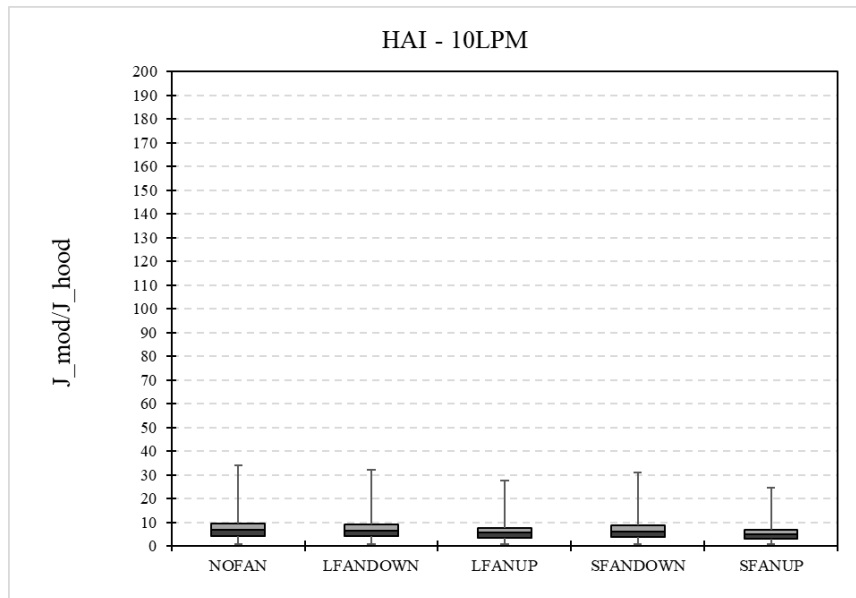
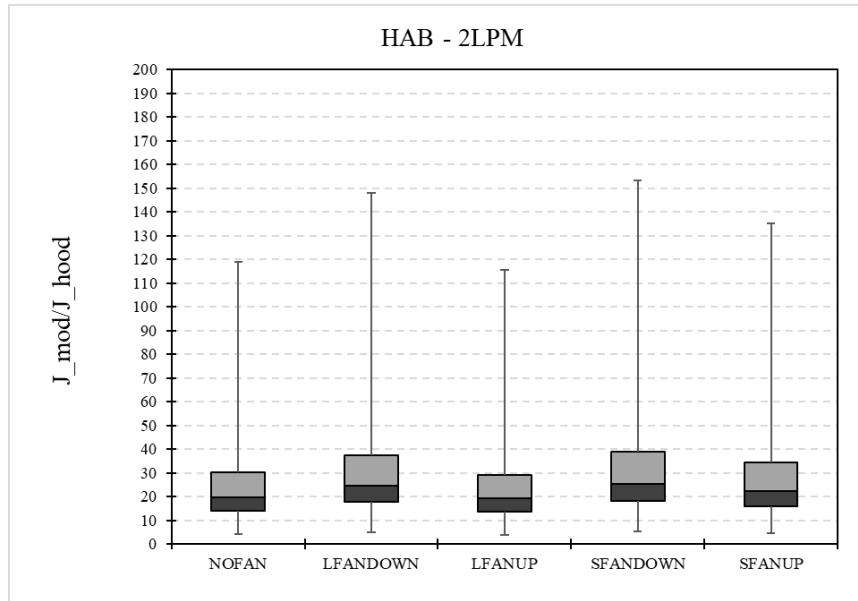


Figure 31 – Emission rate of isobutyric acid (HAI) at Camburi WWTP: Comparison between the values obtained using the k_G model proposed by Prata et al. (2021) and the k_G values from the flux hood with $Q = 10 \text{ L min}^{-1}$. a) roughness 0.005 m and 260° wind direction. b) roughness 0.20 m and 345° wind direction.

(a)



(b)

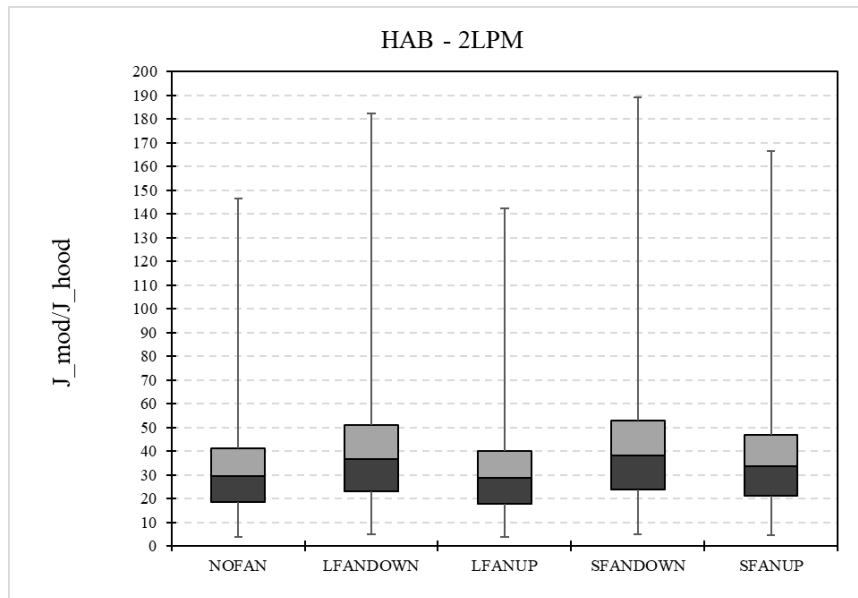
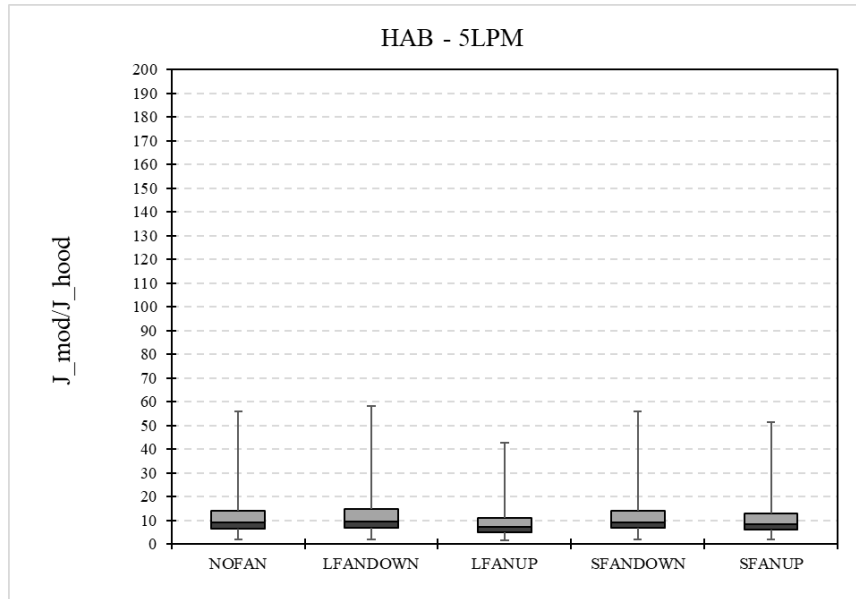


Figure 32 – Emission rate of butyric acid (HAB) at Camburi WWTP: Comparison between the values obtained using the k_G model proposed by Prata et al. (2021) and the k_G values from the flux hood with $Q = 2$ $L \text{ min}^{-1}$. a) roughness 0.005 m and 260° wind direction. b) roughness 0.20 m and 345° wind direction.

(a)



(b)

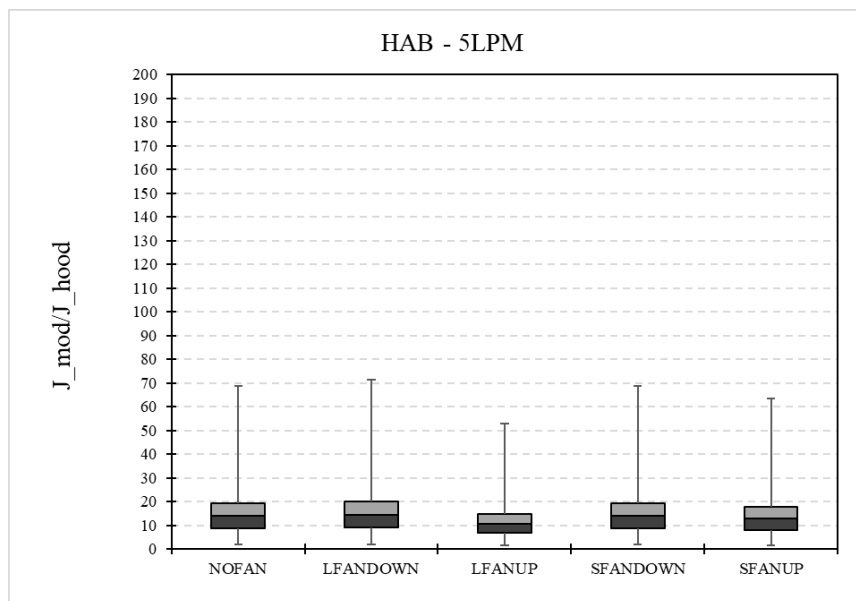
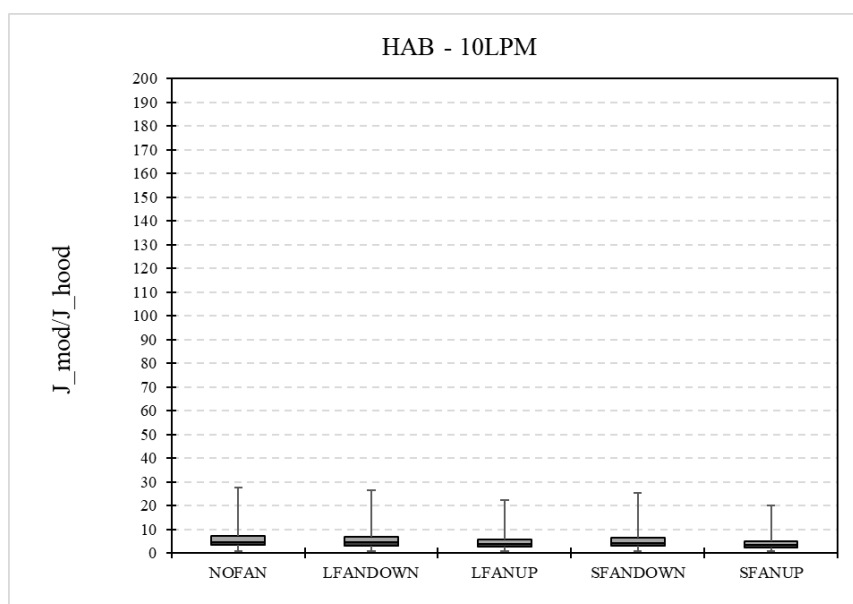


Figure 33 – Emission rate of butyric acid (HAB) at Camburi WWTP: Comparison between the values obtained using the k_G model proposed by Prata et al. (2021) and the k_G values from the flux hood with $Q = 5 \text{ L min}^{-1}$. a) roughness 0.005 m and 260° wind direction. b) roughness 0.20 m and 345° wind direction.

(a)



(b)

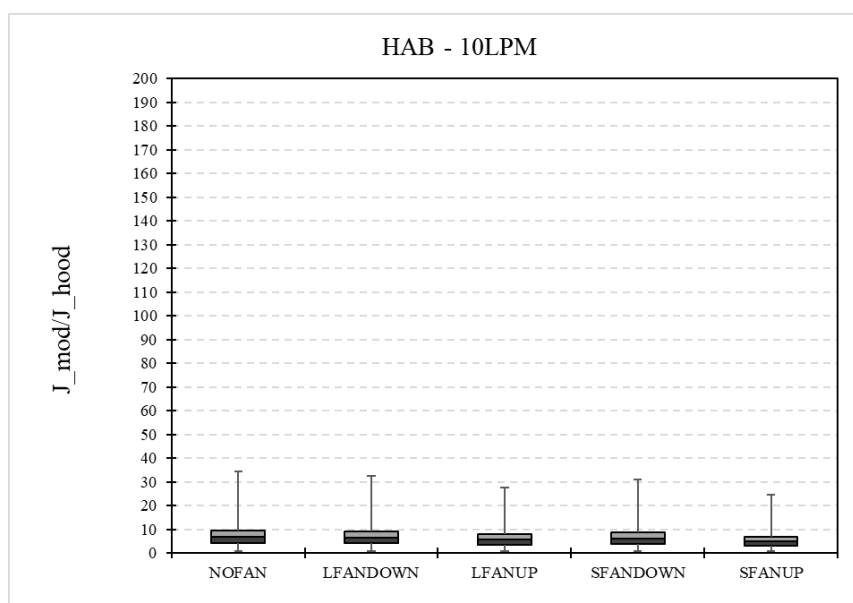


Figure 34 –Emission rate of butyric acid (HAB) at Camburi WWTP: Comparison between the values obtained using the k_G model proposed by Prata et al. (2021) and the k_G values from the flux hood with $Q = 10 \text{ L min}^{-1}$.
 a) roughness 0.005 m and 260° wind direction. b) roughness 0.20 m and 345° wind direction.

Figure 35, Figure 36 and Figure 37 show the relationship between the gas phase mass transfer coefficient estimated by the Prata-Brutsaert model ($k_{G,field}$) and the gas phase mass transfer coefficient measured through the flux hood ($k_{G,hood}$) for the acetic acid compound with $Q = 2, 5$ and 10 L min^{-1} , respectively. Also in each figure it is possible to observe the relationship

$k_{G,field}/k_{G,flux\ hood}$ for the different flux hood configurations evaluated in Section 5.1: No Fan, LFanDown, LFanUp, SFanDown and SFanUp, with U_{10} ranging from 0 to 10 m s⁻¹.

In general terms, k_G in the LFanUp configuration was the closest to the expected k_G in the field, especially for $Q = 2$ and 5 L min⁻¹ (Figure 35 and Figure 36). Here, due to the build-up of concentration in the headspace of the hood (an effect that does not occur for open surfaces in the field), the volatilisation rates inside the flux hood will be lower than the corresponding volatilisation rates in the field, for the same k_G . In addition, the inlet flow rates favor the increase of the mixture inside the headspace, mitigating the effect of the build-up concentration.

It is interesting to notice that the gas phase mass transfer field-to-flux hood ratio of acetic acid that would be observed in the flux hood and LFanUp configuration operating with $Q = 2, 5$ and 10 L min⁻¹ in a low wind panorama ($U_{10} = 2.54$ m s⁻¹) and 260° wind direction is 19.85, 7.10 and 3.81, respectively. On the other hand, for 345° wind direction it would be expected a field-to-flux ratio of 19.31, 6.90 and 3.71. Such equivalencies change depending on the compound (different k_G).

The lowest field-to-flux hood ratio of acetic acid in low wind ($U_{10} = 2.54$ m s⁻¹) was observed in the SFanUp configuration operating with $Q = 10$ L min⁻¹, with a field-to-flux ratio of 3.18 and 3.10 for 260° wind direction and 345° wind direction, respectively (see Figure 37).

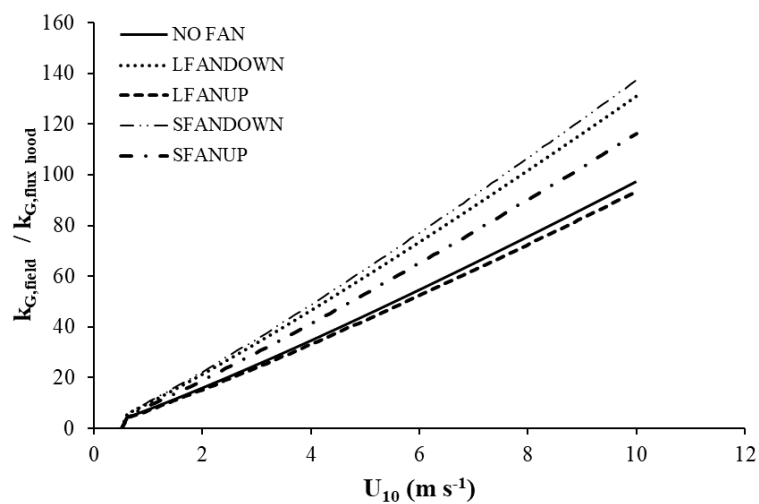
For the compound valeric acid (Figure 38, Figure 39 and Figure 40), even with k_G different from acetic acid, responses similar to those already observed for acetic acid were observed. The lowest field-to-flux hood ratio of valeric acid in low wind ($U_{10} = 2.54$ m s⁻¹) was observed in the SFanUp configuration operating with $Q = 10$ L min⁻¹, with a field-to-flux ratio of 2.71 and 2.65 for 260° wind direction and 345° wind direction, respectively (see Figure 40).

Figure 41, Figure 42 and Figure 43 show the field-to-flux hood ratio of isobutyric acid with responses similar to those already shown for acetic acid. The lowest field-to-flux hood ratio of isobutyric acid in low wind ($U_{10} = 2.54$ m s⁻¹) was observed in the SFanUp configuration operating with $Q = 10$ L min⁻¹, with a field-to-flux ratio of 2.83 and 2.65 for 260° wind direction and 345° wind direction, respectively (see Figure 43).

Figure 44, Figure 45 and Figure 46 present the field-to-flux hood ratio of butyric acid. The lowest field-to-flux hood ratio of butyric acid in low wind ($U_{10} = 2.54$ m s⁻¹) was noted in the SFanUp configuration operating with $Q = 10$ L min⁻¹, field-to-flux ratio of 2.73 and 2.64 for 260° wind direction and 345° wind direction, respectively (see Figure 46). As same as isobutyric compound,

the butyric acid compound showed the lowest $k_{G,field}/k_{G,flux hood}$ ratio, that is, Prata-Brutsaert model fitted better to the experimental results of k_G of these compounds. On the other hand, the results for $k_{G,field}/k_{G,flux hood}$ ratio of the acetic acid compound were the most distant.

(a)



(b)

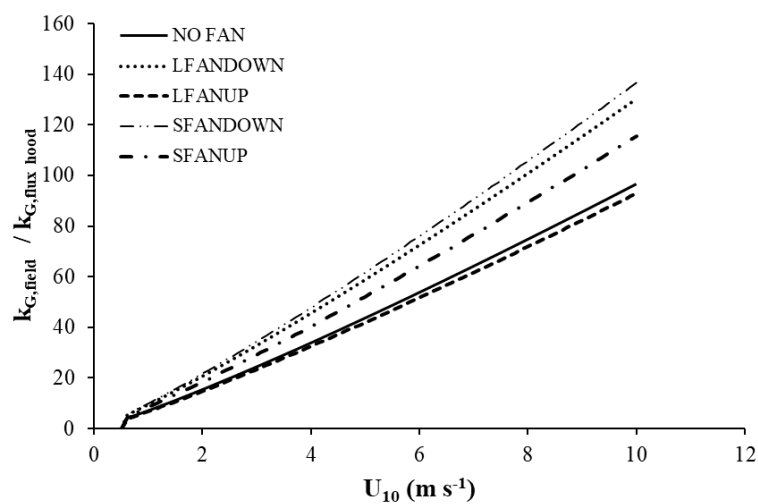
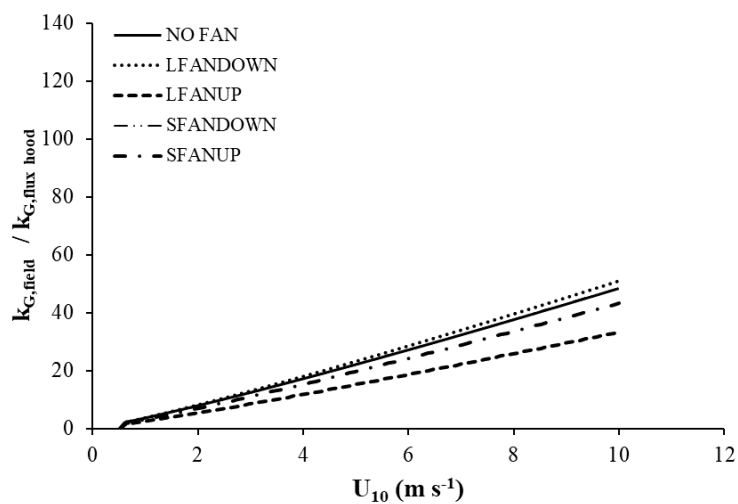


Figure 35 – Comparison of k_G values for acetic acid (AC) obtained using the flux hood with $Q = 2 \text{ L min}^{-1}$ and different fan configurations and those obtained using the Prata-Brutsaert model proposed by Prata et al. (2021) for different wind speeds. a) roughness 0.005 m and 260° wind direction. b) roughness 0.20 m and 345° wind direction.

(a)



(b)

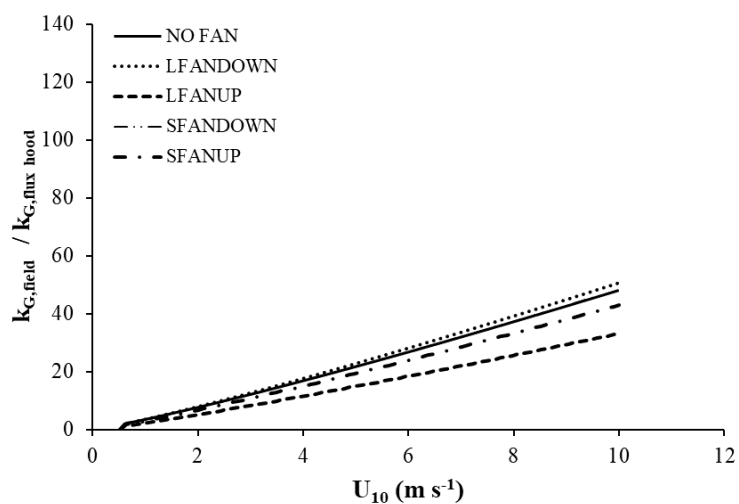
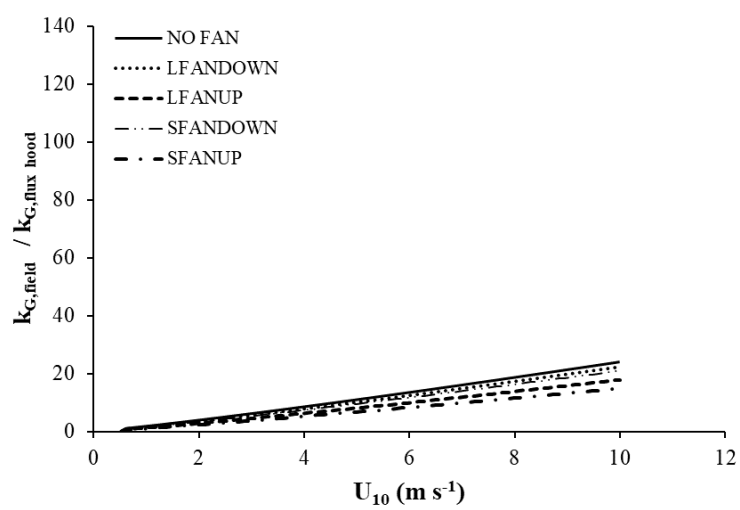


Figure 36 – Comparison of k_G values for acetic acid (AC) obtained using the flux hood with $Q = 5 \text{ L min}^{-1}$ and different fan configurations and those obtained using the Prata-Brutsaert model proposed by Prata et al. (2021) for different wind speeds. a) roughness 0.005 m and 260° wind direction. b) roughness 0.20 m and 345° wind direction.

(a)



(b)

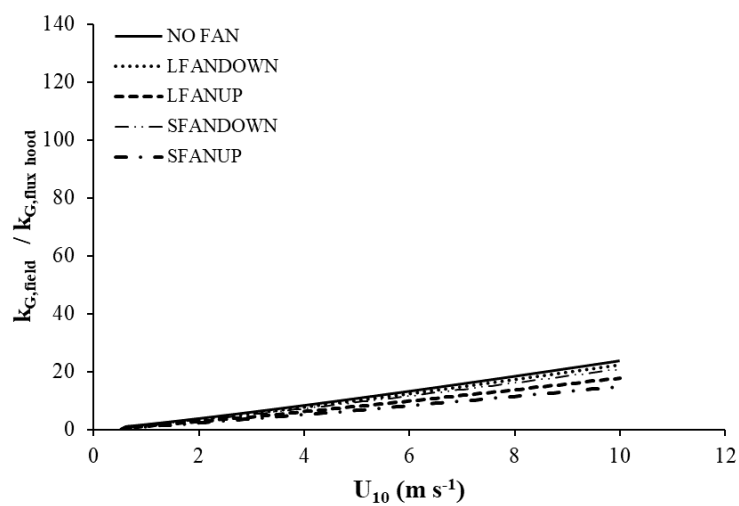
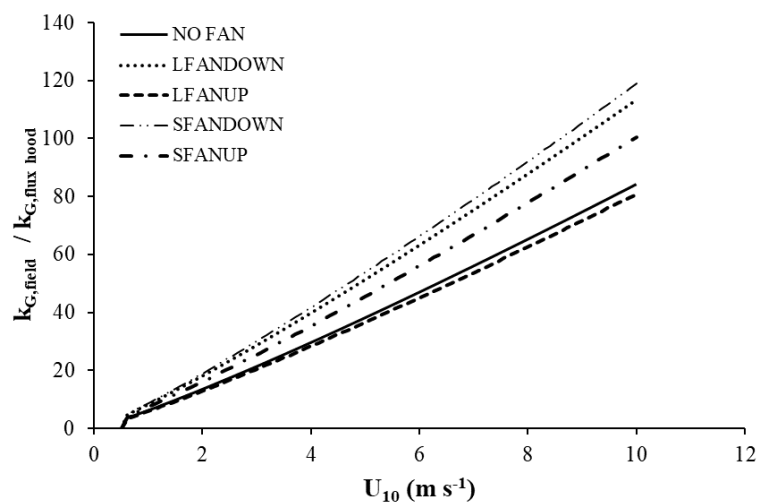


Figure 37 – Comparison of k_G values for acetic acid (AC) obtained using the flux hood with $Q = 10 \text{ L min}^{-1}$ and different fan configurations and those obtained using the Prata-Brutsaert model proposed by Prata et al. (2021) for different wind speeds. a) roughness 0.005 m and 260° wind direction. b) roughness 0.20 m and 345° wind direction.

(a)



(b)

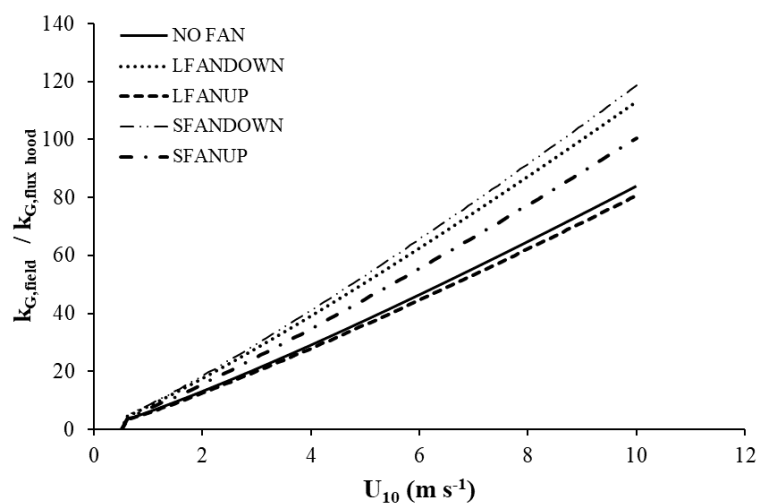
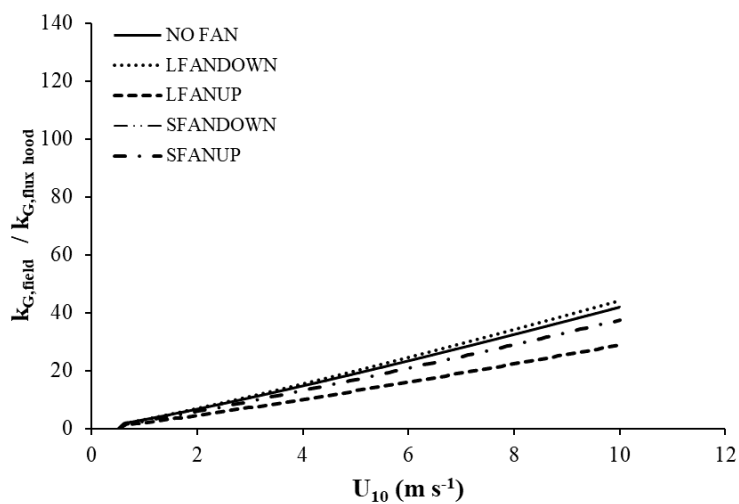


Figure 38 – Comparison of k_G values for valeric acid (HAV) obtained using the Schmidt number and the flux hood with $Q = 2 \text{ L min}^{-1}$ and different fan configurations and those obtained using the Prata-Brutsaert model proposed by Prata et al. (2021) for different wind speeds. a) roughness 0.005 m and 260° wind direction. b) roughness 0.20 m and 345° wind direction.

(a)



(b)

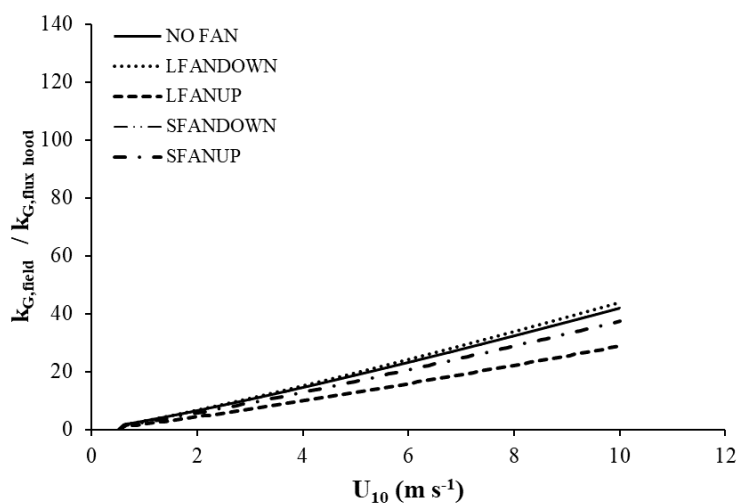
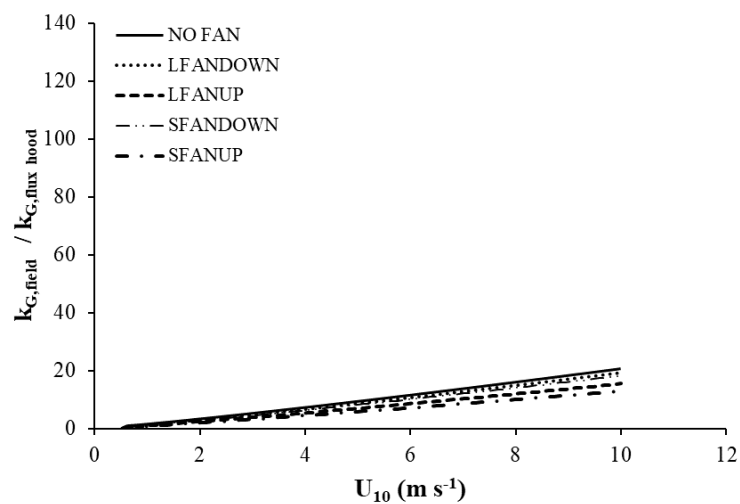


Figure 39 – Comparison of k_G values for valeric acid (HAV) obtained using the Schmidt number and the flux hood with $Q = 5 \text{ L min}^{-1}$ and different fan configurations and those obtained using the Prata-Brutsaert model proposed by Prata et al. (2021) for different wind speeds. a) roughness 0.005 m and 260° wind direction. b) roughness 0.20 m and 345° wind direction.

(a)



(b)

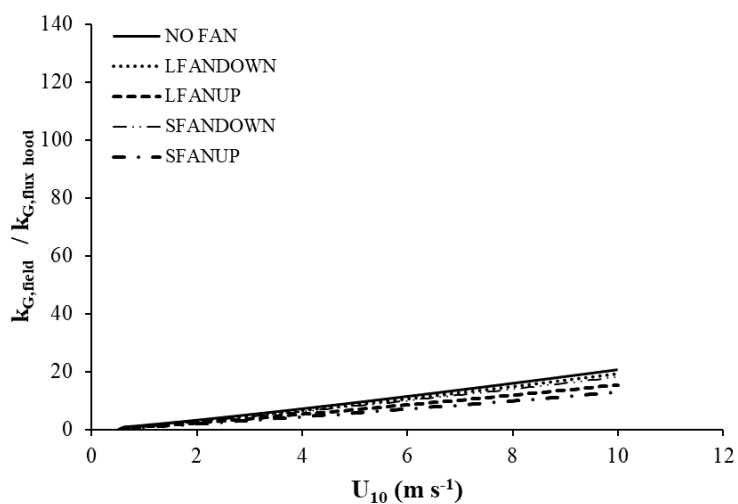
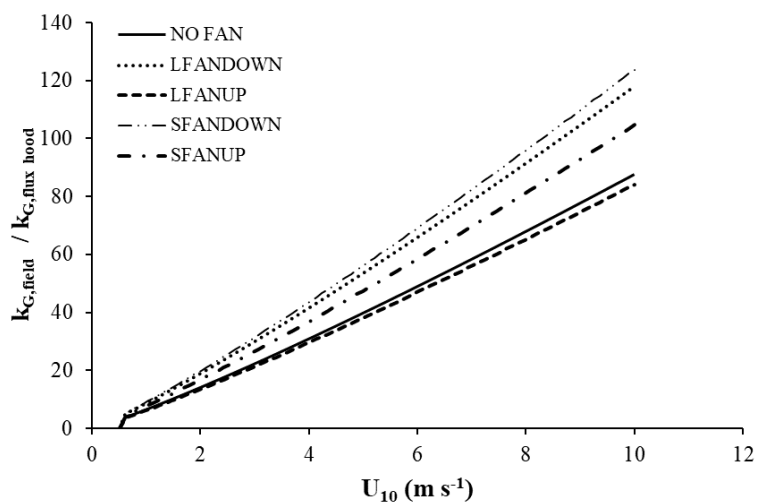


Figure 40 – Comparison of k_G values for valeric acid (HAV) obtained using the Schmidt number and the flux hood with $Q = 10 \text{ L min}^{-1}$ and different fan configurations and those obtained using the Prata-Brutsaert model proposed by Prata et al. (2021) for different wind speeds. a) roughness 0.005 m and 260° wind direction. b) roughness 0.20 m and 345° wind direction.

(a)



(b)

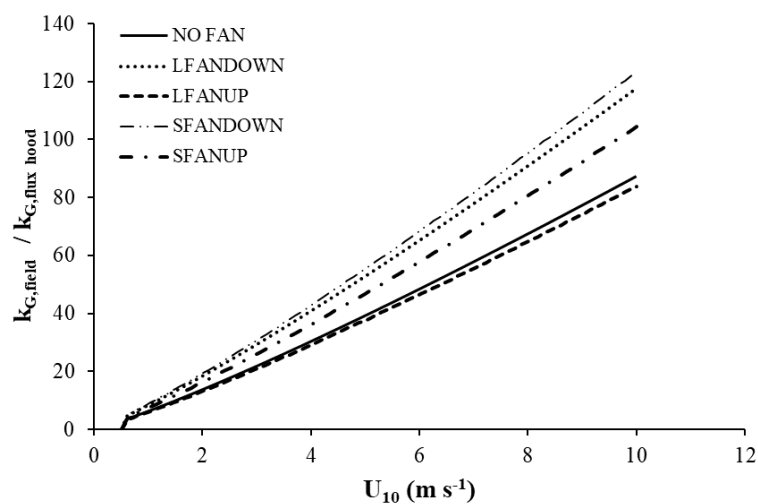
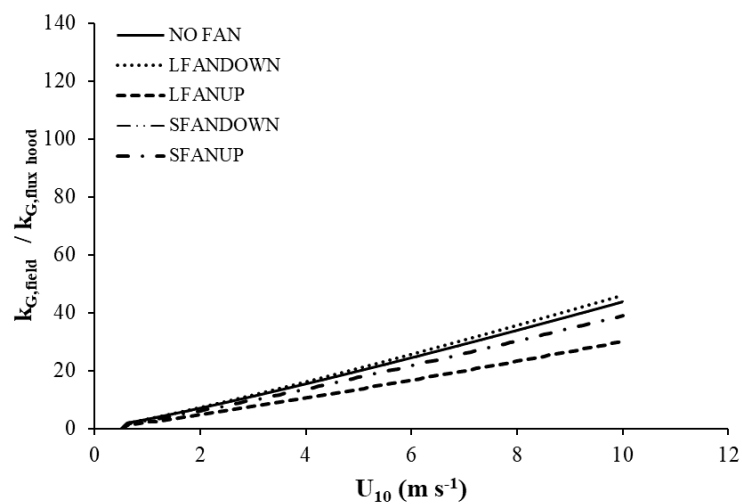


Figure 41 – Comparison of k_G values for isobutyric acid (HAI) obtained using the Schmidt number and the flux hood with $Q = 2 \text{ L min}^{-1}$ and different fan configurations and those obtained using the Prata-Brutsaert model proposed by Prata et al. (2021) for different wind speeds. a) roughness 0.005 m and 260° wind direction. b) roughness 0.20 m and 345° wind direction.

(a)



(b)

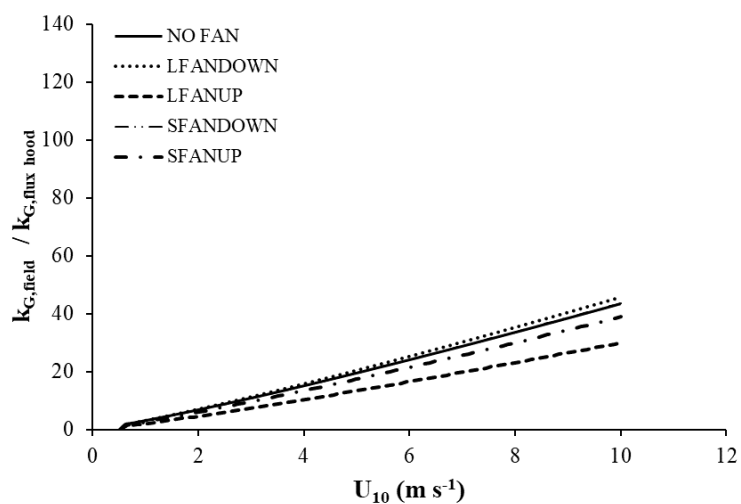
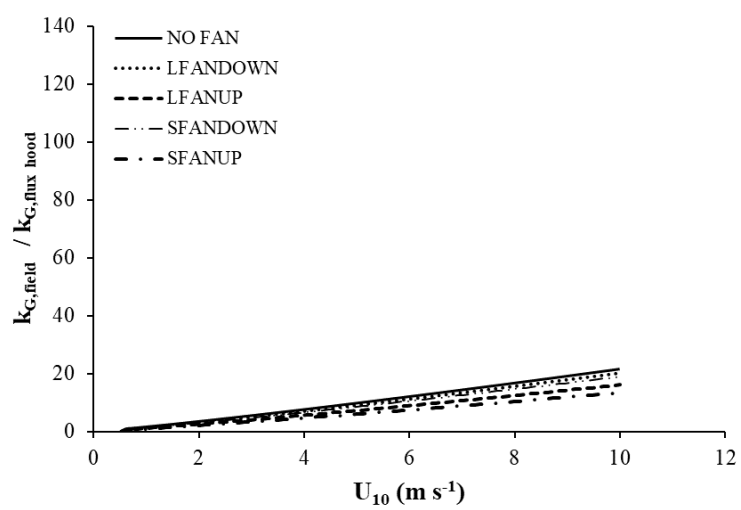


Figure 42 – Comparison of k_G values for isobutyric acid (HAI) obtained using the Schmidt number and the flux hood with $Q = 5 \text{ L min}^{-1}$ and different fan configurations and those obtained using the Prata-Brutsaert model proposed by Prata et al. (2021) for different wind speeds. a) roughness 0.005 m and 260° wind direction. b) roughness 0.20 m and 345° wind direction.

(a)



(b)

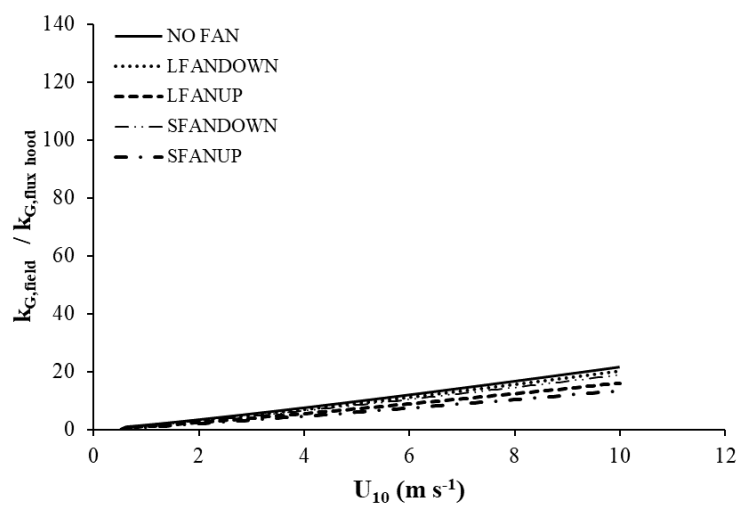
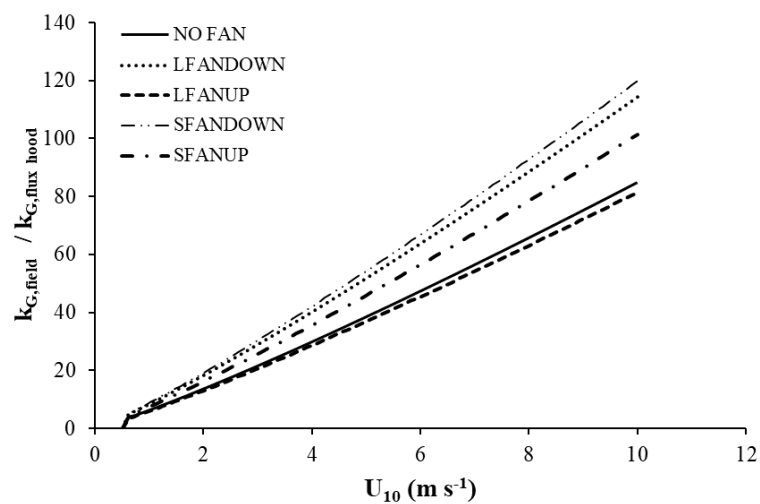


Figure 43 – Comparison of k_G values for isobutyric acid (HAI) obtained using the Schmidt number and the flux hood with $Q = 10 \text{ L min}^{-1}$ and different fan configurations and those obtained using the Prata-Brutsaert model proposed by Prata et al. (2021) for different wind speeds. a) roughness 0.005 m and 260° wind direction. b) roughness 0.20 m and 345° wind direction.

(a)



(b)

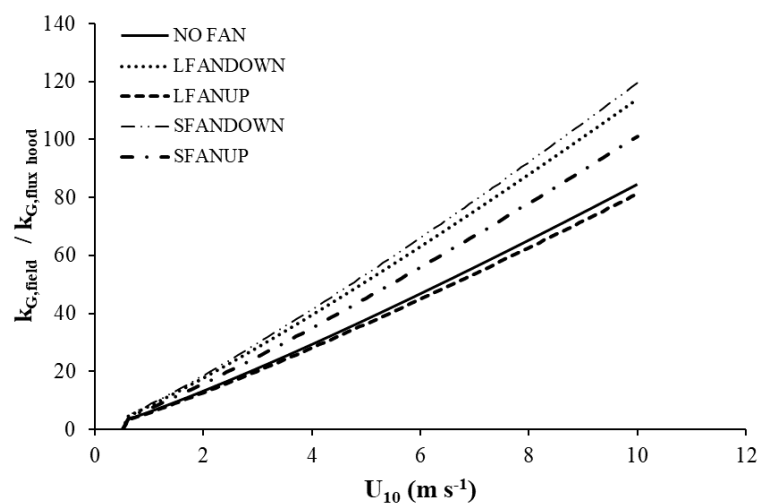
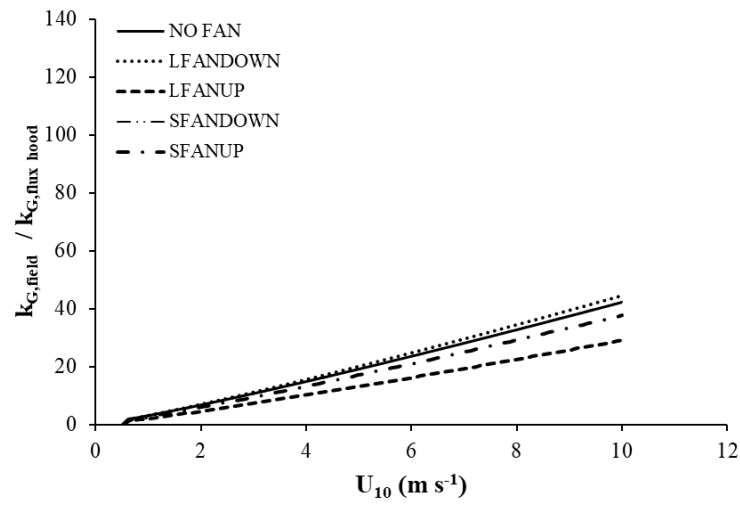


Figure 44 – Comparison of k_G values for butyric acid (HAB) obtained using the Schmidt number and the flux hood with $Q = 2 \text{ L min}^{-1}$ and different fan configurations and those obtained using the Prata-Brutsaert model proposed by Prata et al. (2021) for different wind speeds. a) roughness 0.005 m and 260° wind direction. b) roughness 0.20 m and 345° wind direction.

(a)



(b)

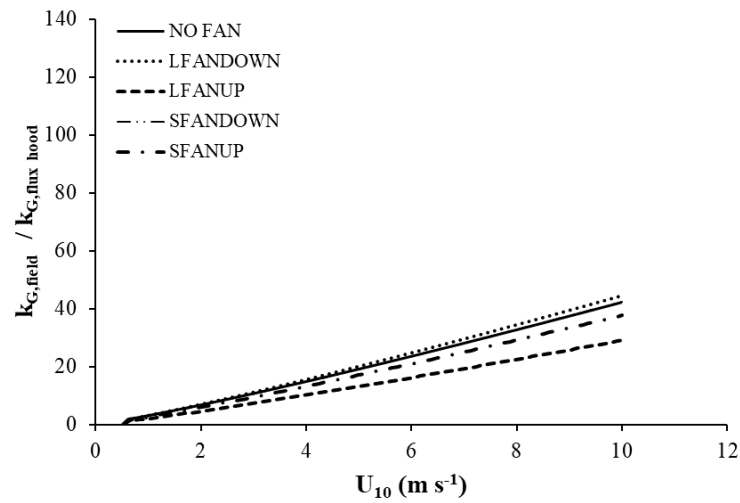
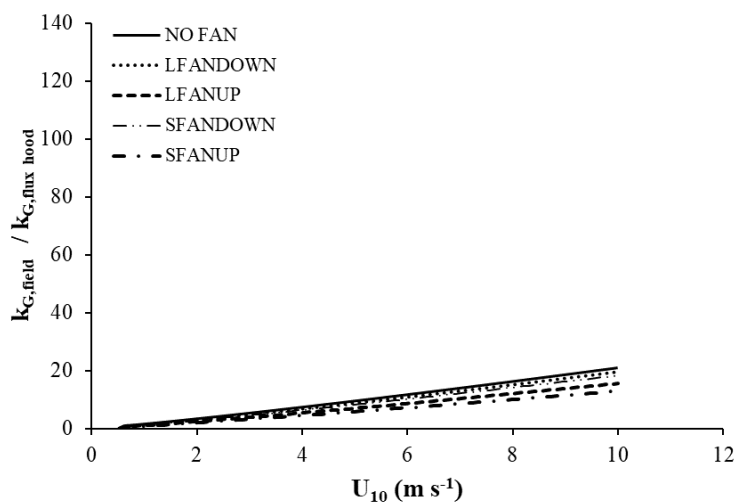


Figure 45 – Comparison of k_G values for butyric acid (HAB) obtained using the Schmidt number and the flux hood with $Q = 5 \text{ L min}^{-1}$ and different fan configurations and those obtained using the Prata-Brutsaert model proposed by Prata et al. (2021) for different wind speeds. a) roughness 0.005 m and 260° wind direction. b) roughness 0.20 m and 345° wind direction.

(a)



(b)

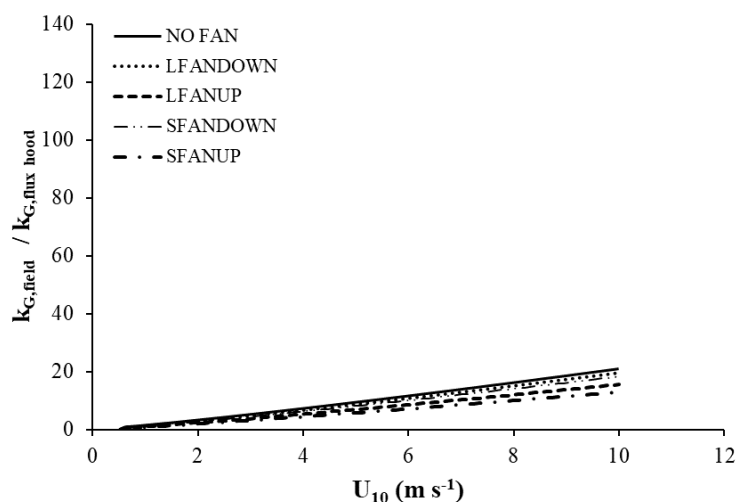


Figure 46 – Comparison of k_G values for butyric acid (HAB) obtained using the Schmidt number and the flux hood with $Q = 10 \text{ L min}^{-1}$ and different fan configurations and those obtained using the Prata-Brutsaert model proposed by Prata et al. (2021) for different wind speeds. a) roughness 0.005 m and 260° wind direction. b) roughness 0.20 m and 345° wind direction.

The bias evaluation presented in this Section for the gas-phase controlled compounds (acetic acid, valeric acid, isobutyric acid, and butyric acid) allows the emission rate measured with the USEPA flux hood in the laboratory to be compared to models that estimate the emission rate expected in the field (J_{mod}/J_{hood}) providing a factor between the parts.

This procedure can be an alternative, for example, for cases in which there are operational difficulties in taking the entire flux hood to the field, including the inlet sweep air flow gas

bottle. Another occasion that limits the use of the flux hood in the field may be related to the distance from the emission source (WWTP) to the laboratory where the analysis of the concentration of the compound is to be carried out, especially for units located in countryside and further away from large urban centers.

Thus, knowing the emission rate bias between flux hood and an expected emission rate in the field for a typical compound concentration in the liquid phase (C_L), mass transfer parameters can be known from Equation (11).

It is worth mentioning that although the build-up concentration is expected inside the flux hood, causing an underestimation of k_G and, consequently, of the emission rate, there is still no convergence between researches to date of a mechanism to interrupt this effect as discussed in Section 5.1.

As the environment within a flux hood is not the same as the environment in the field some authors have also proposed attempts to replicate or scale up:

Parker et al. (2010) proposed three correction methods to improve the accuracy of field-measured flux if using a wind tunnel or flux hood. One of the proposed correction methods, using the term “Evaporative Flux Ratio Correction Method” (EFRCR), that involves a procedure based on water evaporative flux ratios. The method consists of measuring the water evaporative flux inside (J_{in}) and outside (J_{out}) the hood while flux hood measurements are made in the field. Then multiplying by the uncorrected hood-based flux to “evaporative flux ratio correction factor” ($EFRCF = J_{out}/J_{in}$) would give a corrected flux value and greatly improve the accuracy of the flux measurement. This water evaporative correction procedure is similar to that proposed by Teye and Hautala (2008, 2010), who used water evaporative flux to calculate the mass transfer coefficient in a non-steady-state recirculating flux hood (i.e., static chamber). They also measured the field-based mass transfer coefficient within a dairy building by suspending a saturated cloth on a flat plate from an electronic balance and used the measured mass transfer coefficient with a model to predict NH_3 emissions from the dairy.

Parker et al. (2013) demonstrate a methodology for standardizing and comparing different chamber types by measuring water evaporation within the chamber using a gravimetric mass balance approach under controlled laboratory conditions. For the USEPA flux hood, they found a positive correlation between VOC flux and water evaporative flux for the 20 and 60% RH data combined.

Parker et al. (2013b) demonstrated the application of correction factors using the water evaporative flux ratio correction method ($EFRCF \approx J_{out}/J_{in}$) in a case study where the USEPA flux hood and small wind tunnel were used to measure the VOC flux from land-applied swine slurry. Then, water evaporative flux was measured both inside and outside the USEPA flux hood and wind tunnel. The water evaporative flux inside the USEPA flux hood was 6.2 mm d^{-1} compared to 15.0 mm d^{-1} outside the flux hood, for a resulting EFRCF (i.e., J_{out}/J_{in}) of 2.42. Previously, Parker et al. (2009) reported evaporation data resulting in calculated outdoor EFRCF values for the USEPA flux hood of 3.16 and 2.97 for average wind/temperature conditions of $0.1 \text{ m s}^{-1}/24.5 \text{ }^\circ\text{C}$ and $2.9 \text{ m s}^{-1}/31.8 \text{ }^\circ\text{C}$, respectively.

Despite the attempt to standardize the flux hood measurement correction method, (Parker et al. (2013b) recommended scientists and regulatory personnel using flux hood emission data should apply EFRCFs only if there is a strong correlation between water evaporative flux and the flux of the compound being measured.

Recently, Prata et al. (2018) propose the use of emission models for scaling up the emission rates measured experimentally with enclosure sampling devices. They presented a procedure that allows the emission rates of gas-phase controlled compounds measured with the USEPA flux hood to be scaled (at least in order of magnitude) to field conditions different than the mass transfer conditions imposed by the micro-environment inside the flux hood.

Since having k_g and the emission rate (J) measured using the flux hood, it can be obtained $C_{G,i}$ using Equation (32):

$$J = \frac{1}{\frac{1}{k_g} + \frac{A}{Q}} C_{G,i} \quad (32)$$

The main advantage of the proposed procedure is that it takes into account the effects of the concentration build-up in the hood's headspace, which is a feature does not present in other proposed scaling methods such as the water evaporative flux ratio correction factor.

According to Prata et al. (2018), the following aspects are important to be observed:

- The flux hood must present a well-mixed headspace, so that Equation (32) is valid, which is the typical case for the USEPA flux hood.

- Proper recording of the sweep air flow rate Q is necessary for the back-calculation of $C_{G,i}$; which in the present study was met using mass flow control (Section 5.1).
- If k_G for the desired compound inside the flux hood is to be determined experimentally, it is important highlight repetitions and cross-checks in the experiments, to avoid that the k_G retrieved from the experimental results are not significantly affected by the uncertainty in the temperature at the liquid surface and other sources of inaccuracy. Besides, either with k_G determined directly from experiments or calculated based on other compound, it is critical that the operational conditions of the flux hood for which k_G was assessed be as similar as possible to the ones used during the sampling in the field (for instance, same Q , sampling rate and depth of insertion in the liquid); if scums and slick microfilms are present over the liquid surfaces in the field, this may compromise the reproduction of the conditions.
- The accuracy of the scaling approach is directly dependent on the application of a suitable emission model to approximate the field k_G . Here, the application in the Prata-Brutsaert model in Camburi WWTP case was chosen, due to the advantages in the formulation of the IBL.
- The procedure is applicable for scaling emission rates of individual compounds.

With the experimental data and the application of an appropriate model, it is possible to obtain a scaled emission rate. This corrected emission rate is especially important in the USEPA flux hood application, which although it has mechanisms to increase mixing in the headspace, still has limitations due to the build-up of the compound inside headspace (concentration build-up), resulting in an underestimated k_G .

6 CONCLUSIONS AND PERSPECTIVES

The flux hood investigation was carried out through laboratory experiments and numerical simulation, with some results being applied and compared to models proposed in the literature for passive liquid surfaces, as well as observed in real Wastewater Treatment Plants (WWTP). The flux hood was analysed using different configurations concerning an internal fan (No Fan, SFanUp, SFanDown, LFanUp and LFanDown) and inlet air sweep flow (2, 5 or 10 L min⁻¹) for different gas-phase controlled compounds (acetic acid – as reference gas, isobutyric acid, butyric acid and valeric acid). Emission rates and mass transfer coefficients for an acetic acid solution were evaluated from experiments performed with an original USEPA flux hood (No Fan) and flux hoods modified by an internal fan. For all cases with and without a fan, the emission rates and gas-phase mass transfer coefficients generally increased with the inlet sweep air flow rate, showing an approximated linear trend. In the experiments using the flux hood modified by a fan, not all fan configurations tested resulted in higher emissions inside the flux hood compared to the No Fan configuration. Furthermore, for the cases in which the fan promoted an increase in the emission rate, the differences to the No Fan case were rather small. The mass transfer coefficients had different responses depending on the fan size (large or small), the direction of flow (downward or upward) and the inlet sweep air flow rate (2, 5 or 10 L min⁻¹). Compared to the standard No Fan configuration, there was an increase in the emission rate for cases modified by a fan using the inlet sweep air flow rate of 10 L min⁻¹, mainly upward configuration which there was an increase for large and small fan. For the experiments with an inlet sweep air flow rate of 2 L min⁻¹, a slight decrease in the emission rate was observed for the configurations with the fan. For cases with sweep air flow rate of 5 L min⁻¹, emission rates were larger for the fan flow directed upwards, and slightly lower for flow directed downwards. More importantly, however, is the fact that the effects of all the different fan configurations investigated, whether towards increasing or decreasing the emission rates, were overall small. This is contrary to the intuitive hypothesis that the use of a fan inside the flux hood would dramatically enhance the emission of odorants measured on liquid surfaces.

Investigations were carried out using numerical simulations technique to understand the concentration distribution of the compound inside the hood and how it is controlled by the interaction between inlet sweep air flow rate and fan configuration. The numerical simulations were able to reproduce the same behaviour observed in the experiments for the measured outlet probe concentration. Further examination of the flow patterns developed closer to the liquid-gas interface inside the hood revealed that the increase in friction velocity promoted by the fan in some

regions is compensated by a thicker mass transfer boundary layer (compound accumulation due to convergent flow) over the same regions, leading to only small changes in the emission rates. By using the numerical simulation technique, we could better understand the reason the fan inside the flux hood does not produce a significant increase in the emission rate, which is indeed counterintuitive.

Flux hood experiments were performed to estimate the mass transfer parameters of acetic acid and butyric acid (both compounds having their volatilisation controlled by the gas phase) from aqueous solutions inside the flux hood and to assess the validity of adapting results from one compound to another using appropriate powers of their Schmidt numbers. Mass transfer parameters for acetic acid could be successfully measured, however, some reaction with ester formation could be occurring inside the flux hood, which impair the accuracy of the mass transfer coefficient measurement for butyric acid. Mass transfer rates estimated for butyric acid, using the mass transfer parameters of acetic acid, were of the same order of magnitude as the experimental butyric acid mass transfer rates. This indicates an overall successful application of their Schmidt numbers, even though the results for butyric acid indicated the presence of esters in addition to butyric acid, which compromised the precise estimation of the mass transfer parameters for butyric acid. Additional tests were performed to investigate the ester formation and the possibility of inhibiting it: replacement of Milli-Q® water with tap water; replacement of air as a carrier gas by nitrogen; and change in pH of aqueous butyric acid solution with approximately 1 mL of H₂SO₄.

Although some combinations contributed to an increase in the mass transfer coefficient k_G , ester formation was still detected in all tests. Liquid-phase samples were collected during an experiment with the flux hood and no ester formation was identified in them, revealing that the ester formation was occurring in the gas phase.

Finally, the values obtained for the gas side mass transfer coefficients (referred here as $k_{G,flux\ hood}$ with inlet sweep air flow of 2, 3, 5, 7 and 10 L min⁻¹ were compared with the Prata-Brutsaert approach (Equation (28)).

The k_G experimental data were closer to the Prata-Brutsaert model in the inlet sweep air flow 7 and 10 L m⁻¹ configuration. Furthermore, this bias was on the order of up to 40 times at wind speeds close to 20 m s⁻¹. The bias for low wind situation (up to 2.5 m s⁻¹) was around 4 times.

The bias evaluation presented in Section 5.4 for the gas-phase controlled compounds (acetic acid, valeric acid, isobutyric acid, and butyric acid) allows the emission rate measured with the USEPA

flux hood in the laboratory to be compared to models that estimate the emission rate expected in the field (J_{mod}/J_{hood}) providing a factor between the parts, especially, for example, for cases where there are operational difficulties in taking the entire device from the flux hood to the field.

Considering the results presented in the flux hood investigation in both No Fan and Fan configurations, recommendations for future work are suggested:

- It is worth noting that the above conclusions are specific for the fan sizes, rotation speeds and position inside the hood investigated in this work; it is possible that certain variations in these aspects may render stronger effects of the fan flow. In that sense, future studies can utilize the experimental results reported here to improve validation of CFD simulations, which in turn can be applied to explore alternative configurations and positions of the fan.
- It is recommended further research to explore contamination within the flux hood in more detail, since this can impact the accuracy to obtain mass transfer parameters of butyric acid and/or other compounds.
- Further investigations and standardization of procedure are recommended to apply scaling up, especially in situations where the flux hood cannot be used in the field for operational reasons, so that the effect of the build-up concentration inside the flux hood may be considered.

7 REFERENCES

- ANDREÃO, Willian L. et al. Effects of flux chamber configuration on the sampling of odorous gases emissions. **International Journal of Heat and Mass Transfer**, v. 140, p. 918–930, 2019.
- ANDREÃO, Willian Lemker; DE CASSIA FERONI, R. CFD modeling of different mass transfer coefficients on hydrogen sulfide emission in a flux chamber. **Environmental Science and Pollution Research**, v. 29, n. 10, p. 14961–14974, 1 fev. 2022.
- ANEJA, V. Measurement and analysis of atmospheric ammonia emissions from anaerobic lagoons. **Atmospheric Environment**, v. 35, n. 11, p. 1949–1958, abr. 2001.
- ANEJA, V. P.; CHAUHAN, J. P.; WALKER, J. T. Characterization of atmospheric ammonia emissions from swine waste storage and treatment lagoons hog waste TKN of the surface lagoon water ranged from 7 to 8 pH units , and 500 to 750 mg N L⁻¹, decreased through the fall (to a minimum flux during th. **Journal of geophysical research**, v. 105, n. D9, p. 11535–11545, 2000.
- BARCZAK, R. J. et al. Importance of 2,4,6-Trichloroanisole (TCA) as an odorant in the emissions from anaerobically stabilized dewatered biosolids. **Chemosphere**, v. 236, 1 dez. 2019.
- BLUNDEN, J.; ANEJA, V. P.; OVERTON, J. H. Modeling hydrogen sulfide emissions across the gas – liquid interface of an anaerobic swine waste treatment storage system. v. 42, p. 5602–5611, 2008.
- BOUSSINESQ, J. Essai sur la théorie des eaux courantes. **Divers Savants a l'Academie des Sciences de L'Institut de France**, v. 23, p. 1–680, 1877.
- CAPELLI, L. et al. Measuring odours in the environment vs. Dispersion modelling: a review.pdf. **Atmospheric Environment**, v. 79, p. 731–743, 2013.
- CHANTARASUKON, C.; TUKKEEREE, S.; ROHRER, J. Determination of Organic Acids in Wastewater Using Ion-Exclusion Chromatography and Online Carbonate Removal. **Thermo Fisher Scientific Inc**, 2016.
- CHAO, H. P. et al. An alternative method for predicting organic solute volatilization rates under gas and liquid turbulence. **Chemosphere**, v. 59, n. 5, p. 711–720, 2005.

DEMARS, B. O. L.; MANSON, J. R. Temperature dependence of stream aeration coefficients and the effect of water turbulence : A critical review. **Water Research**, v. 47, n. 1, p. 1–15, 2012. Disponível em: <<http://dx.doi.org/10.1016/j.watres.2012.09.054>>.

ECKLEY, C. S. et al. The influence of dynamic chamber design and operating parameters on calculated surface-to-air mercury fluxes. **Atmospheric Environment**, v. 44, n. 2, p. 194–203, 2010.

EKLUND, B. et al. Characterization of landfill gas composition at the Fresh Kills municipal solid-waste landfill. **Environmental Science and Technology**, v. 32, n. 15, p. 2233–2237, 1998.

_____. Practical guidance for flux chamber measurements of fugitive volatile organic emission rates. **Journal of the Air and Waste Management Association**, v. 42, n. 12, p. 1583–1591, 1992.

ENVIROMEGA. **Toxchem+: Fate of Toxics in Wastewater**. . [S.l.: s.n.]. Disponível em: <<https://www.hydromantis.com/request-download.html>>. , 2004

GHOLSON, A. R. et al. Evaluation of an Enclosure Method for Measuring Emissions of Volatile Organic Compounds from Quiescent Liquid Surfaces. **Environmental Science and Technology**, v. 25, n. 3, p. 519–524, 1991.

GOSTELOW, P.; PARSONS, S. A.; STUETZ, R. M. Odour measurements for sewage treatment works. **Water Research**, v. 35, n. 3, p. 579–597, 2001.

GRANT, R. H. et al. Hydrogen sulfide emissions from sow farm lagoons across climates zones. **Journal of Environmental Qualit**, v. 42, p. 1674–1683, 2013.

HUDSON, N. et al. Comparison of odour emission rates measured from various sources using two sampling devices. **Bioresource Technology**, v. 100, n. 1, p. 118–124, 2009.

HUDSON, N.; AYOKO, G. A. Comparison of emission rate values for odour and odorous chemicals derived from two sampling devices. **Atmospheric Environment**, v. 43, n. 20, p. 3175–3181, 2009. Disponível em: <<http://dx.doi.org/10.1016/j.atmosenv.2009.03.050>>.

_____. Odour sampling. 2. Comparison of physical and aerodynamic characteristics of sampling devices: A review. **Bioresource Technology**, v. 99, n. 10, p. 3993–4007, 2008a.

_____. Odour sampling 1: Physical chemistry considerations. **Bioresource Technology**, v. 99, n. 10, p. 3982–3992, 2008b.

JÄHNE, B.; HAUSSECKER, H. Air-water gas exchange. **Annu. Rev. Fluid Mech.**, v. 30, p. 443–468, 1998.

JIANG, K.; BLISS, P. J.; SCHULZ, T. J. The development of a sampling system for determining odor emission rates from areal surfaces: Part i. aerodynamic performance. **Journal of the Air and Waste Management Association**, v. 45, n. 11, p. 917–922, 1995.

JÓZSA, J.; MILICI, B.; NAPOLI, E. Numerical simulation of internal boundary-layer development and comparison with atmospheric data. **Boundary-Layer Meteorology**, v. 123, n. 1, p. 159–175, abr. 2007.

KLENBUSCH, M. **Measurement of gaseous emission rates from land surfaces using an emission isolation flux chamber**. . Austin, Texas: [s.n.], 1986.

LAOR, Y.; PARKER, D.; PAGÉ, T. Measurement, prediction, and monitoring of odors in the environment: A critical review. **Reviews in Chemical Engineering**, v. 30, n. 2, p. 139–166, 2014.

LEWIS, W. K.; WHITMAN, W. G. Principles of Gas Absorption. **Industrial and Engineering Chemistry**, v. 16, n. 12, p. 1215–1220, 1924.

LEYRIS, C. et al. Comparison and development of dynamic flux chambers to determine odorous compound emission rates from area sources. **Chemosphere**, v. 59, n. 3, p. 415–421, 2005.

LIMPT, H. Van et al. Mass transfer relations for transpiration evaporation experiments. v. 48, p. 4265–4281, 2005.

LOTESORIERE, B. et al. Micrometeorological Methods for the Indirect Estimation of Odorous Emissions. **Critical Reviews in Analytical Chemistry**, 2022.

LUCERNONI, F. et al. Sampling method for the determination of methane emissions from landfill surfaces. **Waste Management and Research**, v. 35, n. 10, p. 1034–1044, 2017.

LYMAN, S. N. et al. Emissions of organic compounds from produced water ponds I: Characteristics and speciation. **Science of the Total Environment**, v. 619–620, p. 896–905,

2018.

MACKAY, D.; YEUN, A. T. K. Mass Transfer Coefficient Correlations for Volatilization of Organic Solutes from Water. **Environmental Science and Technology**, v. 17, n. 4, p. 211–217, 1983.

MENTER, F. R. Two-equation eddy-viscosity turbulence models for engineering applications. **AIAA Journal**, v. 32, n. 8, p. 1598–1605, 1994.

PAPE, L. et al. **An automated dynamic chamber system for surface exchange measurement of non-reactive and reactive trace gases of grassland ecosystems**. **Biogeosciences**. [S.l: s.n.], 2009. Disponível em: <www.biogeosciences.net/6/405/2009/>.

PARK, J. W.; SHIN, H. C. Surface emission of landfill gas from solid waste landfill. **Atmospheric Environment**, v. 35, n. 20, p. 3445–3451, 2001.

PARKER, D. et al. Effect of wind tunnel air velocity on VOC flux from standard solutions and CAFO manure/ wastewater. **Transactions of the ASABE**, v. 53, p. 831–845, 2010.

_____. Wind tunnels vs. flux chambers: area source emission measurements and the necessity for VOC and odour correction factors. 2009, Perth, Western Australia: [s.n.], 2009.

PARKER, D. B.; CARAWAY, E.; et al. Effect of Wind Tunnel Air Velocity on VOC Flux Rates from CAFO Manure and Effect of Wind Tunnel Air Velocity on VOC Flux Rates from CAFO Manure and Wastewater. n. June 2014, 2013.

PARKER, D. B.; GILLEY, J.; et al. Odorous VOC emission following land application of swine manure slurry. **Atmospheric Environment**, v. 66, p. 91–100, 2013.

PARKER, David et al. Standardization of flux chamber and wind tunnel flux measurements for quantifying volatile organic compound and ammonia emissions from area sources at animal feeding operations. **Atmospheric Environment**, v. 66, p. 72–83, 2013. Disponível em: <<http://dx.doi.org/10.1016/j.atmosenv.2012.03.068>>.

PATANKAR, S. **Numerical heat transfer and fluid flow**. 2. ed. [S.l: s.n.], 1980.

PEIRSON, W. L.; WALKER, J. W.; BANNER, M. L. On the microphysical behaviour of wind-forced water surfaces and consequent re-aeration. **Journal of Fluid Mechanics**, v. 743, p. 399–447, 2014.

PRATA, A. A.; SANTOS, J. M.; et al. A critical review on liquid-gas mass transfer models for estimating gaseous emissions from passive liquid surfaces in wastewater treatment plants. **Water Research**, v. 130, p. 388–406, 1 mar. 2018. Disponível em: <<https://www.sciencedirect.com/science/article/pii/S004313541730996X>>. Acesso em: 19 fev. 2018.

PRATA, A. A. et al. Dynamic flux chamber measurements of hydrogen sulfide emission rate from a quiescent surface - A computational evaluation. **Chemosphere**, v. 146, p. 426–434, 2016. Disponível em: <<http://dx.doi.org/10.1016/j.chemosphere.2015.11.123>>.

PRATA, A. A.; LUCERNONI, F.; et al. Mass transfer inside a flux hood for the sampling of gaseous emissions from liquid surfaces – Experimental assessment and emission rate rescaling. **Atmospheric Environment**, fev. 2018. Disponível em: <<http://linkinghub.elsevier.com/retrieve/pii/S1352231018301079>>. Acesso em: 19 fev. 2018.

PRATA, A. A. et al. Modelling atmospheric emissions from wastewater treatment plants: Implications of land-to-water roughness change. **Science of the Total Environment**, v. 792, 20 out. 2021.

_____. Wind friction parametrisation used in emission models for wastewater treatment plants: A critical review. **Water Research**, v. 124, p. 49–66, 2017. Disponível em: <<http://dx.doi.org/10.1016/j.watres.2017.07.030>>.

RONG, L. et al. Validation of CFD simulation for ammonia emissions from an aqueous solution. **Computers and Electronics in Agriculture**, v. 75, n. 2, p. 261–271, 2011. Disponível em: <<http://dx.doi.org/10.1016/j.compag.2010.12.002>>.

SAHA, C. K. et al. Assessing effect of wind tunnel sizes on air velocity and concentration boundary layers and on ammonia emission estimation using computational fluid dynamics (CFD). **Computers and Electronics in Agriculture**, v. 78, n. 1, p. 49–60, 2011. Disponível em: <<http://dx.doi.org/10.1016/j.compag.2011.05.011>>.

SANDER, R. Compilation of Henry ' s Law Constants for Inorganic and Organic Species of Potential Importance in Environmental Chemistry. **Database**, v. 20, n. 1, p. 107, 1999.

SANTOS, J. M. et al. An experimental determination of the H₂S overall mass transfer coefficient from quiescent surfaces at wastewater treatment plants. **Atmospheric Environment**, v. 60, p. 18–24, 2012. Disponível em:

<<http://dx.doi.org/10.1016/j.atmosenv.2012.06.014>>.

TEYE, F.; HAUTALA, M. A comparative assessment of four methods for estimating ammonia emissions at microclimate locations in a dairy building. **International Journal of Biometeorology**, v. 54, p. 63–74, 2010.

_____. Adaptation of an ammonia volatilization model for a naturally ventilated dairy building. **Atmospheric Environment**, v. 42, p. 4345–4354, 2008.

TRAN, H. N. Q. et al. Emissions of organic compounds from produced water ponds II: Evaluation of flux chamber measurements with inverse-modeling techniques. **Journal of the Air and Waste Management Association**, v. 68, n. 7, p. 713–724, 2018. Disponível em: <<https://doi.org/10.1080/10962247.2018.1426654>>.

TREYBAL, R. E. **Mass Transfer Operations**. [S.l: s.n.], 1981.

US EPA. USER'S GUIDE FOR WATER9 SOFTWARE, Version 2.0.0. 2001. Disponível em: <<https://www3.epa.gov/ttnchie1/software/water/water9/water9 manual.pdf>>.

VERGOTE, T. L. I. et al. Monitoring methane and nitrous oxide emissions from digestate storage following manure mono-digestion. **Biosystems Engineering**, v. 196, p. 159–171, ago. 2020.

VERSTEEG, H. K. .; MALALASEKERA, W. . **An Introduction to Computational Fluid Dynamics**. [S.l: s.n.], 2007. v. M.

WANG, B. et al. Determination of VOSCs in sewer headspace air using TD-GC-SCD. **Talanta**, v. 137, p. 71–79, 2015. Disponível em: <<http://dx.doi.org/10.1016/j.talanta.2014.11.072>>.

WANG, X.; JIANG, J.; KAYE, R. Improvement of a wind-tunnel sampling system for odour and VOCs. **Water Science and Technology**, v. 44, n. 9, p. 71–77, 2001.

WHITMAN, W. G. The two film theory of gas absorption. **International Journal of Heat and Mass Transfer**, v. 5, n. 5, p. 429–433, 1962.

WOODBURY B. L., PARKER D. B., EIGENBERG R. A., SPIEHS, M. J. Flow characteristics of a dynamic EPA flux chamber. 2011, [S.l: s.n.], 2011.